Dipartimento di Chimica e Tecnologie del Farmaco

PhD Thesis

Facing antibiotic resistance

Presented by
Silvia Corradi

Supervisor:
Prof. Dr. Bruno Botta

Dottorato di Ricerca in Scienze Farmaceutiche – XXXII Ciclo

To my grandfather.

"We are not going in circles, we are going upwards. The path is a spiral; we have already climbed many steps."

Hermann Hesse (Siddhartha)

Curriculum Vitae

Date of Birth: April 14th1991

SILVIA CORRADI

Place of Birth: Rome, RM, Italy

Hometown: Rome, RM, Italy

Nationality: Italian

Scientific Experience

PhD Thesis with Prof. Dr. Bruno Botta, Sapienza Università di Roma, Italy 11/2016-10/2019: identification and synthesis of biologically active natural substances as novel colistin adjuvants in treatment of MDR Gram-negative infections.

Visiting PhD student in Prof. Dr. Filippo Mancia laboratory at the Department of Physiology and Cellular

Biophysics, Columbia University, New York (NY, USA): structural and functional elucidation by cryogenic electron microscopy (Cryo-EM) of RodA-PBP2 protein complex.

Education

Pharmacist Habilitation, 12/2016

Master degree in Medicinal Chemistry at Sapienza Università di Roma, Italy 11/2009-7/2016: "Study of Ring Opening Metathesis Polymerization's mechanism of resorc[4]areni".

High school diploma at Liceo- Ginnasio "Augusto", Rome, Italy, 7/2009.

List of Publications

Corradi, S. *et al*., Synthesis of Bromoundecyl Resorc[4]arenes and Applications of the Cone Stereoisomer as Selector for Liquid Chromatography *J. Org. Chem.* **2018**, *83* (15), 7683-7693; DOI: 10.1021/acs.joc.8b00488

Ghirga, F.; Stefanelli, R.; Cavinato, L.; Lo Sciuto, A.; **Corradi, S.**; Quaglio, D.; Calcaterra, A.; Casciaro, B.; Loffredo, M.R.; Cappiello, F.; Morelli, P.; Mangoni, M.L.; Mancone, C.; Botta, B.; Mori, M.; Ascenzioni, F.; Imperi, F., A novel colistin adjuvant identified by virtual screening for ArnT inhibitors submitted to J. *Antimicrob. Chemother*., **2019.**

List of Oral and Poster Presentations

Silvia Corradi, Elisa De Paolis, Cinzia Ingallina, Simone Berardozzi, Francesca Ghirga, Deborah Quaglio, Mattia Mori, Lucia Di Marcotullio, Paola Infante, Romina Alfonsi, Bruno Botta: "Gli1/DNA interaction is a druggable target for Hedgehog-dependent tumors". "A. Corbella" XLII International Summer School on Organic Synthesis. (Gargnano (BS), Italy, 18-22 June 2017)

Silvia Corradi, Francesca Ghirga, Deborah Quaglio, Bruno Botta, Marco Pierini, Luisa Mannina, Cinzia Ingallina, Elisa De Paolis: "Synthesis of basket recorc[4]arene 3b by intramolecular ring-closing-metathesis andinvestigation of its

aggregation propensity". 22nd International Symposium on Olefin Metathesis and Related Chemistry- ISOM XXII (Zurich, Switzerland, 9-12 July 2017).

Silvia Corradi, Francesca Ghirga, Mattia Mori, Cinzia Ingallina, Simone Berardozzi, Elisa De Paolis, Lucia di Marcotullio, Romina Alfonsi, Bruno Botta, Deborah Quaglio: "Identification of novel natural products chemotypes of Hedgehog-dependent tumors inhibitors". COST ACTION CM1407 2ndTraining School in Synthesis, isolation and structural elucidation of bioactive compounds (Lisbon, Portugal, 18-20 September 2017); 4th COST Action "Challenging organic syntheses inspired by nature- from natural products chemistry to drug discovery" (Lisbon, Portugal, 21-22 September 2017).

Silvia Corradi, Deborah Quaglio, Mattia Mori, Luca Tottone, Cinzia Ingallina, Elisa De Paolis, Isabella Screpanti, Bruno Botta, Rocco Palermo, Francesca Ghirga: "Inhibition of Notch signaling pathway in T-cell acute lymphoblastic leukemia: a challenge faced with a novel chalcone derivative".

8th BeMM PhD Symposium 2017 (Rome, Italy, 20 November 2017).

Elisa De Paolis, Francesca Ghirga, Cinzia Ingallina, Cristina Tortolini, Laura Mangiardi, Franco Mazzei, Bruno Botta, Deborah Quaglio, **Silvia Corradi**: "Synthesis of a new artificial linker resorc[4]arene-based system for immunosensors development". Nanotech Middle East 2017 Conference (Dubai, UAE, 4-6 December 2017).

Silvia Corradi, Francesco Imperi, Mattia Mori, Fiorentina Ascenzioni, Bruno Botta, Francesca Ghirga: "Synthesis of Diterpenoid Derivatives as Putative Arnt Inhibitors". VII EWDSy - European Workshop in Drug Synthesis (Siena, Italy, 20-24 May 2018).

Silvia Corradi, Francesca Ghirga, Deborah Quaglio, Cinzia Ingallina, Elisa De Paolis, Silvia Balducci, Laura Mangiardi, Simone Berardozzi, Mattia Mori and Bruno Botta: "From macrocyclic architectures to small biologically active organic compounds". Second Workshop on Research at the Department of Chemistry and Technologies of Drug (Rome, Italy, 13 July 2018).

Abstract

This PhD thesis is focused on two main topics:

Part A. A novel colistin adjuvant identified by virtual screening for ArnT inhibitors

The spread of multidrug resistance (MDR) Gram-negative bacterial pathogens and the paucity of new drugs prompted the medical community to re-use the old polymyxin antibiotic colistin.

Unfortunately, reintroduction of colistin in clinical practice led inevitably to the emergence of colistin-resistant isolates (Jeannot, K. *et al.* 2017), such as *P. aeruginosa*.

Gram-negative bacteria acquire colistin resistance mostly through mutations of genes responsible for remodeling of the lipopolysaccharide (LPS), primarily *via*

Abstract

the enzymatic addition of 4-amino-4-deoxy-L-arabinose (L-Ara4N) to lipid A by the aminoarabinose transferase ArnT. The resulting positive charge reduces LPS affinity for colistin, leading to resistance (Olaitan, A.O. *et al*., 2014; Baron, S. *et al*., 2016). Accordingly, the pharmacological inhibition of L-Ara4N biosynthetic pathway could represent a suitable approach to extend the clinical lifetime of colistin for the treatment of *P. aeruginosa* infections.

Here, in the attempt to identify potential inhibitors of L-Ara4N-dependent colistin resistance, a docking-based virtual screening of a unique *in house* library of natural products was carried out within the catalytic site of ArnT (Petrou, V.I. *et al.*, 2016). This led to the identification of a natural diterpene (**14**) able to potentiate colistin activity against colistin-resistant *P. aeruginosa* isolates.

A series of semi-synthetic analogs were further synthesized and tested *in vitro* aiming at outlining the

structure-activity relationship (SARs) and improving their activity. Currently, all these compounds are covered by Italian patent.

Part B. A molecular level investigation of the protein machinery essential for bacterial cell wall biosynthesis

The cell wall of most Gram-negative and Gram-positive bacteria is composed of peptidoglycan (PG), a mesh-like structure of repeating glycan chains cross-linked by small peptides. Peptidoglycan is essential for growth, division and viability of the microorganism. Any disruption of its biosynthesis results in bacterial cell lysis or cessation of growth, making it a major target for antibiotics.

It was suggested that many proteins involved in PG synthesis, from the cytoplasmic enzymes that synthesize

Abstract

the precursor Lipid II to the extracellular enzymes that are responsible for its polymerization, function *in vivo* as part of a multi- protein complex "machinery". In particular, recent evidence suggests that the core of the PG biosynthetic complex consists of the class B penicillin binding proteins (PBPs) such as PBP2 and PBP3 that work together with membrane inserted shape, elongation, division and sporulation (SEDs) proteins, FtsW and RodA, respectively. These synthetic machines provide for cell division (FtsW-PBP3) and cell elongation (RodA-PBP2) and are also the key targets of most clinically used ß-lactam compounds.

Though structures of both RodA (a SEDS protein involved in bacterial growth and elongation) and type b PBPs are available, the interaction between these proteins and their joint enzymatic activity is poorly characterized.

Here, the preliminary structural characterization of a RodA-PBP2 protein complex by single-particle cryogenic electron microscopy (cryo-EM) is presented,

Abstract

aiming at a better understanding of these incredibly important enzymes that could enlighten the future of antibiotics research and development.

TABLE OF CONTENTS

Table of contents

Table of contents

List of Compounds

1

2

3

4

5

6

7

8

9

10

11

12

13

14

15

List of compounds, abbreviations, acronyms and symbols

16　　**17**　　**18**

19　　**20**　　**21**　　**22**

23　　**24**　　**25**
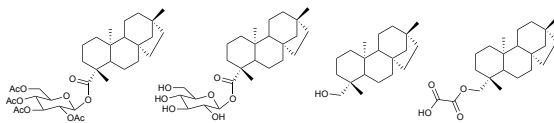
26　　**27**　　**28**　　**29**

30　　**31**　　**32**

33　　**34**　　**35**

X
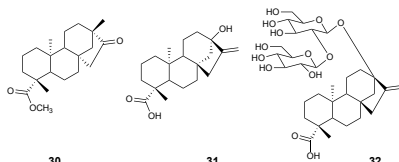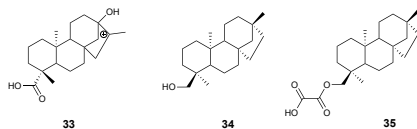
List of Abbreviations, Acronyms and Symbols

A

$[\alpha]_D$: specific optical rotation;

Å: Ångstrom;

Ac: acetyl;

aPBP: class A penicillin-binding protein;

Arg: arginine;

ArnT: aminoarabinose transferase;

ATP: adenosine triphosphate;

B

BD: binding domain

BL-BLI: β-lactam/β-lactamase inhibitors;

bPBP: class B penicillin-binding protein;

br: broad signal;

List of compounds, abbreviations, acronyms and symbols

C

°C: Celsius degree;

^{13}C-NMR: carbon-13 nuclear magnetic resonance;

Calcd: calculated;

CDCl$_3$: deuterated chloroform;

CDDM: conformational dependent domain movement;

CF: cystic fibrosis;

CH$_2$Cl$_2$: dichloromethane;

CH$_3$COOH: acetic acid;

CH$_3$OH: methanol;

CMS: colistimethate sodium;

CRAB: carbapenem-resistant *Acinetobacter baumannii*;

CRE: carbapenem-resistant *Enterobacterales*

CRPA: carbapenem-resistant *Pseudomonas aeruginosa*;

cryo-EM: cryogenic electron microscopy;

List of compounds, abbreviations, acronyms and symbols

CTF: contrast transfer function;

D

d: doublet;

d: doublets or days;

Da: Dalton;

dd: doublet of doublets;

DDM: *n*-Dodecyl β-D-maltoside

DIBMA: diisobutyl-maleic acid copolymer;

dm: doublet of multiplets;

DMF: N,N-dimethylformamide;

DMSO: dimethyl sulfoxide;

dt: doublet of triplets

δ: NMR chemical shift in ppm;

E

E: glutamic acid;

List of compounds, abbreviations, acronyms and symbols

EARS-Net: European Antimicrobial Surveillance Network;

EC-MR: coupling-enabled molecular replacement;

EI: electron ionization;

EM: electron microscopy;

ent-CPP: *ent*-copalyl diphosphate precursor *ent*-CPP;

equiv.   equivalent;

ESI: electrospray ionization;

Et: ethyl;

Et_2O: diethyl ether;

Et_3N: triethylamine;

F

FC: flash chromatography;

FT-ICR: Fourier transform ion cyclotron resonance;

G

g: gram;

List of compounds, abbreviations, acronyms and symbols

HRMS: high resolution mass spectrometry;

HTS: high throughput screening;

Hz: Hertz (s^{-1});

I

IPTG: Isopropyl β-d-1-thiogalactopyranoside;

IR: infrared;

J

J: coupling constant;

JM: juxtamembrane;

K

K: lysine;

K_2CO_3: potassium carbonate;

KDa: KiloDaltons;

KOH: potassium hydroxide

L

List of compounds, abbreviations, acronyms and symbols

L-Ara4N:

L-Ara4N: 4-amino-4-deoxy-L-arabinose;

L-Dab: L-α,γ-diaminobutyric acid;

LiAlH$_4$: lithium aluminum hydride;

LMM-PBP: low molecular mass penicillin-binding protein;

LMM: low molecular mass;

LPS: lipopolysaccharide

Lys: lysine;

M

M: molar;

m: multiplet;

m: multiplet;

m/z: mass to charge ratio;

M$^+$: molecular ion;

MDR: multidrug-resistant;

List of compounds, abbreviations, acronyms and symbols

Me: methyl;

MeOH-d_4: deuterated methanol;

MeOH: methanol;

MeOH: methanol;

mg: milligram;

Mg^{2+}: Magnesium cation;

MH: Mueller-Hinton;

MHz: Megahertz;

MIC: minimum inhibitory concentration;

min: minute;

mL: milliliter;

mM: millimole per liter;

mmol: millimole

Mp: melting point;

MS: mass spectrometry;

List of compounds, abbreviations, acronyms and symbols

MSP: membrane scaffold protein;

MTT: 3-(4,5-dimethylthiazol-2-yl)-2,5-diphenyltetrazolium bromide

MurNAc: N-acetylmuramic acid;

μ: micro;

μL: microliter;

N

Na_2SO_4: sodium sulfate

NaCl: sodium chloride;

$NaIO_4$: sodium periodate;

NMR: nuclear magnetic resonance;

O

OD600: optical density at a wavelength of 600 nm

OprH: outer membrane protein H1

P

List of compounds, abbreviations, acronyms and symbols

PA14 col^R 5: evolved colistin-resistant isolate of *P. aeruginosa* PA14;

PBP: penicillin-binding protein;

PD: pharmacodynamic;

Pd/C: palladium on carbon;

PG: peptidoglycan

PhD: doctor of philosophy;

PK: pharmacokinetic;

PL: periplasmic loops;

PMSF: Phenylmethylsulfonyl fluoride;

ppm: parts per million;

Q

q: quartet;

R

R-: generalized alkyl group or substituent;

List of compounds, abbreviations, acronyms and symbols

R: arginine;

Rf: retention factor;

RNA: ribonucleic acid;

rt: room temperature;

S

s: second or singlet;

SAR: structure-activity relationship;

sas/ss: saturated solution

SD: standard deviation;

SDS-PAGE: sodium dodecyl sulphate- polyacrylamide gel electrophoresis;

SEDS: shape, elongation, division and sporulation

SEMC: Simons Electron Microscopy Center;

SENTRY: Antimicrobial Surveillance Program;

SMA: styrene-maleic acid copolymer;

List of compounds, abbreviations, acronyms and symbols

SNR: signal to noise ratio;

SOCl$_2$: thionyl chloride;

T

t: triplet;

TBAB: tetrabutylammonium bromide;

TCEP: tris(2-carboxyethyl)phosphine

TCs: two-component systems;

td: triples of doublet;

TEG: triethylene glycol;

Th: threonine;

THF: tetrahydrofuran;

TLC: thin layer chromatography;

TM: transmembrane;

TMD: transmembrane domain;

List of compounds, abbreviations, acronyms and symbols

TMS: tetramethylsilane;

TPase: transpeptidases;

Tyr: tyrosine;

U

UDP: uridine diphosphate;

UndP: undecaprenyl phosphate;

UV: ultraviolet;

V

VAP: ventilator-associated pneumonia

W

WHO: World Health Organization;

WT: wild type;

X

-

Y

-

Z

Zn^{2+}: Zinc cation;

General Introduction

<u>Bacterial cell wall: a unique feature of prokaryotic cells</u>

Bacteria are one of the three taxonomic domains of cellular organisms. They are prokaryotic cells and differ mainly from the eukaryotic ones for: the dimension; the lack of a membrane-bound nucleus and other intracellular membranous organelles, such as mitochondria; the reproductive strategies; and the presence of distinctive features, such as motility structures and cell wall (Figure 1) (Rogers, K. and Kadner, R.J., 2019; Parker, J., 2001).
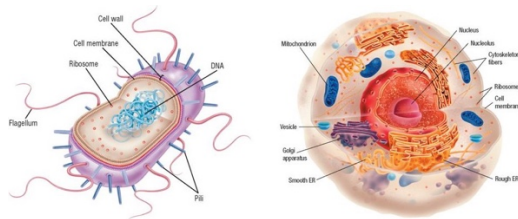
Figure 1 Prokaryotic and eukaryotic cell structures.

General introduction

Unlike cells of higher organisms, bacteria face unpredictable and hostile environments. Thus, to survive, they evolved a unique cell envelope, which acts as the primary protective barrier. The cell wall varies between types of bacteria giving them distinctive structural characteristics and pathogen-host interaction profiles (Messner, P. *et al*., 2013). Based on the structure of this feature, bacterial cells were first classified by Hans Christian Gram in two main groups: Gram- positive and Gram-negative bacteria (Cabeen, M.T. and Jacobs-Wagner, C., 2005). Thus, Gram-positive cell walls are composed of a thick, multilayered peptidoglycan (PG) coat that includes embedded teichoic and lipoteichoic acids. While Gram-negative cell walls consists of an outer membrane (OM) that surrounds a thin PG layer, and a periplasmic space between the inner and outer membranes (Figure 2).
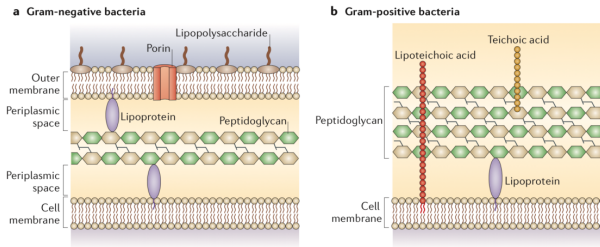
Figure 2 Cell wall structure of Gram-negative bacteria **(a)** and Gram-positive bacteria **(b)** (Brown, L., *et al*., 2015).

The major conserved component of the cell wall in almost all Gram-negative and Gram-positive bacteria is peptidoglycan (Vollmer, W. *et al*., 2008).

PG is a mesh-like structure made up of strands of repeating sugar units, N-acetylmuramic acid (MurNAc) and N-acetylglucosamine (GlcNAc), which are cross-linked by small peptides. The biosynthesis of PG starts in the cytosol, where the hydrophilic PG precursor (UDP-MurNAc-pentapeptide) is attached to the lipid carrier undecaprenyl phosphate (UndP). The lipid-linked precursor (undecaprenyl-pyrophosphoryl-MurNAc-

pentapeptide or Lipid I) is modified further to undecaprenyl-pyrophosphoryl-MurNAc-(pentapeptide)-GlcNAc (Lipid II) by addition of a GlcNAc moiety. Lipid II is then flipped across the membrane to the periplasm where its sugars are polymerized to form the glycan strands of the peptidoglycan mesh (Figure.3).

Figure **3** Peptidoglycan biosynthesis and cleavage (Typas, A. *et al*., 2012).

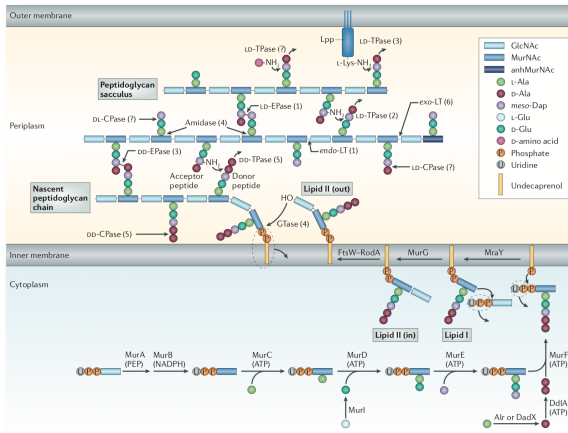PG acts to stabilize the membrane and overall structure of the bacterial cell. It is also essential for growth,

division and viability of bacterial organisms. Thus, enzymes contributing to the peptidoglycan biosynthetic pathway are attractive antibiotic targets (Silhavy, T.J. *et al.*, 2010; Brown, D.G., 2016).

Antibiotic resistance: a rising threat to global health

Antibiotics revolutionized medicine in many aspects and improved significantly the quality of life, reducing childhood mortality, increasing life expectancy and saving numerous lives (Li, B. and Webster T.J., 2018; Gould, K., 2016; Fernandes, P. and Martens, E., 2017; Aminov, R.I, 2014).

The birth of the antibiotic era comes from the work of several pioneering scientists. In 1929, the isolation of penicillin from *Penicillium* mold and its potential use in surgical dressings were reported by Alexander Fleming. In 1935, the synthesis of sulfanilamide, the prototype for all sulfa drugs, was presented by Gerhard Domagk. In 1939, the isolation of tyrothricin, which was the first antibiotic established as a therapeutic substance, was reported by René Dubos.

In the early 1940s, thanks to that and the industrialized production of penicillin numerous antibiotics were isolated and developed. The so-called "Golden Age" of antibiotic discovery began and the major classes of antibiotics in use, even nowadays, were produced (Fernandes, P., 2006).

From the late 1960s, resistance to existing antibiotics emerged powerfully and became the driving force for searching for new drugs. The antibiotic discovery largely abandoned natural product sources and redirected efforts on synthetic and high-tech approaches (Lewis, K., 2017). Unfortunately, the output of novel antibiotic agents fell dramatically, and only few drugs were putted on market in the last years (Figure 4) (Silver, L.L., 2011; O'Neill, J., 2016).

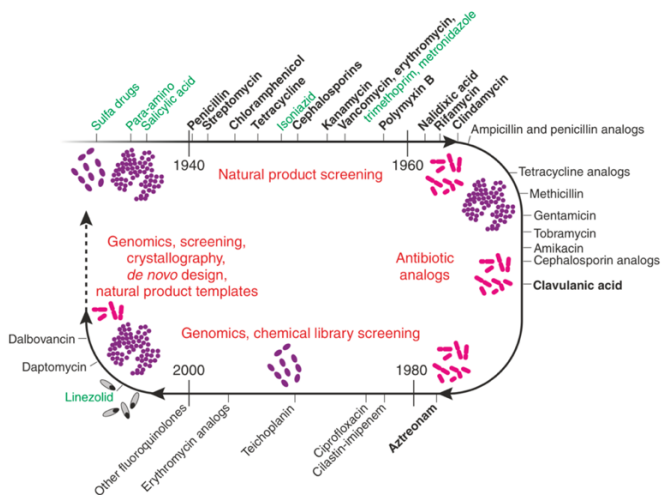**Figure 4** A timeline for antibiotic research. (Fernandes, P., 2006).

The decreased interest in antibiotic research of pharmaceutical companies is probably related to difficulties in clinical development and regulatory, and economic issues. However, the stimulation of antibiotic research has a pivotal role in finding new strategies to address the global threat of antibiotic- resistance (Tacconelli, E. *et al*., 2018).

10

General introduction

Resistance to antibiotics is a natural process that was observed since they were discovered (Fleming, A., 1945). In recent times, it is causing a public health crisis. Indeed, as a direct evolutionary consequence of widespread antibiotic use and overuse, bacteria resistance against all available antibiotics is rapidly outpacing the speed of human innovation (Wright, G.D., 2016; Tyer, M. and Wright, G.D., 2019; Hernando-Amado, S. *et al*., 2019). Nowadays, about 700,000 people die every year from drug- resistant strains of common bacterial infections and the burden of deaths could rise to 10 million lives each year by 2050, unless action is taken (O'Neill, J., 2016).

Bacteria can be intrinsically resistant to certain antibiotics. For example, an individual species can be resistant due to absence of a specific antibiotic susceptible target. In addition, they can acquire or develop resistance to antibiotics through the mutation of genes coding for drug targets and other compensatory proteins, or by the introduction of new genes by horizontal gene transfer

(Blair, J.M. *et al.*, 2015; Frieri, M. *et al*., 2016). The acquired resistance can be mediated by several mechanisms, which fall into three main groups (Figure 5):

1. prevention of access of antibiotics to target, as a result of poor penetration into the bacterium or of antibiotic efflux;

2. changes of antibiotic targets *via* genetic mutations or post-translational modifications;

3. inactivation of antibiotic through their hydrolysis or modification.
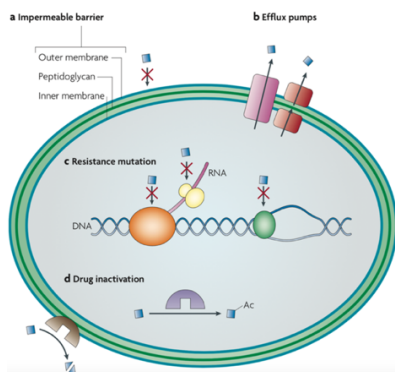
Figure 5 Mechanisms of antibiotic resistance (Allen, H.K. *et al.*, 2010).

The first group of resistant mechanisms minimize the intracellular concentrations of the antibiotic. As example, in Gram- negative and many Gram-positive bacteria, efflux pumps are major contributors to the resistance. They can have narrow substrate specificity or a wide range of structurally dissimilar substrates (known as multidrug resistance efflux pumps); and when overexpressed, they can confer high levels of resistance to previously clinically useful antibiotics. The second group, usually, requires a mutational change in the genes encoding the antibiotic target. It comprises alterations to the target structure that prevent efficient antibiotic binding, but that still enable the target to carry out its normal function. The third one can degrade or modify antibiotics of different classes, using enzymes that catalyse their hydrolysis or add chemical groups (acyl, phosphate, nucleotidyl and ribitoyl groups) to vulnerable sites on the antibiotic molecule preventing the drug from binding to its target.

In summary, as a result of the widespread use of antibiotics in several fields the emergence of antibiotic resistance is great. Thus, the current challenge is to develop novel drugs investigating the mechanisms of resistance, and exploiting available technologies and expertise (Blair, J.M. *et al.*, 2015).

Part A

A novel colistin adjuvant
identified by virtual
screening for ArnT
inhibitors

The present part of the thesis deals with a research activity carried out at the Dipartimento di Chimica e Tecnologie del Farmaco at Sapienza Università di Roma, under the supervision of Prof. Bruno Botta.

CHAPTER A1

Introduction

A1.1 Current treatment options for multidrug-resistant Gram-negative bacteria infections

Global resistance to most available antibiotics is threatening human health and making antibiotic choices for infection control limited and more expensive (Li, B. and Webster, T.J., 2018). In particular, the emergence of multidrug-resistant (MDR) mechanisms in opportunistic Gram-negative bacterial pathogens such as *Pseudomonas aeruginosa*, *Acinetobacter baumannii* and *Enterobacteriaceae* is alarming. Hence, in 2017 the World Health Organization (WHO) included these pathogens in the list of bacteria for which antibiotics are urgently needed as first priority (https://www.who.int/en/news-room/detail/27-02-2017-who-publishes-list-of-bacteria-for-which-new-antibiotics-are-urgently-needed). In the past few years, new treatment options for MDR Gram-

negative bacteria infections in critically ill patients became available (Figure A1.1), even though pharmacokinetic (PK) and pharmacodynamic (PD) optimization of their dosages and treatment has still some areas of uncertainty (Bassetti, M. *et al*., 2019).

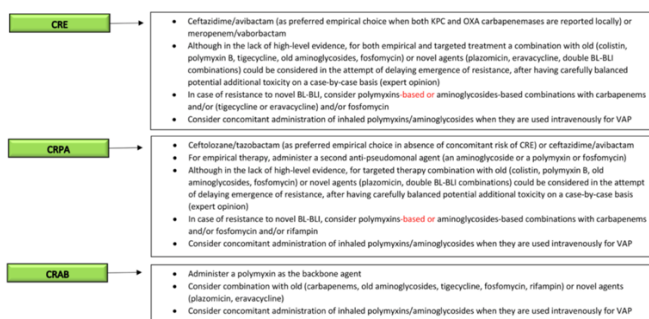**Figure A1.1** Current clinical reasoning for the treatment of serious MDR Gram-negative bacteria infections in critically ill patients. CRE, carbapenem-resistant *Enterobacterales*; CRPA, carbapenem-resistant *Pseudomonas aeruginosa*; CRAB, carbapenem-resistant *Acinetobacter baumannii*; BL-BLI, β-lactam/β-lactamase inhibitors; VAP, ventilator-associated pneumonia (Bassetti, M. *et al*., 2019).

However, resistance to these treatments already started to emerge. Thus, because of the emergence of MDR Gram-negative organisms and lack of new drugs, medical community re-evaluated the use of the old antibiotics, such as polymyxins (Giamarellou, H., 2016; Poirel, L. *et al*., 2017; Velkov, T. *et al*., 2013).

Polymyxins were discovered more than 50 years ago (Velkov, T., 2010). They derive from various species of *Paenibacillus* (*Bacillus*) *polymyxa* and their chemical structure is similar to that of cationic antimicrobial peptides (defensins and gramicidins), which represent the first line of defense against bacterial colonization in eukaryotic cells. Polymyxins are cationic polypeptides that consist of a cyclic heptapeptide possessing a tripeptide side chain acylated at the N-terminus by a fatty acid tail, which accounts for most of the polymyxins antimicrobial activity and toxicity as well (Poirel, L. *et al*., 2017).

The antibacterial mechanism of action (Velkov, T. *et al.*, 2010; Velkov, T. *et al.*, 2013; Li, Z. and Velkov, T.,

2019; Kaye, K.S. *et al.*, 2016; Sabnis, A. *et al*., 2019) of polymyxins is not yet completely understood. However, they are believed to target the lipopolysaccharide in Gram-negative outer and cytoplasmic membranes, leading to disruption of the cell envelope and bacterial lysis (Sabnis, A. *et al*., 2019) (Figure A1.2).
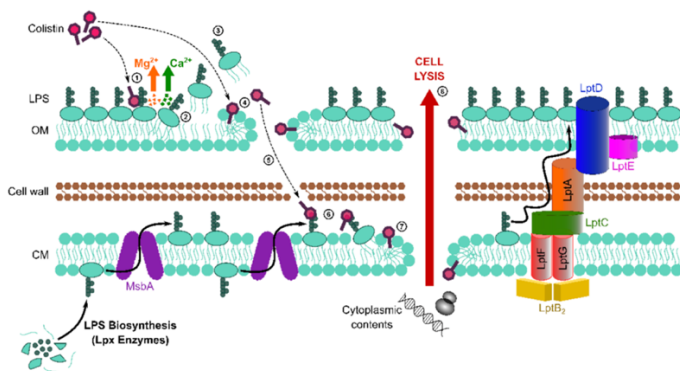
Figure A1.2 Schematic representation of antibacterial mechanism of action of colistin (Sabnis, A. *et al*., 2019).

Thus, the electrostatic interaction of polymyxin cationic L-α,γ-diaminobutyric acid (L-Dab) side-chains with the phosphate groups of lipid A moiety of LPS

displaces stabilizing cations Ca^{2+} and Mg^{2+}, that bridge adjacent LPS molecules. The polymyxin molecules*,* then, enter into the fatty acyl chain layer of the lipid A molecules, causing derangement of outer and cytoplasmic membranes (Li, Z. and Velkov, T., 2019). This in turn results in increased membrane permeability, leakage of cell content and ultimately cell death (Storm, D.R. *et al*., 1977).

Based on available evidences, bactericidal activity of polymyxins also involves a secondary mode of action, which is responsible for the inhibition of bacterial respiration. In particular, it seems that the ability of polymyxins to disrupt the inner membrane structure is coincident with their inhibition of the alternative type 2 nicotinamide adenine dinucleotide dehydrogenase: the inner membrane respiratory enzyme of a number of pathogenic Gram- negative bacteria. Indeed, the downstream secondary target-polymyxin interactions trigger redox-related physiological alterations that result

in the formation of toxic reactive oxygen species as well as stimulating repairing responses, which further contribute to cellular damage, mutations and death (Li, Z. and Velkov, T., 2019).

To date, several distinct groups of polymyxins (polymyxins A to E) were isolated and structurally identified from *Paenibacillus polymyxa*. Of these different groups, only two are used in the clinical setting (Velkov, T. *et al.*, 2013; Landman, D., 2008): polymyxin B and colistin (Figure A1.3).
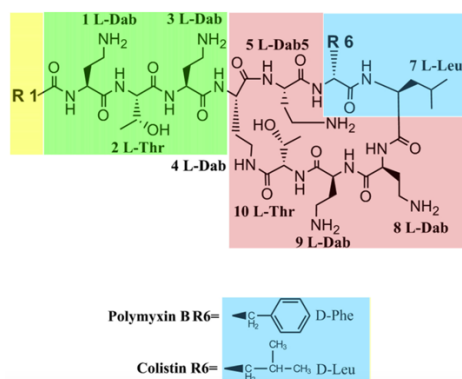
Figure A1.3 Chemical structures of polymyxin B and colistin (Velkov, T. *et al.*, 2010).

In particular, colistin is the last-resort therapeutic option in infections by recalcitrant Gram-negative bacteria when no other less toxic or effective antibiotics are suitable. It is a multicomponent polypeptide antibiotic, comprised mainly of colistin A and B (Li, J. *et al.*, 2006; Li, J. and Nation, R.L., 2009). Colistin was isolated from the soil bacterium *Paenibacillus polymyxa* subsp. *Colistinus* in 1947 (Poirel, L. *et al.*, 2017; Vaara, M., 2019) and it became available for clinical use in the 1960s. However, it was used in human medicine only for few years. During the 1970s, colistin was replaced by more potent and less toxic drugs due to severe side effects such as neuro- and nephrotoxicity. Currently, it is re-assessed as a critically important antibiotic in humans due to its efficacy against MDR Gram-negative bacteria (Apostolakos, I. and Piccirillo, A., 2018). There are two forms of colistin commercially available (Li, J. *et al.*, 2006): colistin sulfate and colistimethate sodium (CMS or colistin methanesulfonate). Because of toxicity, colistin

sulfate is used only for topical therapy. While, CMS is a less toxic formulation for parenteral use than colistin sulfate. It is the polyanionic colistin prodrug, which is converted into colistin and several inactive compounds in aqueous media and biological (Poirel, L. *et al*., 2017). However, based upon recent studies it is evident that colistin monotherapy is not likely to be reliably efficacious with currently recommended daily doses of CMS (Velkov, T. *et al.*, 2013).

Furthermore, worrisome trends of increasing resistance to this antibiotic were reported in some countries. Thus, the use of colistin should be optimized as much as possible in terms of dosages and indications improving effectiveness and minimizing the emergence of further resistance (Bassetti, M. *et al*., 2019; Tsuji, B.T. *et al.*, 2019).

A1.2 Resistance to polymyxins in Gram-negative bacteria

Resistance to polymyxins by bacilli that are normally susceptible to these drugs was reported. There are also reports of increases in infections caused by naturally polymyxin-resistant bacteria, such as *Proteus*, *Providencia, Morganella*, and *Serratia* (Olaitan, A.O., 2014). Colistin resistance in *Klebsiella pneumoniae*, *P. aeruginosa* and *A. baumannii* appears in less than 10% of the isolates, although higher rates (50%) were reported (Jeannot, K. *et al*. 2017; Poirel, L. *et al*., 2017; Kaye, K.S. *et. al*., 2016; Giamarellou, H., 2016). In a recent study by SENTRY Antimicrobial Surveillance Program on isolates collected worldwide in 2017, the frequency of colistin resistance was still very rare. In 2015, the European Antimicrobial Surveillance Network (EARS-Net) registered 33,100 deaths due to infections caused by antibiotic-resistant bacteria. Among them, only 0.5% was

caused by colistin-resistant *A. baumannii* or *P. aeruginosa* (Vaara, M., 2019). However, it should be noted that colistin resistance epidemiology may be underestimated due to the absence of powerful automated methods in clinical setting (Jayol, A. *et al*., 2018). Thus, identifying new strategies in order to decrease polymyxin resistance development and preserve the activity of these antibiotics gets imperative.

Gram-negative bacteria employ several means to protect themselves from adverse environmental stimuli, including exposure to cationic antimicrobial peptides, such as polymyxin B and colistin. Some bacteria, such as *K. pneumoniae*, *P. aeruginosa* and *A. baumannii*, develop resistance to polymyxins; whereas other bacteria, such as *Proteus* spp., *Serratia* spp., and *Burkholderia* spp., are naturally resistant to these drugs. This intrinsic resistance is mainly due to L-Ara4N modified lipopolysaccharides (Olaitan, A.O. *et al*., 2014), whereas in some species it was associated with defects in UDP-glucose dehydrogenase

and UDP-glucose phosphorylase, enzymes involved in the biosynthesis of the LPS precursor (Velkov, T. *et al.*, 2013). The acquired resistance is made of different strategies, including a variety of LPS modifications or its complete loss from the bacterial surface; the production of capsular polysaccharides; the expression of efflux pump systems (Moffatt, J.H. *et. al.*, 2019); the expression of the outer membrane proteins such as OprH, which stabilizes the membrane under conditions of Mg^{2+} lack; and presence hopanoids, sterol-like compounds that are believed to perform a barrier function in the outer membrane of certain bacterial species (Velkov, T. *et al.*, 2013) (Figure A1.4).
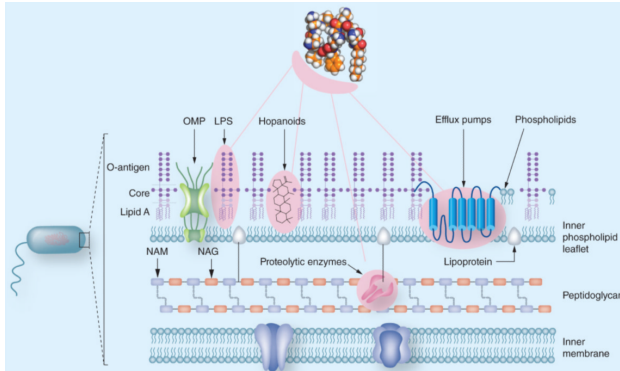
Figure A1.4 Key mechanisms of polymyxin resistance in Gram-negative bacteria (Velkov, T. *et al.*, 2013)

A1.2.1 Resistance Mechanisms involving LPS structure modifications: addition of L-Ara4N to lipid A

The first step in the action of polymyxin antibiotics on the Gram-negative bacterial outer membrane involves an electrostatic interaction between the positive charge of the five L-Dab residues of the polymyxin molecule and the negatively charged phosphate groups on lipid A (Velkov, T. *et al.*, 2013). Thus, the majority of resistance mechanisms involves modifications that alter structure and charge of LPS (Moffatt, J.H. *et. al.*, 2019). Indeed, by decreasing the net negative charge of LPS phosphate residues, these alterations tend to prevent the binding of polymyxin molecules to the bacterial surface and their further penetration into the cell interior, where they are supposed to exert the bactericidal activity (Jeannot, K. *et al.,* 2017).

LPS is composed of three domains: the lipid A hydrophobic anchor, the core oligosaccharide and the O antigen (Needham, B.D. and Trent, M.S., 2013). Lipid A is the endotoxic portion of LPS and the site also for many LPS modifications. The various possible modifications include the addition of 4-amino-4-deoxy-L-arabinose (L-Ara4N) moieties and phosphoethanolamine moieties, as well as phosphorylation, deacylation, acylation and hydroxylation (Figure A1.5) (Nowicki, E.M. *et al*., 2015).
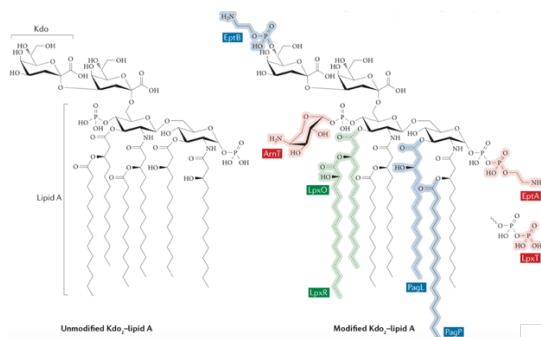

Figure A1.5 Unmodified lipid A and inner core (Kdo or 3-deoxy-d-*manno*-octulosonic acid) portion of LPS; Modified lipid A and inner core (Needham, B.D. and Trent, M.S., 2013).

All of these alterations are subjected both transcriptional and post-translational regulation by many enzymes. Two-component systems (TCs), which are typically composed of a sensor kinase and a response regulator, small RNAs, peptide feedback loops and substrate availability are all involved in directing the activity of these enzymes. To date, widespread TCs are PhoPQ and PmrAB systems, and the ParRS, ColRS and CprRS systems in *P. aeruginosa* (Needham, B.D. and Trent, M.S., 2013).

In Gram negative bacteria, the most common LPS modification mainly occurs by covalent addition of L-Ara4N to lipid A moiety. Environmental stimuli and specific mutations within the TCSs trigger the activation of phosphorelay systems PhoPQ and PmrAB, which overexpress LPS-modifying genes (Figure A1.6). For example, the activation of the PmrAB TCS leads to the upregulation of the *pmrCAB* and *arnBCADTEF-pmrE* operons that mediate the synthesis and transfer of L-

Ara4N to lipid A. (Olaitan, A.O. *et al*., 2014; Baron, S. *et al*., 2016).
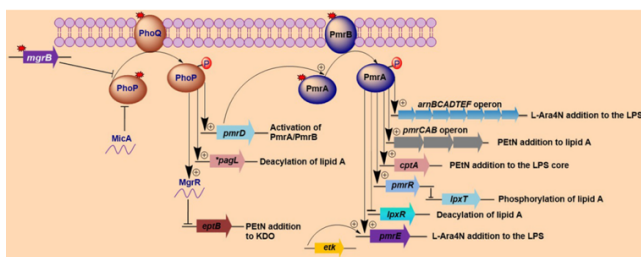
Figure A1.6 Activation of lipopolysaccharide-modifying genes involved in polymyxin resistance in Gram-negative bacteria (Olaitan, A.O. *et al*., 2014).

In particular, *P. aeruginosa* colistin resistance correlates with mutations in PhoPQ two-component system leading to activation of the *arn* operon and increased production of L-Ara4N. The *arn* operon is also controlled by PmrA/PmrB, ParR/ParS, ColR/ColS and CprR/CprS (Figure A1.7). The absolute requirement of Arn-mediated lipid A aminoarabinosylation for acquired

colistin resistance in *P. aeruginosa* was definitely demonstrated by showing that L-Ara4N defective mutants are unable to develop colistin resistance (Lo Sciuto, A. and Imperi, F., 2018).

Figure A1.7 Schematic representation of regulation of genes contributing to colistin resistance in clinical strains of *P. aeruginosa* (Jeannot, K. *et al.,* 2017).

This evidence strongly supports the notion that pharmacological inhibition of L-Ara4N biosynthetic enzymes is a proper approach to extend the anti- *P. aeruginosa* colistin activity.
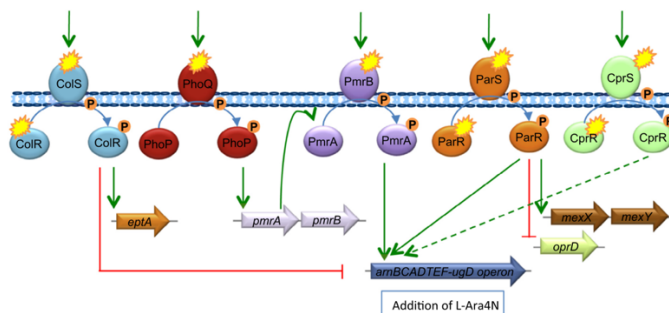
The biosynthesis of L-Ara4N starts with the conversion of UDP-glucose to UDP-glucuronic acid. The ArnA enzyme then catalyzes the oxidative decarboxylation of UDP-glucuronic acid to generate a novel UDP-4-ketopentose (Yan, A. *et al*., 2007). The resulting UDP-4-ketopentose is transaminated by ArnB to generate UDP-L-Ara4N, which is then formylated by the *N*- terminal domain of ArnA. ArnC enzyme then transfers the *N*-formylated L-Ara4N moiety to undecaprenyl phosphate. The resulting product is further rapidly deformylated by ArnD enzyme, generating undecaprenyl phosphate L-Ara4N. After transport of undecaprenyl phosphate-L-Ara4N to the outer surface of the inner membrane, ArnT transfers the L-Ara4N residue to the 4′-phosphate group of lipid A (Raetz, C.R.H. *et al*., 2007) (Figure A1.8).
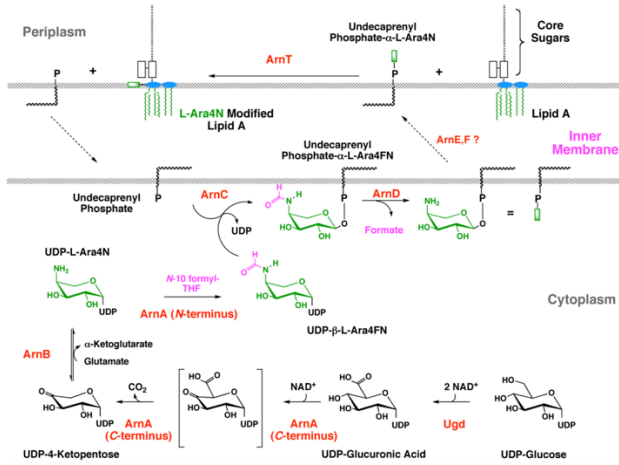
Figure A1.8 Biosynthesis of the L-Ara4N unit and its attachment to lipid A (Raetz, C.R.H. *et al*., 2007).

A1.2.3 Aminoarabinose transferase ArnT structure and catalytic mechanism

ArnT enzyme is a member of the GT-C family of glycosyltransferases (Lairson, L.L. *et al*., 2008). In 2016, the ArnT structure from *Cupriavidus metallidurans* CH34 ($ArnT_{Cm}$) was determined alone and in complex with its natural lipid carrier undecaprenyl phosphate (UndP), yielding crystals in lipid cubic phase (LCP).

The structure of $ArnT_{Cm}$ was determined to 2.8 Å resolution and appears as a monomer, consisting of (Figure A1.9):

- a transmembrane domain (TMD), which shows 13 TM helices in an intricate arrangement;

- a soluble periplasmic domain (PD) positioned above it;

- three juxtamembrane (JM) helices (JM1, JM2, JM3), which are parts of periplasmic loops (PL).
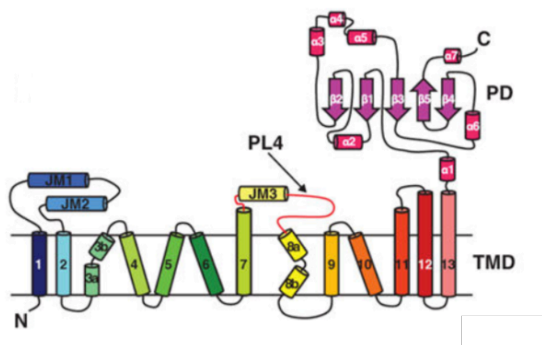
Figure A1.9 Schematic representation of the connectivity and structural elements of $ArnT_{Cm}$ (Petrou, V.I. *et al.*, 2016).

The structure of $ArnT_{Cm}$ shows, also, three cavities that differ in their electrostatic nature (Figure A1.10):

- cavity 1 is the largest one. It is amphipathic with a lower hydrophobic portion located below the level of the membrane and an upper hydrophilic one;

- cavity 2 is the smallest one. It is connected to cavity 1 through a narrow passage and it is primarily hydrophilic;

- cavity 3 is entirely hydrophobic and located close to the cytoplasmic side of the molecule;
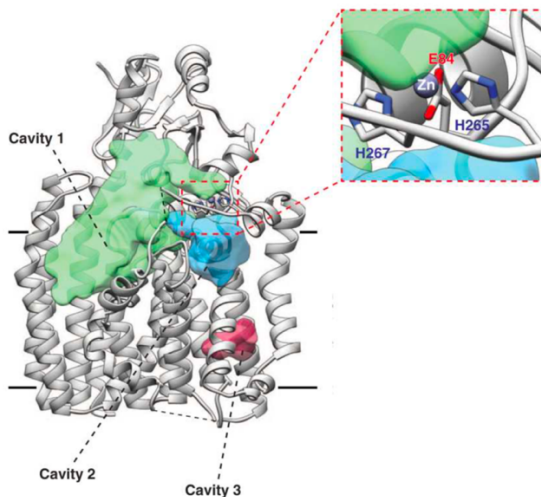
Figure A1.10 Ribbon representation of $ArnT_{Cm}$ showing the cavities in the structure and close-up of the metal coordination site in $ArnT_{Cm}$ (Petrou, V.I. *et al.*, 2016).

Cavity 1 hydrophobic portion is directly accessible from the outer leaflet of the inner membrane, and it seems to be where lipid A binds to ArnT. Whereas, both cavity 2

and cavity 3 are involved in binding of lipid carrier UndP to ArnT$_{Cm}$. This enzyme binds also between JM1 and PL4 a Zn^{2+} ion, which is coordinated by glutamic acid at position 84 (E84), histidines at positions 265 and 267 (H265 and H267, respectively), and likely by a water molecule. All the three metal-coordinating residues appear to be important for the enzymatic function (Petrou, V.I. *et al.*, 2016; Hall, B.E. *et al.*, 2002).

To investigate how ArnT interacts with its lipid substrates, ArnT$_{Cm}$ was cocrystallized with UndP (ArnT$_{Cm}$-UndP) and its structure was determined to 3.2 Å resolution (Figure A1.11).
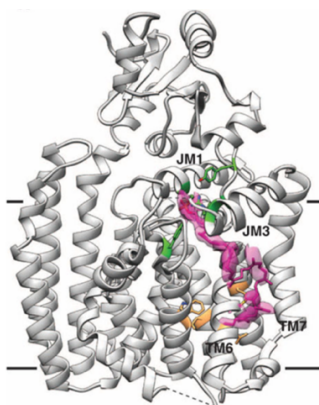
Figure A1.11 Binding of undecaprenyl phosphate (UndP) to ArnT$_{Cm}$ (Petrou, V.I. *et al.*, 2016).

Overall, the structures of ArnT$_{Cm}$ and ArnT$_{Cm}$-UndP suggest that the binding of substrates may be sequential, and the active site is completed by elements of the extended JM3 helix only with UndP bound (Figure A1.12).
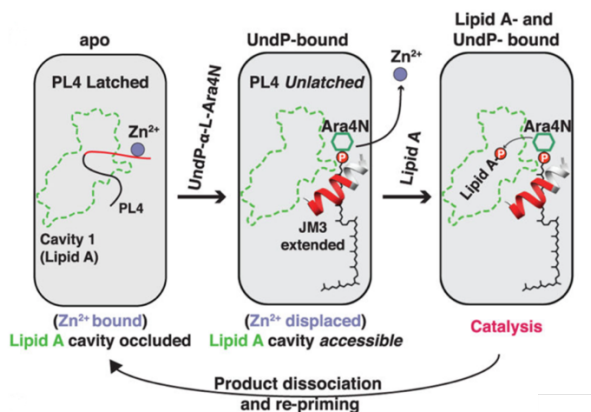
Figure A1.12 Schematic representation of substrate-binding–induced conformational changes and catalytic cycle of ArnT$_{Cm}$ (Petrou, V.I. *et al.*, 2016).

According with the structures reported above, ArnT catalytic mechanism involves the lipid A phosphate group, which is coordinated with two conserved aspartic acid residues (D55 and D158, respectively). Thus, the nucleophilic attack of the phosphate group on the anomeric carbon of L-Ara4N donor pushes off the lipid

carrier UndP and leads to the formation of lipid A-L-Ara4N bond (Figure A1.13) (Petrou, V.I. *et al.*, 2016).
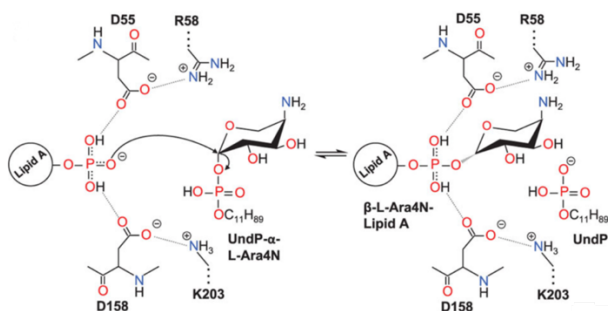
Figure A1.13 Putative catalytic mechanism of ArnT$_{Cm}$ (Petrou, V.I. *et al.*, 2016).

A1.3 Aim of the work

Colistin resistance is expected to critically impair the treatment options against MDR Gram-negative infections. Epidemiology studies and experimental evidences support the hypothesis that the prevalent molecular mechanism conferring colistin resistance in Gram-negative bacteria is the enzymatic transfer of Ara4N to lipid A, by the aminoarabinose transferase ArnT (PmrK).

If this mechanism of lipid A modification could be disabled, colistin-resistant bacteria might be returned to a susceptible state. Thus, an agent capable of this restoration could enhance colistin activity, expand its repertoire of utility and allow also the durable therapeutic utility of the newer antibiotics. Up to now, only one molecule was reported interfering with Lipid A modification. It is a 4-deoxy-L-arabinose analog and it was designed to impair the L-Ara4N unit biosynthesis, mimicking the N-formylation transition state of 4-amino function of

aminoarabinose or serving as surrogate for the formylated amine (Kline, T. et al., 2008). Accordingly, it was a goal of this PhD thesis to identify small natural molecules that could disable this lipid A modification and use as novel adjuvants to colistin activity to treat MDR Gram-negative infections.

CHAPTER A2

Identification of a natural diterpene as a novel colistin adjuvant

A2.1 Natural Products in drug discovery: a unique *in house* library of Natural Compounds

Natural products are mostly plant secondary metabolites, which are involved in physiological responses during plants interactions with their environments. They represent an important source of remedies since ancient times (Newman, D.J., 2008; Newman, D. J. and Cragg, G. M., 2007; Cragg, G.M, and Newman, D.J., 2013; Newman, D.J. and Cragg, G.M., 2016; Thomford, N.E. *et al*., 2018). Thus, the use of plants and preparations derived from them was the basis for medical treatments in Oriental civilizations and ancient Western world for many thousands of years, and even today, herbal and traditional medicines constitute primary health care for ~80% of the world population (Kingston,

D.G.I and Newman, D.J., 2012). Natural products play also a fundamental role in modern drug discovery due to their high structural variety and chemical diversity. Since the late 20th century, however, many pharmaceutical companies scaled significantly down or abandoned their natural product programs, because of the advances in both high throughput screening (HTS) and combinatorial synthesis, and the development of huge synthetic libraries of small molecules (Shen, B., 2015). Despite it, this trend is changing and a renewed interest in nature is emerging. Indeed, natural products are evolutionary refined as drug-like molecules and they possess enormous structural and chemical diversity that cannot be matched by any synthetic libraries of small molecules. Thus, natural compounds continue to remain the most abundant source of leads as valued platforms to identify and develop novel drugs

(Casciaro, B. *et al.*, 2019; Shen, B., 2015; Harvey, A.L. *et al.*, 2015; Brown, D.G, 2014).

In this scenario, a unique in *house* library of about one thousand natural compounds, mostly isolated from plants used in the traditional medicine of South America and collected in the years, is available at the Organic Chemistry Laboratory of the Department of Chemistry and Technology of Drugs (Sapienza University of Rome, Italy). This library consists of natural products from different classes, previously published and fully characterized, and it was also enlarged with natural compounds from commercially sources and synthetic and semisynthetic compounds. The library is characterized by a satisfactory chemical diversity, offering a unique chance to identify unexpected new scaffolds for the development of therapeutically relevant molecules. Accordingly, it is yet successfully screened in *silico* and in *vitro* for the

identification of hit and lead compounds in previous early-stage drug discovery projects (Mascarello, A. *et al.*, 2013; Infante, P. *et al.* 2015 and 2016; Casciaro, B. *et al.*, 2019).
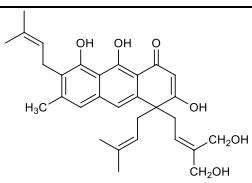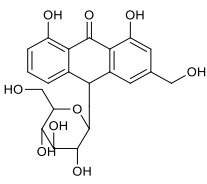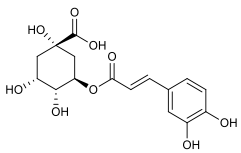
A2.2 In *silico* screening of an in house Library of Natural Products: identification of putative ArnT inhibitors

In the attempt to identify potential inhibitors of Ara4N-dependent colistin resistance, we carried out a docking-based virtual screening of our *in house* library of natural products within the catalytic site of ArnT, whose crystal structure was recently solved (Petrou, V.I. *et al.*, 2016). By virtual screening, compounds were ranked based on their predicted binding mode and theoretical affinity within the ArnT catalytic site, and further filtered by chemical diversity criteria, leading to the final selection
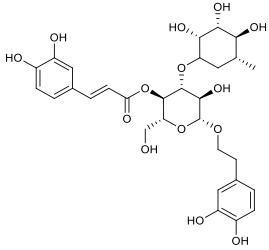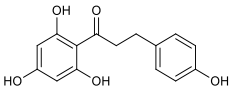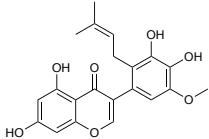
of 18 candidate hits (Table A2.1), that were submitted to biological investigations.
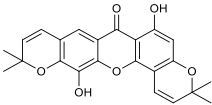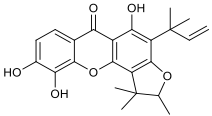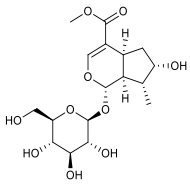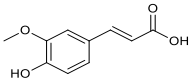
Mol	Chemical structure	MW	Molecular formula	Ref.
1		492.60	$C_{30}H_{36}O_6$	Delle Monache F. *et al.*, 1979
2		418.39	$C_{21}H_{22}O_9$	Peng C. *et al.*, 2019
3		354.31	$C_{16}H_{18}O_9$	Leitão S.G. *et al.*, 2008
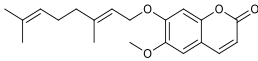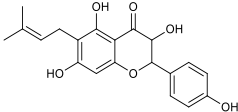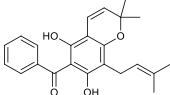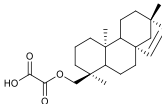
4		622.62	$C_{30}H_{38}O_{14}$	Scarpati M.L., Delle Monache, F., 1963
5		274.27	$C_{15}H_{14}O_5$	Hu, Q. *et al.*, 2017
6		384.38	$C_{21}H_{20}O_7$	Tahara S. *et al.*, 1992

7		392.41	$C_{23}H_{20}O_6$	Delle Monache F. *et al*., 1981
8		396.44	$C_{23}H_{24}O_6$	Delle Monache F. *et al*., 1981
9		390.39	$C_{17}H_{26}O_{10}$	Garaev E.E. *et al*., 2014
10		194.19	$C_{10}H_{10}O_4$	Gießel J.M. *et.al*., 2019

11		328.41	$C_{20}H_{24}O_4$	Torres R. *et al.*, 1979
12		356.37	$C_{20}H_{20}O_6$	Harbore J.B., 1993
13		364.44	$C_{23}H_{24}O_4$	Delle Monache G. *et al.*, 1980
14		360.49	$C_{22}H_{32}O_4$	Erazo S. *et al.*, 2002
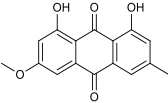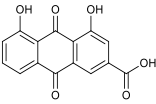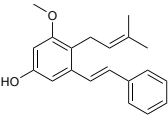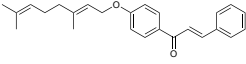
15		284.27	$C_{16}H_{12}O_5$	Camele G. *et.al*, 1982
16		284.22	$C_{15}H_8O_6$	Lee J.H. *et al.*, 2002
17		294.39	$C_{20}H_{22}O_2$	Delle Monache F. 1977
18		360.50	$C_{25}H_{28}O_2$	Gugliel mi P. *et al.*, 2019

Table A2.1 List of compounds **1-18** selected and tested.

The potential ArnT inhibitors 1-**18** identified in *silico* show a remarkable range of chemical diversity and differ also for their source, which is either natural or synthetic. They are anthranoids (namely, **1**, **2**, **15** and **16**), chalcones (namely, **5** and **18**), xanthones (namely, **7** and **8**), flavonoids (namely, **6** and **12**), cinnamic acid derivatives (namely, **3** and **10**), terpenoids (namely, **9**, **13** and **14**), a phenylpropanoid glycoside (namely, **4**), a coumarin (namely, **11**) and a stilbene (namely, **17**).

The chemical identity of compounds **1**-**18** was assessed by re-running nuclear magnetic resonance (NMR) experiments and proved to be in agreement with the literature data reported for each compound. The purity of all compounds was, also, checked by reversed- phase HPLC and it proved to be always higher than 95%.

A2.3 In *vitro* screening of compounds 1-18 as colistin adjuvants

Compounds identified by virtual screening were subjected to biological validation by using an *in vitro* evolved colistin-resistant isolate of *P. aeruginosa* PA14 (PA14 col[R] 5, colistin minimum inhibitory concentration (MIC) = 64 µg/mL), which overexpresses the *arn* operon responsible for lipid A aminoarabinosylation resistance (Lo Sciuto, A. and Imperi, F., 2018). First, in order to verify whether the *in silico* selected compounds were able to reduce or abrogate the growth of the reference strain PA14 col[R] 5, they were tested at a fixed concentration (50 µM) in the presence of a sub-inhibitory concentration of colistin (8 µg/mL).

Three compounds (namely, **8**, **14** and **17**) showed significant inhibition (>60%) of PA14 col[R] 5 growth in the

presence of colistin, without notable effects on growth in the absence of the antibiotic (Figure A2.1 **A**). None of the other compounds showed relevant inhibitory activity on either colistin treated or untreated cells. For the three hit compounds, we further determined the dose-dependent effect on PA14 col^R 5 growth in the presence of 8 µg/mL colistin.
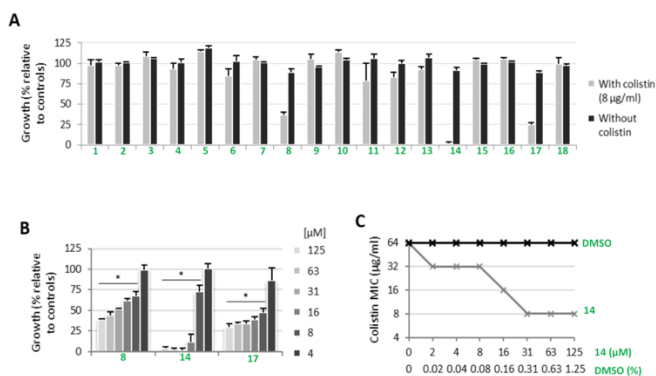
Figure A2.1 In *vitro* screening of compounds **1-18**.

Compounds **14** and **17** caused a significant growth reduction at concentrations ≥ 8 µM, although they did not completely inhibit bacterial growth at any concentrations tested. In contrast, compound **14** significantly inhibited PA14 col^R 5 growth at 8-16 µM and completely abrogated it at ≥ 31 µM (Figure A2.1 **B**). In agreement with the screening results, we confirmed that **14** has no inhibitory activity *per se*, as demonstrated by its marginal effect on PA14 col^R 5 cultured in the absence of colistin, even at the highest concentration tested (125 µM). The potentiating effect of **14** on colistin activity was also corroborated by checkerboard assays, that showed a dose-dependent reduction of colistin MIC for PA14 col^R 5 in the presence of increasing concentrations of **14** (Figure A2.1 **C**). Colistin MIC decreased to the lowest level (8 µg/mL, corresponding to an 8-fold reduction) with 31 µM of **14**,

and remained stable at higher concentrations of **14** (up to 125 μM).

Overall, these results demonstrated that one of the compounds identified by *in silico* docking of ArnT, namely **14**, actually potentiates colistin activity against a colistin-resistant *P. aeruginosa* strain.

A2.4 A diterpene from Fabiana densa var. *ramulosa* endowed with promising biological activity

Compound **14** is the diterpene "*ent*-beyer-15-en-18-O-oxalate" (Figure A2.2).
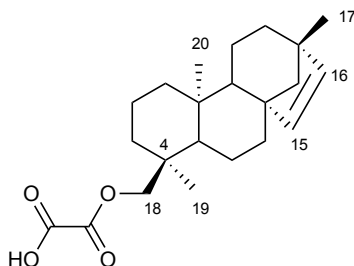
14

Figure A2.2 Structure of *ent*-beyer-15-en-18-O-oxalate (**14**).

It was isolated from the leaves of Fabiana densa var. *ramulosa* (*Solanaceae*) (Figure A2.3), which is a native shrub of Chile that grows from the Altiplano region

to the Puna (Erazo, S. *et al*., 2002). This plant was botanically classified by the French botanist Esprit Alexandre Remy in 1847 and it is commonly called "checal" "tolilla" or "tola-checal". In 2002 the chemical composition of resinous exudate from the leaves of Fabiana densa var. *ramulosa* and its biological properties were carried out by Erazo, S. *et al*. at Faculty of Chemical and Pharmaceutical Sciences at University of Chile.

Figure A2.3 Fabiana densa var. *ramulosa (Solanaceae)*.

In particular, a "novel" diterpenoid, the *ent*-beyer-15-en-18-O-oxalate (**14**), and the know *ent*-beyer-15-en-18-ol (**19**) (Figure A2.4) (San Martìn, A. *et al*. in 19839), were isolated and characterized. Currently, these diterpenoids occur in our library of natural compounds.

19
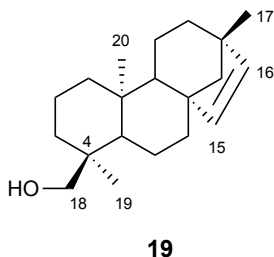
Figure A2.4 Structure of *ent*-beyer-15-en-18-ol (**19**).

They demonstrated, also, an interesting antimicrobial activity of the resinous exudate and its components against *S. aureus*, which could explain its use in traditional medicine to immobilize fractured limbs and

as an infusion for the cough and illness of the lungs (Erazo, S. *et. al*., 2002).

The chemical structure of **14** was assessed by ^{1}H NMR, ^{13}C NMR and high-resolution mass spectrometry (HRMS) experiments. The ^{1}H NMR (CDCl$_3$) spectrum of compound **14** shows the peculiar signals of the *ent*-beyerene scaffold. In particular, it reveals a pair of doublets at 5.45 ppm and 5.69 ppm for the two olefinic protons (H-15 and H-16), and three intense singlets for the three methyl groups at 0.99 ppm (CH$_3$-17), 0.91 ppm (CH$_3$-19) and 0.99 ppm (CH$_3$-17). The presence of oxalate group at C-18 was confirmed by comparing ^{1}H NMR and ^{13}C NMR spectra of *ent*-beyer-15-en-18-O-oxalate (**14**) with those of *ent*-beyer-15-en-18-ol (**19**). Accordingly, the ^{1}H NMR spectral data are almost coincident with those of the *ent*-beyerene scaffold of **19**, except for the signals (a pair of doublets) of H-18a and H-18b which were

downfield at 3.90 ppm and 4.10 ppm (Figure A2.5 **A**). Comparison of the ^{13}C NMR spectral data of **14**, with those of alcohol diterpene **19**, evidence two signals at 158.65 ppm and 157.77 ppm, which were assigned to the carbonyl groups at C-21 and C-22 of oxalate function of **14**, respectively **(**Figure A2.5 **B**).

Furthermore, the purity of **14** was assessed by reversed- phase HPLC (Wellsow, J. *et al*., 2006; Wölwer-Rieck, U., 2012) and it proved to be higher than 95%
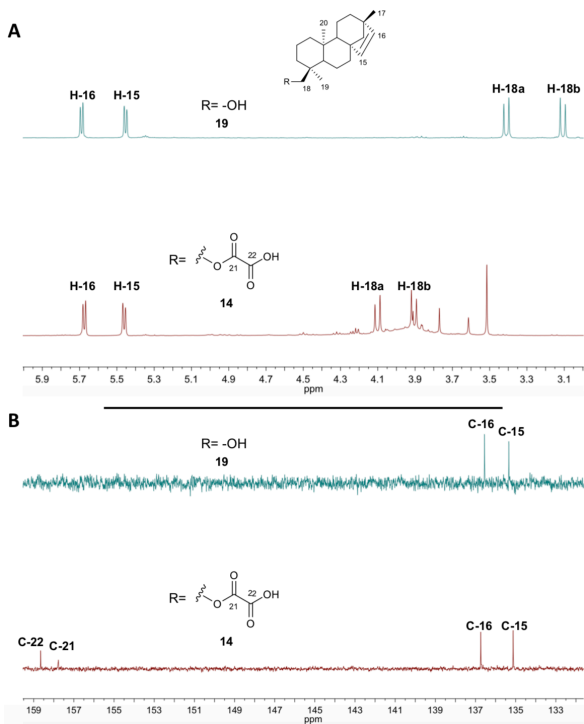
Figure A2.5 Comparison of the NMR spectral data of *ent*-beyer-15-en-18-O-oxalate (**14**) and *ent*-beyer-15-en-18-ol (**19**). (**A**) ^{1}H NMR (CDCl$_3$, 400MHz) spectra of **14** and **19**; (**B**) ^{13}C NMR (CDCl$_3$, 100MHz) spectra of **14** and **19**.

A2.5 Range of activity, specificity and cytotoxicity of compound 14

To verify the specificity of **14** towards colistin resistance, MIC of colistin for the colistin-sensitive parental strain PA14 was determined in the presence and absence of a concentration of **14** active against PA14 col^R 5 (30 µM) (Table A2.2).

Species	Strain	MIC (µg/mL)	
		14	**DMSO**
P. aeruginosa	PA14 col^R 5	8	64
	PA14	1	0.5
	KK1 col^R 1	8	128
	KK1	1	0.5
	KK27 col^R 6	4	64
	KK27	1	0.5
	TR1 col^R 6	4	16
	TR1	1	0.5
	ND76	4	32
	MG75	8	32

K. pneumoniae	KP-Mo-3	16	128
	KP-Mo-5	8	128
	KP-Mo-6	4	32
	KP-Mo-11	8	64
	KP-Mo-16	8	64

Table A2.2 Colistin MIC for *P. aeruginosa* and *K. pneumoniae* strains in the presence of 30 µM of **14** or 0.3% DMSO as the control.

Notably, compound **14** did not decrease colistin MIC for PA14, suggesting that the compound may exert adjuvant activity only on colistin-resistant isolates. This hypothesis was confirmed by testing three other *in vitro* evolved colistin resistant mutants of *P. aeruginosa* together with their parental cystic fibrosis (CF) isolates (Lo Sciuto, A. and Imperi, F., 2018). While **14** efficiently reduced the MIC of colistin for all resistant strains, it did not enhance colistin activity against their colistin-sensitive parental isolates. Indeed, for all colistin-sensitive isolates (PA14

and the three CF isolates) we observed a slight (2-fold) increase in colistin MIC in the presence of **14**, which however remained below the breakpoint for colistin-resistant *P. aeruginosa* (4 µg/mL, Clinical and Laboratory Standards Institute, 2016).

Finally, the potentiating effect of **14** on colistin activity was also observed in two colistin-resistant clinical isolates, namely ND76 and MG75, directly isolated from the sputum of chronically infected CF patients, indicating that **14** is also effective against colistin resistance strains evolved *in vivo* during the infection. These strains were kindly provided by Dr. P. Morelli from Istituto Giannina Gaslini, Genoa, Italy.

To rule out that the adjuvant activity of **14** could be due to a general destabilizing effect on the *P. aeruginosa* cell envelope, we assessed whether this compound also affects the MIC of other antibiotics with

different mechanisms of action and intracellular targets, *i.e.* ofloxacin, gentamicin and meropenem. As result, **14** did not cause any relevant variation in the susceptibility levels to these antibiotics. either in the parental strain PA14 or in its derivative PA14 col^R 5.

In order to verify whether the putative ArnT inhibitor **14** can also potentiate colistin activity against other Gram-negative pathogens, we assessed its ability to counteract colistin resistance in a panel of colistin-resistant *K. pneumoniae* clinical strains. As shown in Table A2.2, **14** at 30 μM strongly reduced colistin MIC for all the colistin-resistant *K. pneumoniae* strains, implying that the inhibitory activity of this compound on colistin resistance is not restricted to *P. aeruginosa.* To evaluate cytocompatibility of **14**, in particular for the antibiotic therapy of the lung, cytotoxicity was tested against the bronchial epithelial cells 16HBE. Cells were treated with

14 at concentrations ranging from 4 to 125 µM, for 3 or 18 hours, and viability was assessed by the MTT assay. As shown in figure A2.6, **14** did not affect cell viability at any concentration after 3 hours of incubation while, after 18 hours, a slight decrease in cell viability (about 25%) was observed for the two highest concentration tested (125 and 63 µM).
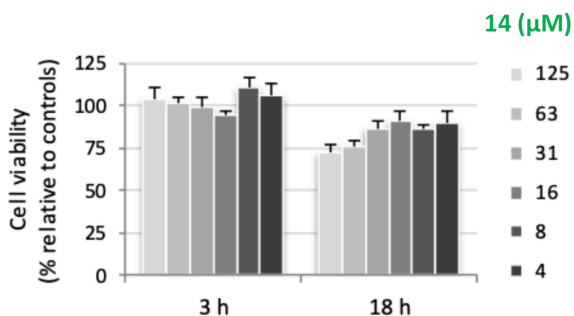
Figure A2.6 Viability of 16HBE epithelial cells exposed to **14** at the indicated concentrations for 3 or 18 hours.

A2.6 Predicted binding mode of 14 to ArnT

The binding mode of **14** within the catalytic site of ArnT was further investigated by molecular docking simulations carried out by the Fred docking program (OpenEye).

Two main binding poses were identified, one extending towards the putative binding site of Lipid A (Petrou, V.I. *et al.*, 2016), and the other occupying the undecaprenyl phosphate binding site with a very good overlapping with the crystallographic ligand.
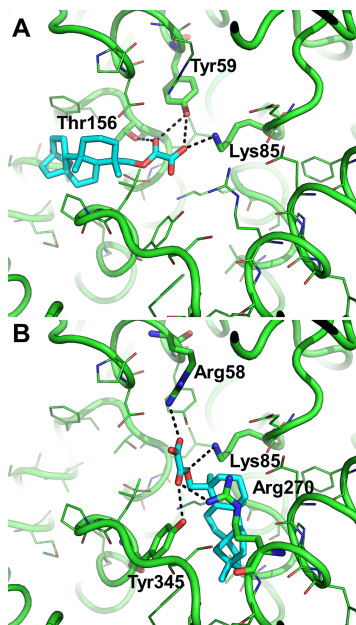
Figure A2.7 Predicted binding mode of **14** to ArnT crystallographic structure. Two different docking poses are shown in **A** and **B**.

Notably, these poses might account for the inhibitory effect observed *in vitro*, and are endowed with a comparable docking score calculated by the Chemgauss4 function, i.e. -4.98 and -5.05 respectively. In both poses, the oxalyl group nicely overlaps with the crystallographic phosphate moiety.

In the case compound **14** extends towards the Lipid A binding site (Figure A2.7 **A**), H-bond interactions are established with Tyr59, Lys85, and Thr156 while the lipophilic part of the molecule is well inserted in the hydrophobic cavity that projects towards the transmembrane region of the receptor. In the alternative pose, the oxalyl group establishes H-bond interactions with Arg58, Lys85, Arg270, and Tyr345, while the lipophilic part fulfill the undecaprenyl phosphate binding site (Figure A2.7 **B**).

CHAPTER A3

Design, synthesis and biological activity evaluation of *ent*-beyer-15-en-18-o-oxalate diterpene analogs

A3.1 Structural relationship between *ent*-beyerene and *ent*-kaurene diterpenes

Diterpenes are a wide family of natural products with different biological activities and very unique chemical structures (Murillo, J.A. *et al.*, 2019). They represent the major constituents of numerous plant resins and some of these ones are of commercial importance (as antibiotics, phytohormones, cattle poisons and perfumery constituents).

Compound **14** belongs to the family of tetracyclic *ent*-beyerene diterpenes. Polycyclic diterpenes (Hanson, J.R., 1968; Hanson, J.R, 1971) form a class of more than ten thousand natural products, which can be further classified on the basis of hydrocarbon ring biosynthesis. However, they mostly derive from four units of isopentenyl pyrophosphate namely geranylgeranyl

diphosphate (GGPP), through a number of cyclization and enzyme catalyzed skeleton rearrangement (Peters, R.J., 2010). Interestingly, some of these rearrangements are triggered by pyrophosphate removal forming various diterpenes such as *ent*-beyerene, *ent*-kaurene, *ent*-trachylobane and *ent*-atiserene, which are widespread in plants (Hong, Y.J. *et al*., 2010).

Regarding *ent*-kaurene (**20**) and *ent*-beyerene (**21**) diterpenoids, they are closely related compounds. Indeed, they have a common skeleton that presents the "*ent*" configuration, in which the absolute stereochemistry of the A/B ring junction (C-5βH, C-10αMe) is opposite to that of the steroids. Both scaffolds are featured by the presence of the bicyclo[3.2.1]octane moiety, a bridged ring system (for rings C and D) attached to C-8 creating a spiro centre at this position, and a 1:3-diaxial interaction between the C-10 methyl group and a bridge carbon at C-8. While they

differ for the double bond between C15 and C16, which is exocyclic in *ent*-kaurene structures (Figure A3.1) (Hanson, J.R., 2018).
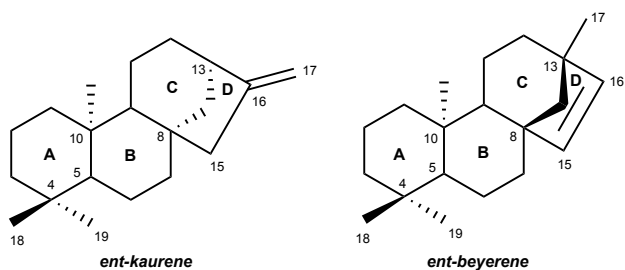
Figure A3.1 Structures of *ent*-kaurene (**20**) and *ent*-beyerene (**21**).

The structural relationship between **20** and **21** arises from their common biosynthetic pathway. Indeed, the tetracyclization of tricyclic carbocation *ent*-pimara-15-en-8-yl intermediate (**A**), arising from *re*-face

tricyclization of *ent*-copalyl diphosphate precursor (***ent-CPP***), forms the secondary carbocation *ent*-beyer-15-yl intermediate (**B**). This intermediate can be directly deprotonated on the neighboring *endo*-methylene to form *ent*-beyer-15-ene. Alternatively, the secondary carbocation *ent*-beyer-15-yl intermediate can undergo ring rearrangement to form the tertiary carbocation *ent*-kaur-16-yl intermediate (**C**). Deprotonation of this carbocation on the neighboring methyl group gives rise to the *ent*-kaur-16-ene (Figure A3.2), which is a well-established intermediate in the biosynthesis of the sweet-tasting diterpenoid glycoside stevioside naturally occurring in *Stevia Rebaudiana* (Bertoni) (Roy, A. *et al*., 2007; Peters, R.J., 2010; Hong, Y.J. *et al*., 2010).
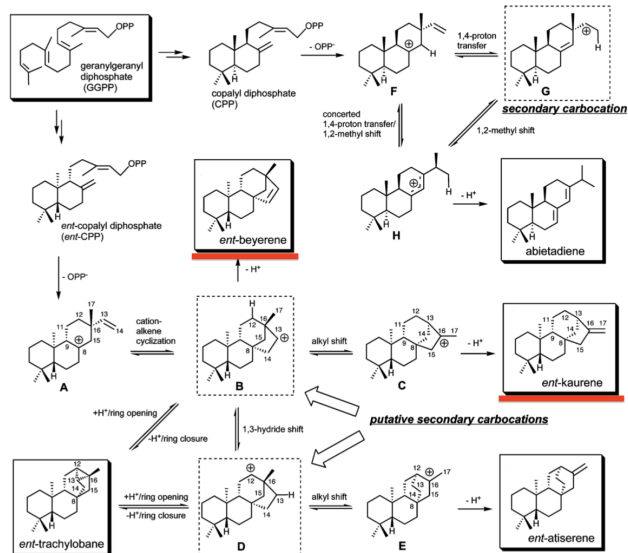
Figure A3.2. Biosynthetic pathway of *ent*-beyerene, *ent*-kaurene and other polycyclic diterpenes (Hong, Y.J. *et al*., 2010).

A3.2 Steviol glycosides from Stevia rebaudiana Bertoni

Stevia rebaudiana Bertoni (Kinghorn, A.D., *et al*., 1984; Kinghorn, A.D., 2002) (Figure A3.3) is a branched shrub, native to the Amambay region in the north east of Paraguay.

Figure A3.3 *Stevia rebaudiana* Bertoni.

Its cultivation occurs in Brazil and Argentina and is spreading also to other regions of the world, including Canada and some parts of Asia and Europe. This plant was botanically classified in 1899 by Moisés Santiago Bertoni. Initially called Eupatorium rebaudianum, its name changed to S. *rebaudiana* (Bertoni) Bertoni in 1905. For centuries, the Guarani tribes of Paraguay and Brazil used *Stevia* species, primarily S. *rebaudiana*, which they called ka'a he'ê (''sweet herb''), as a sweetener in yerba mate and medicinal teas for treating heartburn and other ailments. Nowadays, it mainly attracts economic and scientific interests due to the use of its leaves extract as a sweet-tasting calorie- free sugar substitute or as an alternative to artificial sweeteners (Lemus-Mondaca, R. *et al.*, 2012). Indeed, natural high sweeteners, named steviol glycosides, are found tipically in large amounts within the

leaves of S. *rebaudiana* Bertoni (Wölwer-Rieck, U., 2012).

Glycosides are compounds containing a sugar molecule (from which they get their name) bound to a non-carbohydrate moiety (aglycone). These compounds are mainly found in plants, and they can be converted, by hydrolytic cleavage, into a sugar and a non-sugar component. The steviol glycosides are diterpenes, isolated and identified as stevioside, steviolbioside, rebaudioside A, B, C, D, E, F and dulcoside A (Ceunen, S. and Geuns, J.M.C., 2013; Lemus-Mondaca, R. *et al.*, 2012; Napolitano, J.G. *et al.*, 2015). All of these compounds present the same aglycone **22** (steviol backbone) and differ in the content of carbohydrate residues (mono-, di-, and tri-saccharides), containing glucose and/or rhamnose at positions C19 and C13 (R1 and R2, respectively) (Figure A3.4).

22
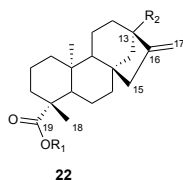
Compound	R1	R2
Steviol	H	H
Steviolbioside	H	β-Glc-β-Glc(2→1)
Stevioside	β-Glc	β-Glc-β-Glc(2→1)
Rebaudioside A	β-Glc	β-Glc-β-Glc(2→1) | β-Glc(3→1)
Rebaudioside B	H	β-Glc-β-Glc(2→1) | β-Glc(3→1)
Rebaudioside C (Dulcoside B)	β-Glc	β-Glc-α- Rha(2→1) | β-Glc(3→1)
Rebaudioside D	β-Glc-β-Glc(2→1)	β-Glc-β-Glc(2→1) | β-Glc(3→1)
Rebaudioside E	β-Glc-β-Glc(2→1)	β-Glc-β-Glc(2→1)
Rebaudioside F	β-Glc	β-Glc-β-Xyl(2→1) | β-Glc(3→1)
Dulcoside A	β-Glc	β-Glc-α- Rha(2→1)

Figure A3.4 Structures of the major glycosides of Stevia *rebaudiana* Bertoni leaves. Glc, Xyl, and Rha represent glucose, xylose, and rhamnose sugar moieties, respectively (Geuns, J.M.C., 2003).

In particular, stevioside was reported to be the most abundant steviol glycoside found in the plant leaves and its chemical structure was elucidated in 1960s (Geuns, J.M.C., 2003; Ogawa, T. *et al.*, 1980; Wood, H.B.jr *et al.*, 1955; Mosettig, E. *et al.*, 1955).

A3.3 Design and synthesis of *ent*-beyer-15-en-18-O-oxalate (14) analogs

The microbiological data (Chapter A2) suggested the promising synergic activity of *ent*-beyerene diterpenoid **14** with colistin in the treatment of colistin-resistant bacterial infections. Since **14** emerged as the hit compound in the first screening, a series of semi-synthetic analogs were designed and synthesized aiming at outlining the structure-activity relationship (SARs) and improving their activity.

Since the low concentration of **14** in the Chilean plant Fabiana densa var. *ramulosa* and its difficult isolation, a different source for the starting material was found. Based on the structural similarities of *ent*-kaurene (**20**) and *ent*-beyerene (**21**) scaffolds, a first generation of nine analogs of compound **14** (**24-32**) (Figure A3.5) were designed and synthesized from the commercially available stevioside (**23**), featuring a steviol aglycone (**22**) linked to three β-glucopyranosyl moieties at C19 and C13.
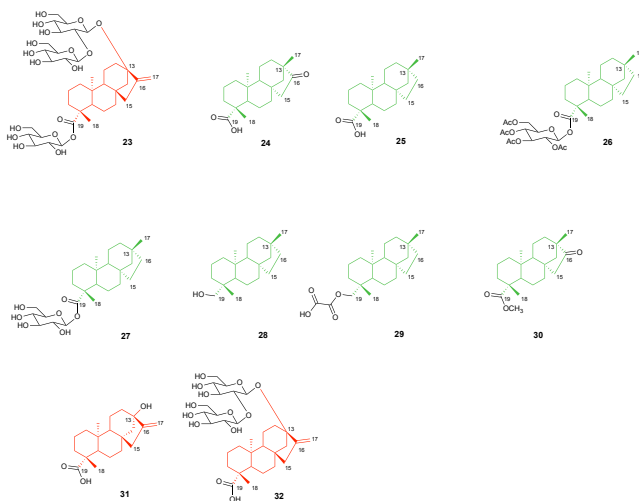
Figure A3.5 Structures of compounds **23-32**.

The semi-synthetic analogs are featured by the *ent-*kaurene skeleton (**31-32**) and an opposite configuration at C4 with respect to compound **14**, and the *ent*-beyerane skeleton (**24-30**) that can be obtained by acid hydrolysis of **23**. Compounds **24-30** differ from the parental *ent-*beyerene scaffold of diterpenoids from Fabiana densa var.

ramulosa for the lack of the unsaturation between C15 and C16 and a different absolute configuration at C4 (R rather than S) (Mosettig, E. *et al*., 1963).

More in detail, the first analog, namely **24 (***ent*-16-ketobeyeran-19-oic acid or isosteviol), was obtained *via* hydrolysis of **23** with a strong mineral acid like hydrobromic acid (yield 89%). This reaction consists of sugar groups removal, followed by acid-catalyzed steviol aglycone rearrangement and inversion of ring D (Avent, A.G. *et al*.,1990; Kinghorn, A.D., *et al*., 1984). Thus, the presence of the bicyclo[3.2.1]octane moiety that forms rings C and D of these diterpenoids makes them particularly prone to skeletal rearrangements (Hanson, J.R. and De Oliveira, B.H., 1993; Hanson, J.R, 2018) (Figure A3.6).
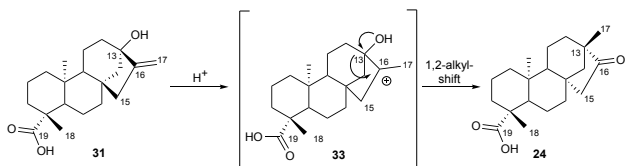
Figure A3.6 Wagner-Meerwein rearrangement of steviol (**31**) to isosteviol (**24**).

In particular, the steviol aglycone (**31**): isosteviol (**24**) conversion is an example of a Wagner-Meerwein rearrangement, a class of 1,2-rearrangement of carbocation intermediates (Wang, Z., 2010), which is promoted by the presence of a hydroxyl group adjacent to the 16-alkene.

Compound **24** is a unique building block in organic synthesis due to its quite rare structural features (Lohoelter, C. *et al*., 2013; Lohoelter, C. *et al*., 2012; Moons, N. *et al*.,2011). Thus, it was used as starting material to synthesize compounds **25-30** by making

chemical transformations at positions C16 and C19, respectively (Scheme A3.1).
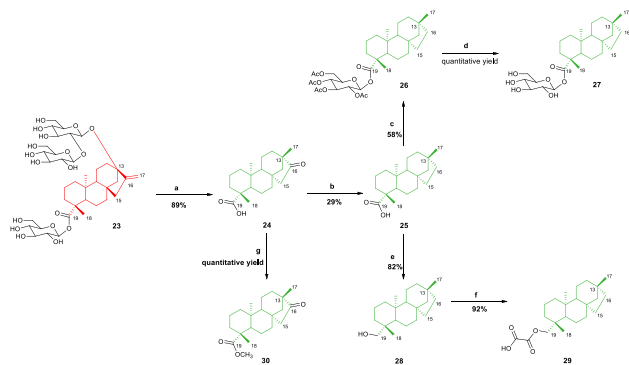
Scheme A3.1 Synthetic pathway of compounds **25-30** synthesis; Reagents and conditions: a) HBr, r.t., 12 h; b) 95% $H_2NNH_2xH_2O$/KOH, TEG, 150-200 °C, 24h; c) Acetobromo-α-D-glucose, K_2CO_3/TBAB/CH_2Cl_2/H_2O, reflux, 24h; d) Et_3N/MeOH/H_2O/hexane, 48 h; e) $LiAlH_4$ in THF 2M, THF dry, r.t. 3h; f) Et_2O, oxalyl chloride 0°C, r.t. 20 min; g) 1. $SOCl_2$, DMF dry, r.t. 2h; 2. MeOH dry, Et_3N, r.t. 2h.

First of all, **24** was subjected to the Huang-Minlon modification of Wolff-Kishner reaction: the carbonyl group at C16 was reduced to hydrocarbon by strongly heating it in presence of an alkaline solution and hydrazine hydrate, in refluxing triethylene glycol (Mosettig, E. and Nes, W.R., 1955; Huang-Minlon, 1946). This reaction led to **25** (yield 29%), namely *ent*-beyeran-19-oic acid or isostevic acid, which was then used to synthesize the other derivatives by chemical modifications of carboxylic group at C19. In particular, **26** was obtained *via* glycosylation reaction with 2,3,4,6-tetra-*O*-acetyl-α-D-glucopyranosyl bromide (acetobromo-α-D-glucose) with a yield of 58%, using as catalyst the phase transfer catalyst tetrabutylammonium bromide (TBAB). Further, the deacetylation of hydroxyl groups of sugar moiety of **26** with triethylamine, followed by alkaline hydrolysis, furnished **27** (quantitative yield) (Chaturvedula, V.S.P. *et*

al., 2011; Das, R. and Mukhopadhyay, B., 2016), which was designed to mimic L-Ara4N unit. Compound **28** was synthesized reducing **25** with lithium aluminium hydride to the corresponding alcohol with a yield of 82 % (Batista, R. *et al*., 2007; Murillo, J.A. *et al*., 2019). Then, the esterification of hydroxyl group with oxalyl chloride led to **29** (yield 92%) (Zhang, X. and MacMillan, D.W. C., 2016), which differs from **14** only for the absence of the double bond between C15 and C16 and the opposite configuration of C4. Finally, compound **30** (methyl (methyl *ent*-16-ketobeyeran-19-oate or isosteviol methyl ester) was quantitatively obtained by activating **24** in the corresponding acid chloride, followed by the esterification with methanol (Wang, T.T. *et al*., 2014).

Compounds **31** (*ent*-13-hydroxykaur-16-en-19-oic acid or steviol) and **32** (steviolbioside) were synthesized

from **23** (Wood, H.B.jr *et al*.1955; Ogawa, T. *et al*., 1980) (Scheme A3.2).
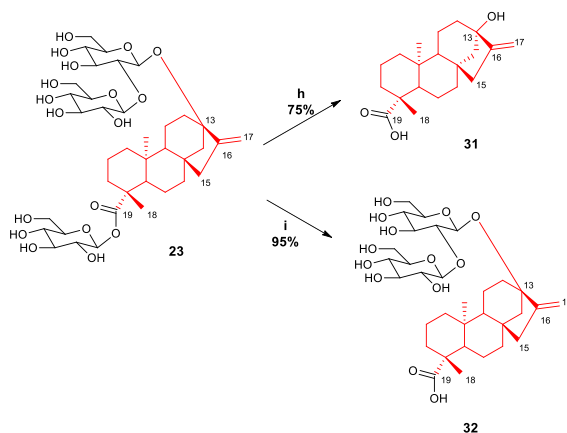
Scheme A3.2 Synthetic pathway of compounds **31-32**; Reagents and conditions: h) 1. NaIO$_4$ in H$_2$O, r.t., 16 h, 2. KOH, reflux, 1h; i) KOH 10%, 100°C, 1h.

Accordingly, **23** was at first oxidized by using sodium periodate to the corresponding hexaaldehyde, which was further hydrolysed in a strong alkali

Chapter A3

environment to yield **31** (75%). These experimental conditions thus avoided the acid-catalyzed Wagner-Meerwein rearrangement. Compound **32** was obtained by alkaline hydrolysis of **23** with a yield of 95%.

Further, in order to investigate the role of C15-C16 unsaturation of *ent*-beyerene diterpenoid **14** in the biological activity, the unsaturated derivative **35** was synthesized from compound **19** available in our *in house* library. In particular, it was prepared *via* hydrogenation of **19** using palladium on carbon (Pd/C) as catalyst in dry ethanol (Murillo, J.A. *et al*., 2019), followed by the esterification to oxalate ester starting from the alcohol **34** (*ent*-beyer-18-ol) (Zhang, X. and MacMillan, D.W. C., 2016) (Figure A3.7).
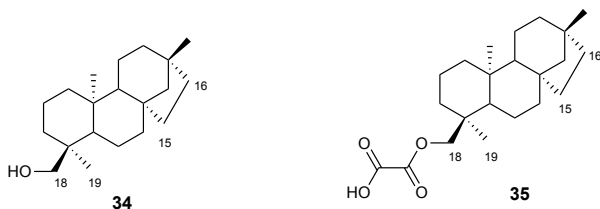
Figure A3.7 Structures of compounds **34** and **35**.

Finally, chemical identity of all of these compounds was confirmed by NMR and HRMS experiments. To date compound **14** and its analogs are covered by Italian patent.

A3.4 In *vitro* screening of compounds 23-35

To verify the colistin synergistic activity of the newly synthesized compounds, the screening assay that allowed the identification of compound **14** as a colistin adjuvant (chapter A2) was repeated. Briefly, growth of the

colistin-resistant tester strain *P. aeruginosa* PA14 col^R 5 was monitored in the presence of sub-MIC colistin (8 μg/mL) and each compound of interest at different concentrations (4-125 μM). As control, the effect of each compound on PA14 col^R 5 growth in the absence of colistin was also assessed.

Compounds **23**, **24**, **26**, **28**, **30**, **31** and **32** had no relevant effect on bacterial growth (Figure A3.8 **A** and data not shown) and were therefore not further investigated in this thesis. In contrast, compounds **25**, **27**, **29** and **32** showed some inhibitory activity on PA14 col^R 5 cultured in the presence of colistin (Figure A3.8 **A**), without affecting bacterial growth in the absence of the antibiotic (data not shown). This implies that, as for the compound **14**, these compounds likely synergize with colistin. Notably, while compound **27** caused only a partial inhibition (about 70-75%) of PA14 col^R 5 growth in the

presence of 8 μg/mL colistin, compounds **29** and **35** were able to completely inhibit growth at an intermediate concentration (31-32 μM) although, surprisingly, they lost activity at higher concentrations ($\geq$ 62 μM) (Figure A3.8 **A**). Whether this effect could be due to poor solubility and/or aggregation of these compounds at high concentrations remains to be determined.

The potentiating effect of compounds **27**, **29** and **35** on colistin activity was also corroborated by checkerboard assays, and directly compared to that of compound **14**. As shown in figure A3.8 **B**, all compounds caused some dose-dependent reduction of colistin MIC for PA14 col^R 5, thus confirming that these compounds can synergize with colistin. However, compounds **27** and **29** appeared to be less effective than compound **14** in potentiating colistin activity (Figure A3.8 **B**). Conversely, compound **35** was found to be more active than compound

14 at lower concentrations (4-8 μM), although, in line with the results described above (Figure A3.8 **B**), the colistin potentiating effect was partially lost at higher concentrations (Figure A3.8 **B**).
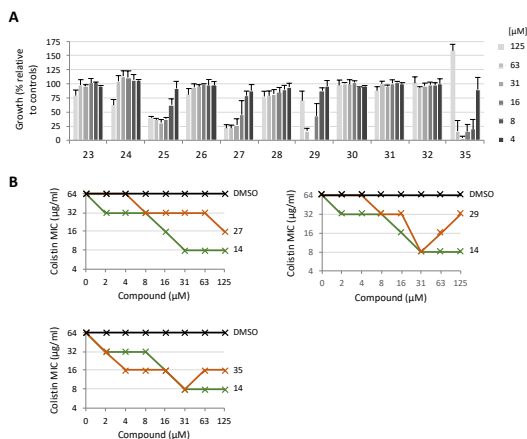
Figure A3.8. (A) Dose-dependent effect of compounds **23-32** and compound **35** on PA14 col^R 5 growth after 24 hours at 37°C in MH supplemented with 8 μg/mL colistin. Growth values are expressed as percentage relative to the cultures treated with equivalent concentrations of DMSO, and represent the mean (±SD) of at least

three independent experiments. **(B)** Effect of different concentrations of compounds **27**, **29** or **35** on the MIC of colistin for PA14 col^R 5 (orange lines) as determined by checkerboard assays. As control, DMSO was used at equivalent concentrations (0.02-1.25%; black lines). The results previously obtained with compound **14** (chapter A2) are reported in each graph for comparison (green lines). The graphs are representative of at least three independent experiments.

The most active compounds **27**, **29** and **35** were also tested at different concentrations in combination with colistin against the two clinical isolates *P. aeruginosa* MG75 and ND76. The results were compared with those obtained with compound **14**. Interestingly, as reported for MG75 (Figure A3.9 **A**), compounds **27** and **35** showed a potent activity in restoring the antimicrobial effect of colistin causing a reduction of its MIC up to 16-fold when used at a concentration of 32   M. A potent coadjuvant activity was also demonstrated for **27** against *P.*

aeruginosa ND76 (Figure A3.9 **B**), while **14** and **35** showed almost the same profile.
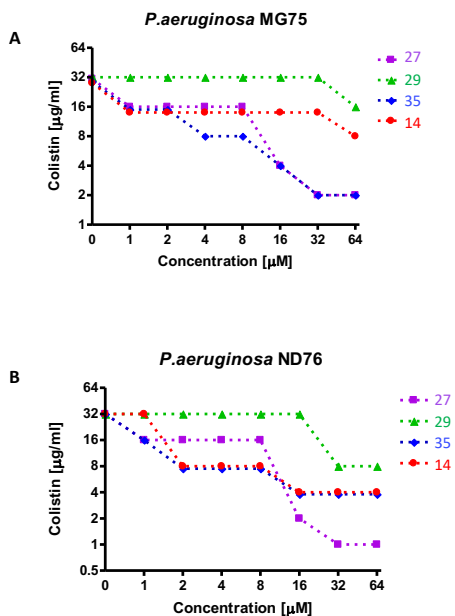
Figure A3.9 Effect of different concentrations of compounds **27**, **29** and **35** on the MIC of colistin for clinical isolates *P. aeruginosa* MG75 and ND76.

A3.5 Structure-activity relationships (SARs) analysis of compound 14 and its analogs

Taking into account the microbiological data reported in chapter A2, the diterpenoid **14**, featuring an *ent*-beyerene scaffold, at a concentration of 32 µM showed a high activity in restoring the colistin effect, with an 8 folds reduction of colistin MIC for the PA14 col^R 5 and ND76 clinical isolates of *P. aeruginosa*. Thus, emerging as a promising adjuvant to this antibiotic in the treatment of MDR Gram-negative bacteria infections, several analogs of **14** were synthetized and tested *in vitro*.

Accordingly, SARs were investigated for **14** and its analogs. Among them, compounds **27, 29** and **35** showed the most interesting activity. Compound **35** featuring the same stereochemistry and structure of **14**

except for the double bond between C15 and C16, proved to be more active in potentiating colistin activity with a MIC reduction up to 8 and 16-fold (32 µM of **14**) in the PA14 col^R 5 and MG75 clinical isolate of *P. aeruginosa*, respectively. The results obtained with the saturated derivative **35** suggested that the restricted flexibility of ring B is not required for the activity. Compound **29**, which is the almost stackable *ent*-beyerane analog of **14** bearing the opposite stereochemistry at C4 showed slightly less colistin adjuvant activity reducing MIC up to 2 and 4 fold (32 µM of **29**) in PA14 col^R 5 and ND76 clinical isolate of *P. aeruginosa*. In addition, analog **27**, which shares the same structural features of **29** except for the sugar moiety at C19 position, showed a good inhibitory profile with 2 and 16-fold reduction of MIC (32 µM of **27**) in the same colistin resistant *P. aeruginosa* strains, although it was active at high concentrations against PA14

col^R 5. According to the in *silico* studies of **14** within the catalytic site of ArnT (chapter A2), these data confirmed that a functional group at C18 (C19 for analogs obtained from *ent*-kaurane scaffold) able to establish H-bond interactions within the binding site is essential, and suggested that the C4 stereochemistry probably plays a determinant role in the correct orientation of the same group in the binding pocket. Taking into account all the other diterpene analogs, the microbiological data showed no effect as colistin adjuvants. In particular, in the case of *ent*-kaurane analogs SAR indicated that: a carboxyl acid or the ß-D-glucose ester at C19 and a hydroxyl group or a -2-*O*-β-D-glucose-β-D-glucose moiety at C13 completely abrogate biological effects. The analysis of the biological activity related to *ent*-beyerene scaffold (Figure A3.10) indicated that: 1) the *ent*-beyerane scaffold shows a higher activity than the *ent*-beyerene one, highlighting that the

unsaturation between C15- C16 is not essential for the activity; 2) an oxalate like groups at C18 or at C19 are essential for the activity; 3) the presence of a sugar moiety at C19 retains the activity, likely mimicking L-Ara4N; 4) a carboxylic group, an alcohol or a methyl ester at C19 and a carbonyl group at C16 completely abrogate biological effects. In addition, the importance of stereochemistry at C4 (S configuration for *ent*-beyerene diterpenoids from Fabiana densa var. *ramulosa*) is going to be investigated synthesizing a derivative of **29** containing a double bond between C15-C16.
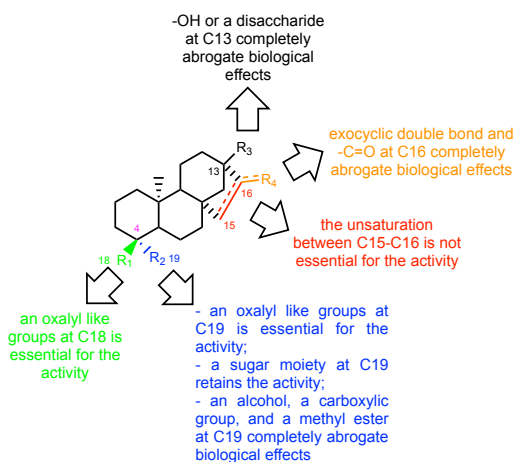
Figure A3.10 Structure activity relationships of **14** and its analogs.

A3.6 Conclusions

The old antibiotic colistin is our last-resort therapeutic option in infections by many MDR Gram-negative. However, reports of colistin-resistant isolates are rising. Thus, alternative therapeutic strategies and efforts to preserve the clinical efficacy of colistin are necessary.

Here, we reported the identification of a natural diterpene (**14**) able to potentiate colistin activity against colistin-resistant *P. aeruginosa* isolates (without affecting growth *per se* and with no activity on colistin-sensitive strains), and colistin-resistant clinical isolates of *K. pneumoniae*.

Since **14** emerged as a promising adjuvant to colistin activity, several analogs were synthetized and tested *in vitro*. Among them, **35**, **29** and **27** showed to be the most interesting compounds. In particular, compound

35 turned out to be the most powerful one. SARs were investigated highlighting the importance of *ent*-beyerane scaffold and oxalate like groups at C18 or at C19 for the biological activity.

In conclusion, our results revealed some natural small compounds able to enhance colistin activity. Thus, we hope they could trigger the development of agents capable to restore colistin activity in colistin-resistant isolates and improve the therapeutic utility of the newer antibiotics.

CHAPTER A4

General Methods

113

General Methods

All non-aqueous reactions were performed under an argon atmosphere using flame-dried glassware and standard syringe/septa techniques.

All absolute solvents were purchased as anhydrous grade from Sigma Aldrich and used without further purification unless otherwise stated. Solvents for extractions, flash column chromatography (FC) and thin layer chromatography (TLC) were purchased as commercial grade from Sigma Aldrich and used without further purification unless otherwise stated. Reactions were magnetically stirred and monitored by TLC performed on Merck TLC aluminum sheets (silica gel 60 F254). Spots were visualized with UV light (λ = 254 nm). Chromatographic purification of products (FC) was

performed using Sigma Aldrich silica gel 60 for preparative column chromatography (particle size 40-63 μm).

Melting points (**Mp**) were obtained in open capillary tubes using a Büchi melting point apparatus B-545 and are uncorrected.

^{1}H- and ^{13}C-NMR spectra were recorded in CDCl$_3$, acetone-*d$_6$*, DMSO-*d$_6$* or methanol-*d$_4$* on a Bruker AV-400 400 MHz spectrometer (operating at 400 MHz for ^{1}H and 100 MHz for ^{13}C) at room temperature and tetramethylsilane (TMS) as internal standard. Chemical shifts (δ) are reported in parts per million (ppm) and are referenced to CDCl$_3$ (δ = 7.26 ppm for ^{1}H, δ = 77.16 ppm for ^{13}C), acetone-*d$_6$* (δ = 2.05 ppm for ^{1}H, δ = 29.84 ppm for ^{13}C) DMSO-*d$_6$* (δ = 2.50 ppm for ^{1}H, δ 39.52 ppm for

^{13}C), or MeOH-d_4 (δ = 3.31 ppm for ^{1}H, δ 49.00 ppm for ^{13}C). All ^{13}C-NMR spectra were measured with complete proton decoupling. Data for NMR spectra are reported as follows: s=singlet, d= doublet, t= triplet, q= quartet, m= multiplet, br= broad signal, J= coupling constant in Hz.

High-resolution mass spectra (HRMS) were recorded on Bruker BioApex Fourier transform ion cyclotron resonance (FT-ICR) mass spectrometer.

Mass spectra (MS) were recorded on Bruker Esquire 3000 PLUS (Esi Ion Trap LC/MSn System)

HPLC analysis was performed on a Waters 2690 Separation Module, equipped with a Rheodyne Model 8125 20-µL injector and a Model M486 programmable multi-wavelength detector (PDA). Chromatographic data

were collected and processed using the Empower Chromatography Manager software. The purity of the compounds was always higher than 95 %.

The compounds are referred to by increasing numbers **X**, following the sequential references in the main text

Plant material Aerial parts of *Fabiana densa* var. *ramulosa* were collected and identified by the School of Chemistry and Pharmacy, University of Chile.

A4.1 Characterization of 18 hits compounds of an in *house* library of natural products

All the tested compounds (**1-18**) are known structures belonging to our *in house* library of natural products. Chemical identity of compounds **1-18** was assessed by re-running NMR experiments and proved to be in agreement with the literature data reported below for each compound. The purity of all compounds, checked by reversed-phase HPLC, was always higher than 95%.

Compound **1** (γ-γ'-OH Ferruginin A or 4,5,10-trihydroxy-1-[4-hydroxy-3-(hydroxymethyl)but-2-enyl]-7-methyl-1,6-bis(3-methylbut-2-enyl)anthracen-2-one) showed NMR spectra identical to the literature Delle Monache, F. et al., 1979.

Compound **2** (aloin or (10*S*)-1,8-dihydroxy-3-(hydroxymethyl)-10-[(2*S*, 3*R*, 4*R*, 5*S*, 6*R*)-3,4,5-trihydroxy-6-(hydroxymethyl)oxan-2-yl]-10*H*-anthracen-9-one) was purchased from Sigma-Aldrich (CAS Number: 1415-73-2) and used without further purification.

Compound **3** (chlorogenic acid or (1*S*, 3*R*, 4*R*, 5*R*)-3-[(*E*)-3-(3,4-dihydroxyphenyl)prop-2-enoyl]oxy-1,4,5-trihydroxycyclohexane-1-carboxylic acid) was purchased from Sigma-Aldrich (CAS Number: 327-97-9) and used without further purification.

Compound **4** (verbascoside or [(2*R*, 3*R*, 4*R*, 5*R*, 6*R*)-6-[2-(3,4-dihydroxyphenyl) ethoxy]-5-hydroxy-2-(hydroxymethyl)-4-[(2*S*, 3*R*, 4*R*, 5*R*, 6*S*)-3,4,5-trihydroxy-6-methyloxan-2-yl)oxyoxan-3-yl]-(*E*)-3-(3,4dihydroxyphenyl) prop-2-enoate) was purchased from Sigma-Aldrich (CAS Number: 61276-17-3), and used without further purification.

Compound **5** (phloretin or 3-(4-hydroxyphenyl)-1-(2,4,6-trihydroxyphenyl)propan-1-one) was purchased from Sigma-Aldrich (CAS Number: 200-488-7) and used without further purification.

Compound **6** (piscidone or 3-[3,4-dihydroxy-6-methoxy-2-(3-methylbut-2-enyl) phenyl]-5,7-dihydroxychromen-4-one) showed NMR spectra identical to the literature Tahara, S. et al., 1992.

Compound **7** (rheediaxanthone A or 11,22-dihydroxy-7,7,19,19-tetramethyl-2,8,20-trioxapentacyclo[12.8.0.03,12.04,9.016,21]docosa 1(14),3(12),4(9), 5,10,15,17, 21-octaen-13-one showed NMR spectra identical to the literature Delle Monache, F. et al., 1981.

Compound **8** (rheediaxanthone B or 5,9,10-trihydroxy-1,1,2-trimethyl-4-(2-methylbut-3-en-2-yl)-

2*H*-furo[2,3-*c*] xanthen-6-one) showed NMR spectra identical to the literature Delle Monache, F. et al., 1981.

Compound **9** (loganin or methyl (1*S*, 4a*S*, 6*S*, 7*R*, 7a*S*)-6-hydroxy-7-methyl-1-[(2*S*, 3*R*, 4*S*, 5*S*, 6*R*)-3, 4, 5-trihydroxy-6-(hydroxymethyl) oxan-2-yl] oxy1, 4*a*, 5, 6, 7, 7*a*-hexahydrocyclopenta[*c*]pyran-4-carboxylate) was purchased from Sigma-Aldrich (CAS Number: 18524-94-2) and used without further purification.

Compound **10** (3-hydroxy-4-methoxycinnamic acid or 3-(3-hydroxy-4-methoxyphenyl) prop-2-enoic acid) was purchased from Sigma-Aldrich (CAS Number: 537-73-5) and used without further purification.

Compound **11** (6-methoxy-7-O-geranyl-coumarin or 6-methoxy-2-oxochromen-7-yl-(2*E*)-3,7-dimethylocta-2,6-dienoate) showed NMR spectra identical to the literature Torres, R. et al., 1979.

Compound **12** (6-prenyl-aromadendrin or 3-methyl-2-butenyl (2*R*,3*R*)-3,5,7-trihydroxy-2-(4-hydroxyphenyl)-2,3-dihydrochromen-4-one) showed NMR spectra identical to the literature J.B. Harborne, J. B., 1993.

Compound **13** (vismiaphenone B or [5,7-dihydroxy-2,2-dimethyl-8-(3-methylbut-2-enyl) chromen-6-yl] phenylmethanone) showed NMR spectra identical to the literature Delle Monache, G. et al., 1980.

Compound **14** (*ent*-beyer-15-en-18-O-oxalate) showed NMR spectra identical to the literature Erazo, S. et al., 2002.

Compound **15** (physcion or 1,8-dihydroxy-3-methoxy-6-methylanthracene-9,10-dione) was purchased from Sigma-Aldrich (CAS Number: 521-61-9) and used without further purification.

Compound **16** (rhein or 4,5-dihydroxy-9,10-dioxoanthracene-2-carboxylic acid) showed NMR spectra identical to the literature Manshuo, L. et al., 2017.

Compound **17** (longistilin C or 3-methoxy-4-(3-methylbut-2-enyl)-5-[(*E*)-2-phenylethylen] phenol) showed NMR spectra identical to the literature Delle Monache, F., 1977.

Compound **18** (chalcon 19 or 4'-O-geranyl-chalcon or (*E*)-4'-O- 3,7-dimethyl-2,6-octadiene-1,3-diphenylprop-2-en-1-one) showed NMR spectra identical to the literature Guglielmi, P. et al., 2019.

A4.2 Characterization of diterpenes 14 and 19 from *Fabiana densa* var. *ramulosa*
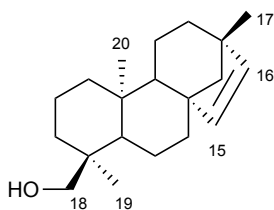
19

Compound 19. *ent*-beyer-15-en-18-ol. White powder (yield 10%); m.p. 110 ºC ± 0.5 ºC; [α]$_D$ +29.7° (CHCl$_3$). **¹H NMR** (CDCl$_3$, 400 MHz): δ (ppm) = 5.69 (d, 1H, J = 5.7 Hz, H-15); 5.45 (d, 1H, J = 5.6 Hz, H-16); 3.41 (d, 1H, J = 10.8 Hz, H-18a); 3.11 (d, 1H, J = 10.8 Hz, H-18b); 0.99 (s, 3H, CH$_3$-17); 0.78 (s, 3H, CH$_3$-19); 0.77 (s,

3H, CH$_3$-20); **^{13}C NMR** (CDCl$_3$, 100 MHz): δ (ppm)= 136.59, 135.38, 72.48, 61.34, 52.94, 49.19, 49.14, 43.81, 38.90, 37.74, 37.28, 37.16, 35.54, 33.34, 25.11, 20.38, 20.02, 18.12, 17.96, 15.76. **ESI-MS** (positive) m/z: [M+Na]$^+$ calcd. for C$_{20}$H$_{32}$ONa 311.25, found 311.3.
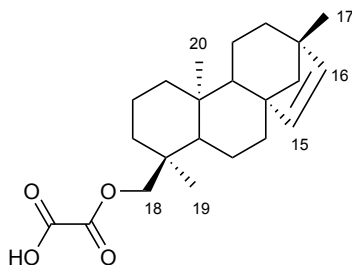
14

Compound 14. *ent*-**beyer-15-en-18-O-oxalate.** White powder (yield 5%); m.p. 169.5 ºC ± 0.5 ºC; [α]$_D$ +10° (CHCl$_3$). **^{1}H NMR** (CDCl$_3$, 400 MHz): δ (ppm) = 5.67 (d, 1H, J = 5.7 Hz, H-15,); 5.46 (d, 1H, J = 5.7 Hz,

H-16,); 4.10 (d, 1H, J = 10.8 Hz, H-18a); 3.90 (d, 1H, J = 10.8 Hz, H-18b); 0.99 (s, 3H, CH_3-17); 0.91 (s, 3H, CH_3-19); 0.79 (s, 3H, CH_3-20). **^{13}C NMR** (CDCl$_3$, 100 MHz): δ (ppm)= 158.65, 157.77, 136.74, 135.13, 76.54, 61.17, 52.83, 50.08, 49.01, 43.77, 38.57, 37.36, 36.98, 36.94, 35.92, 33.21, 25.03, 20.35, 20.29, 17.78, 17.62, 15.63. **ESI-HRMS** (negative) m/z: [M-H]$^-$ calcd. for $C_{22}H_{31}O_4$ 359.22278; found 359.22245

A4.3 Synthesis and characterization of compounds 24-32

A4.3.1 Synthesis and characterization of compound 24
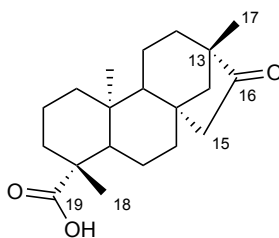
24

Compound **23** (SIGMA-ALDRICH 260-975-5) (8.68 mmol, 7.0 g) was dissolved in 21 ml of hydrobromic acid (HBr 48% in water) and the dark reaction mixture was stirred for 16 hours at room temperature. Then the

precipitate was filtered and solubilized with AcOEt. The organic layer was extracted with water and brine, dried over anhydrous Na_2SO_4 and evaporated to dryness under reduced pressure. The residue was crystallized with CH_3OH yielding compound **24** (7.72 mmol, 2,45 g, 89%). (Lohoelter, C. *et al.*, 2013; Avent, A.G. *et al.*, 1990).

Compound 24. Brown powder (yield 89%); m.p. 230 ºC ± 0.5 ºC; $[\alpha]_D$ -69.3° (EtOH). **^{1}H NMR** (CDCl$_3$, 400 MHz): δ (ppm) = 2.64 (dd, 1H, J = 18.6 Hz e J = 3.7 Hz, 1H, H-15a); 2.07 (d, 1H, J = 13.3 Hz, H-3eq); 1.93-1.32 (m, 13H); 1.25 (s, 3H, CH_3-18); 1.23-1.01 (m, 4H); 0.97 (s, 3H, CH_3-17); 0.96-079 (m, 1H, H-1ax); 0.78 (s, 3H, CH_3-20); **^{13}C NMR** (CDCl$_3$, 100 MHz): δ (ppm) = 222.90, 183.50, 57.17, 54.90, 54.44, 48.89, 48.61, 43.81, 41.60, 39.90, 39.63, 38.34, 37.84, 37.46, 29.11, 21.77, 20.49, 19.99, 19.01, 13.48. **ESI-HRMS** (positive) m/z:

[M+Na]$^+$ calcd. for C$_{20}$H$_{30}$O$_3$Na 341.20872; found 341.20902

A4.3.2 Synthesis and characterization of compound 25
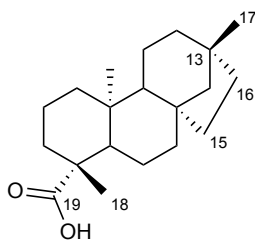
25

A mixture of **24** (3.14 mmol, 1.0 g), triethylene glycol (12.5 ml), 95% hydrazine (2.5 ml) and KOH (22.3 mmol, 1.25 g) was distilled at 180 °C until around 1.25 ml were removed. Then the reaction was stirred at reflux at 200 °C for 2 hours. After that, the reaction mixture was cooled down and 162.5 ml of distilled water were added. The solution was neutralized with glacial acetic acid (CH₃COOH) (1N) and the precipitate (which formed on

acidification) was filtered and dissolved with Et_2O. The organic layer was extracted with water for two times, dried over anhydrous Na_2SO_4 and evaporated to dryness under reduced pressure giving compound **25** (0.911 mmol, 277 mg, 29%). (Mosettig, E. *et al*., 1955).

Compound 25. White powder (yield 29%); m.p. 190 ºC ± 0.5 ºC; $[\alpha]_D$ -42.0° (CHCl$_3$). **¹H NMR** (CDCl$_3$, 400 MHz): δ (ppm)= 2.13 (d, 1H, J = 12 Hz, H-3eq); 2.02-1.24 (m, 15H); 1.22 (s, 3H, CH$_3$-18); 1.18-0.95 (m, 5H); 0.93 (s, 3H, CH$_3$-17); 0.89 (m, 1H, H-1ax); 0.84 (s, 3H, CH$_3$-20). **¹³C NMR** (CDCl$_3$, 100 MHz): δ (ppm) = 184.04, 60.54, 57.52, 56.33, 45.13, 43.83, 41.54, 40.19, 40.18, 39.45, 38.36, 37.96, 37.69, 33.63, 29.19, 27.26, 21.92, 20.95, 19.09, 14.32. **ESI-HRMS** (negative) m/z: [M-H]⁻ calcd. for $C_{20}H_{31}O_2$ 303.23295; found 303.23288.

A4.3.3 Synthesis and characterization of compound 26

26
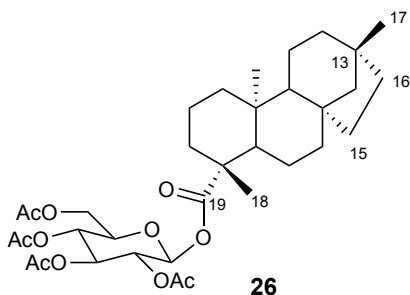
To a solution of **25** (0.986 mmol, 300 mg) in CH$_2$Cl$_2$ (6.73 ml) and water (1.79 ml) tetrabutylammonium bromide (TBAB) (0.02 mmol, 6.72 mg), K$_2$CO$_3$ (3.26 mmol, l450 mg) and acetobromo-α-D-glucose (1.36 mmol, 560 mg) were added. The reaction mixture was stirred at reflux at 50 °C for 24 hours. Then the aqueous layer was extracted with CH$_2$Cl$_2$ and the

organic layer was washed with water for two times, with brine and evaporated to dryness under reduced pressure obtaining compound **26** (0,572 mmol, 363 mg, 58%). (Chaturvedula, V.S.P. *et al.*, 2011).

Compound 26. Brown powder (yield 58%); m.p. 140 ºC ± 0.5 ºC; $[\alpha]_D$ -8.7° (CHCl$_3$). **^{1}H NMR** (CD$_3$OD, 400 MHz): δ (ppm) =5.82 (d, J= 8.4 Hz, 1H, H-1'); 5.34 (t, 1H, J = 9.4 Hz, H-3'); 5.12-5.05 (m, 2H, H-2'e H-4'); 4.33 (dd, 1H, J= 12.1 Hz, J = 4.8 Hz, H-6'); 4.02 (dd, 1H, J = 12.0 Hz, J = 2.4 Hz, H-6''); 4.02-3.98 (m, 1H, H-5'); 2.04 (s, 3H, CH$_3$CO); 2.02 (s, 6H, 2 x CH$_3$CO); 1.98 (s, 3H, CH$_3$CO); 1.80-1.25(m, 16H); 1.17 (s, 3H, CH$_3$-17); 1.41-0.97 (m, 5H); 0.94 (s, 3H, CH$_3$-18); 0.77 (s, 3H, CH$_3$-20). **^{13}C NMR** (CD$_3$OD, 100 MHz): δ (ppm) = 177.16, 172.23, 171.55, 171.23, 170.79, 92.50, 74.54,73.57, 71.77, 69.45, 62.66, 58.53, 58.48,57.48, 46.16, 45.18, 42.51,

41.12, 41.09, 40.34, 39.29, 39.03, 38.52, 34.82, 29.23, 27.51, 22.96, 21.89, 20.93, 20.52, 14.42. **ESI-HRMS** (positive) m/z: $[M+Na]^+$ calcd. for $C_{34}H_{50}O_{11}Na$ 657.32453; found 657.32481.

A4.3.4 Synthesis and characterization of compound 27
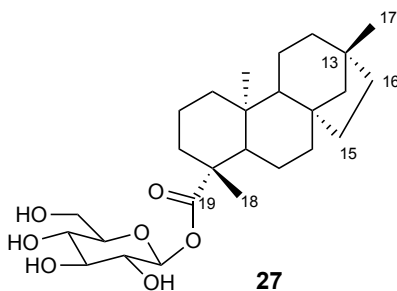
10% of Et$_3$N (7.6 ml) was added to a solution of **26** in CH$_3$OH: H$_2$O: hexane (10: 2: 1). The reaction mixture was stirred at room temperature for 48h. Further, it was evaporated to dryness under reduced pressure and the residue was crystallized with Et$_2$O at room temperature leading to compound **27** (0.511 mmol, 238 mg, quantitative yield). (Oulmi, D. *et al*., 1995; Chaturvedula, V.S.P. *et al*., 2011).

Compound 27. White powder (quantitative yield); m.p. 160 ºC ± 0.5 ºC; [α]$_D$ -22.7° (MeOH). **^{1}H NMR** (CD$_3$OD, 400 MHz): δ (ppm) = 5.42 (d, 1H, J = 8.3 Hz, H-1'); 3.83 (dd, 1H, J = 12.1 Hz, J = 1.6 Hz, H-6'); 3.67 (dd, 1H, J = 11.6 Hz, J = 4.4 Hz, H-6''); 3.40-3.34 (m, 4H, H-2', H-3', H-4', H-5'); 2.20-2.17 (d, 1H, J = 13.2, H-3eq); 2.09-2.03 (m, 1H, H-5eq); 1.91-1.34 (m, 14H); 1.21 (s, 3H, CH$_3$-17); 1.18-0.97 (m, 5H); 0.94 (s, 3H, CH$_3$-18); 0.87 (s, 3H, CH$_3$-20). **^{13}C NMR** (CD$_3$OD, 100 MHz): δ (ppm) = 178.27, 95.55, 78.69, 78.66, 74.03, 71.11, 62.42, 59.10, 58.56, 57.57, 46.25, 45.10, 42.75, 41.29, 41.23, 40.32, 39.37, 39.04, 38.53, 34.51, 29.24, 27.60 22.86, 21.93, 20.07, 14.42. **ESI-HRMS** (positive) m/z: [M+Na]$^+$ calcd. for C$_{26}$H$_{42}$O$_7$Na 489.28227; found 489.28264.

A4.3.5 Synthesis and characterization of compound 28
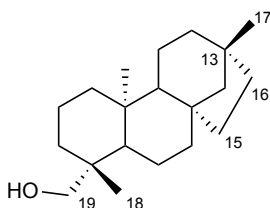
28

To a stirred solution of **25** (1 mmol, 304 mg) in anhydrous THF (0.0854 n/l, 11.70 ml) LiAlH$_4$ (9 mmol, 4.5 ml) was added dropwise and the reaction mixture was stirred at reflux for 3 hours. Further, it was cooled down, quenched by the slow addition of EtOAc and saturated aqueous solution of Rochelle's salt (sodium potassium tartrate), and evaporated to dryness under reduced

pressure removing excess of THF. After that, the aqueous layer was extracted with EtOAc and dried over anhydrous Na_2SO_4 yielding compound **28** (0.82 mmol, 238 mg, 82%). (Batista, R. *et al*., 2007; Murillo, J.A. *et al*., 2019).

Compound 28. White powder (yield 82%); m.p. 115 ºC ± 0.5 ºC; [α]$_D$ -0.7° (CHCl$_3$). **^{1}H NMR** (CDCl$_3$, 400 MHz): δ (ppm) = 3.75 (d, 1H, J = 8 Hz, H-19b); 3.41 (d, 1H, J = 8 Hz, H-19a,); 1.75 (d, 1H, J = 12Hz, H-3eq); 1.72-1.16 (m, 19H); 0.95 (s, 3H, CH$_3$-17); 0.93 (s, 3H, CH$_3$-19); 0.89 (s, 3H, H-20). **^{13}C NMR** (CDCl$_3$, 100 MHz): δ (ppm) = 65.82, 57.78, 57.32, 57.14, 45.09, 41.78, 40.10, 39.91, 39.42, 38.67, 37.75, 37.69, 35.69, 33.74, 27.30, 27.21, 20.74, 20.50, 18.25, 15.85. **ESI-MS** (positive) m/z: [M+Na]$^+$ calcd. for C$_{20}$H$_{34}$ONa 313.26; found 313.7.

A4.3.6 Synthesis and characterization of compound 29
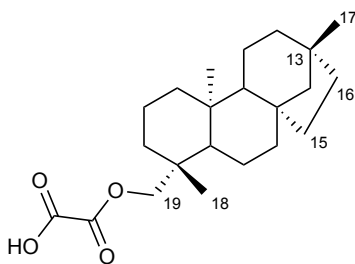
29

To a solution of **28** (0.207 mmol, 60 mg, 1 equiv.) in Et₂O (0.192 mmol/ml, 1.08 ml) oxalyl chloride (0.414 mmol, 0.207 ml, 4 equiv.) was added dropwise at 0 °C and the reaction mixture was stirred at reflux for 30 minutes. Then the reaction mixture was cooled down and quenched by slow addition of distilled water. The aqueous layer was extracted with Et₂O and the organic layer was washed with

water for two times and with brine, dried over anhydrous Na$_2$SO$_4$ and evaporated to dryness under reduced pressure. The residue was purified by flash column chromatography on silica gel and a mixture of CHCl$_3$: CH$_3$OH: HCOOH (98: 2: 1%) was used as eluent affording compound **29** (0.190 mmol; 69 mg, 92%). (Zhang, X. *et al*., 2016).

Compound 29. Pale yellow oil (yield 92%); [α]$_D$ -14.3° (CHCl$_3$). **^{1}H NMR** (CDCl$_3$, 400 MHz): δ (ppm) = 4.52 (d, 1H, J = 10.8 Hz, H-19a); 4.10 (d, 1H, J = 10.8 Hz, H-19b); 2.04-1.3 (m, 17H); 1.16-1.03 (m, 5H); 1.00 (s, 3H, CH$_3$-17); 0.94 (s, 3H, CH$_3$-19); 0.92 (s, 3H, H-20). **^{13}C NMR** (CDCl$_3$, 100 MHz): δ (ppm) = 158.59, 158.18, 71.10, 57.70, 57.15, 57.01, 45.03, 41.51, 40.03, 39.52, 39.42, 37.67, 37.66, 37.37, 36.06, 33.69, 27.42, 27.26, 20.72, 20.35, 18.05, 15.86. **ESI-HRMS** (negative) m/z: [M -H]$^-$ calcd. for C$_{22}$H$_{34}$O$_4$ 361.23843; found 361.23820.

A4.3.7 Synthesis and characterization of compound 30
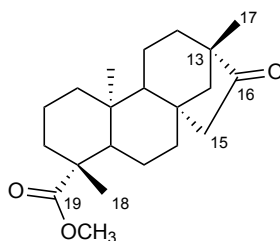
30

To compound **24** (0.943 mmol, 300 mg) cooled in ice bath, SOCl$_2$ (13.6 ml) and anhydrous DMF (0.3 ml) were added. The reaction mixture was stirred at room temperature for 2 hours and, then, evaporated to dryness under reduced pressure. The residue was dissolved in anhydrous CH$_3$OH (54.5 ml) and Et$_3$N (12.3 ml) was added. The solution was stirred at room temperature for 2

hours and evaporated to dryness under reduced pressure. The residue was dissolved in CH_2Cl_2 and the organic layer was washed with brine for three times and dried by anhydrous Na_2SO_4 overnight. After filtration, the solution was evaporated to dryness under reduced pressure giving compound **30** (0.943 moli, 313 mg, quantitative yield). (Batista, R. *et al*., 2007).

Compound 30. Yellow powder (quantitative yield); m.p. 184 ºC ± 0.5 ºC; [α]$_D$ -46.0° (CHCl$_3$). **^{1}H NMR** (CDCl$_3$, 400 MHz): δ (ppm) = 3.63 (s, 3H, COOCH$_3$); 2.63 (dd, 1H, J = 18.6 Hz, J = 3.8 Hz, H-15ax); 2.18 (d, 1H, J = 14.1 Hz, H-3eq); 2.02-1.33 (m, 15H); 1.19 (s, 3H, CH$_3$-18); 1.14-0.10 (m, 5H); 0.97 (s, 3H, CH$_3$-17); 0.89 (m, 1H, H-1ax); 0.68 (s, 3H, CH$_3$-20). **^{13}C NMR** (CDCl$_3$, 100 MHz): δ (ppm) = 177.98, 57.22, 54.89, 54.47, 51.40, 48.86, 48.62, 43.94, 41.64, 39.97, 39.60, 38.10, 37.47, 29.00, 21.86, 20.48, 20.00, 19.10, 13.32. **ESI-**

HRMS (positive) m/z: [M+Na]$^+$ calcd. for $C_{21}H_{32}O_3Na$ 355.22437; found 355.22466.

A4.3.8 Synthesis and characterization of compound 31

31
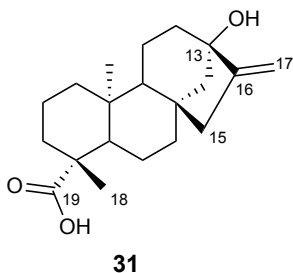
A solution of **23** (1.36 mmol, 1.1 g) and NaIO$_4$ (7 mmol, 1.5 g) in water (75 ml) was stirred at room temperature for 16 hours. Then KOH (134 mmol, 7.5 g) and the reaction mixture was stirred at reflux for 1 hour. After that, the mixture was cooled and neutralized with CH$_3$COOH. The aqueous layer was extracted with Et$_2$O and the organic layer was washed with water, dried over

anhydrous Na$_2$SO$_4$ and evaporated to dryness under reduced pressure. The residue was crystallized with CH$_3$OH affording compound **31** (1,02 mmol, 324,58 mg, 75%). (Batista, R. *et al*., 2007; Ogawa, T. *et al*., 1980).

Compound 31. White powder (yield 75 %); m.p. 205 ºC ± 0.5 ºC; [α]$_D$ -45.7°(CDCl$_3$). **^{1}H NMR** (CDCl$_3$, 400 MHz): δ (ppm) = 4.98 (s, 1H, H-17a); 4.81 (s, 1H, H-17b); 2.22-2.07 (m, 4H); 1.95-1.30 (m, 14H); 1.23 (s, 3H, CH$_3$-18); 1.10-0.99 (m, 2H); 0.95 (s, 3H, CH$_3$-20). **^{13}C NMR** (CDCl$_3$, 100 MHz): δ (ppm) = 183.30, 155.85, 103.17, 80.48, 56.99, 53.93, 47.52, 47.03, 43.71, 41.84, 41.35, 40.64, 39.62, 39.45, 37.86, 28.92, 21.92, 20.57, 19.13, 15.55. **ESI-HRMS** (negative) m/z: ([M -H]$^-$) calcd. for C$_{20}$H$_{29}$O$_3$ 317.21222; found 317.21250.

A4.3.9 Synthesis and characterization of compound 32
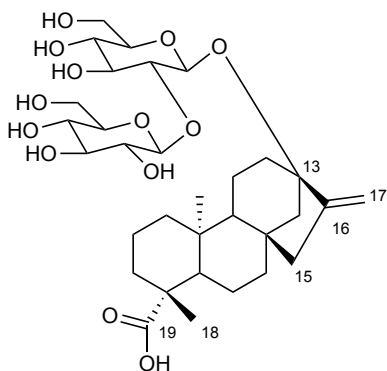
32

A solution of **23** (0.62 mmol, 500 mg) in 10% aqueous KOH (12.5 ml) was stirred at 100 °C for 1 hour. Then the reaction mixture was cooled down, neutralized with a solution of CH_3COOH 1N and evaporated to dryness under reduced pressure. The residue was

crystallized with CH$_3$OH yielding the compound **32** (0.589 mmol, 390 mg, 95%). (Wood, J.R. *et al*., 1955, Chaturvedula, V.S.P. *et al.*, 2011).

Compound 32. White powder (yield 95 %); m.p. 213 ºC ± 0.5 ºC; [α]$_D$ -32.5° (MeOH). **¹H NMR** (DMSO-d$_6$, 400 MHz): δ (ppm) = 5.08 (s, 1H, H-17); 4.74 (s, 1H, H-17b); 4.46 (d, 1H, J = 8 Hz, H-1'); 4.35 (d, 1H, J = 8 Hz, H-1''); 3.63-2.98 (m, 12 H); 2.17-1.22 (m, 17H); 1.07 (s, 3H, H-18); 0.89 (s, 3H, H-20);0.80-0.70 (m, 2H,); **¹³C NMR** (DMSO-d$_6$, 100 MHz): δ (ppm) = 179.50, 153.41, 104.75, 103.97, 96.36, 84.90, 82.45, 76.98, 76.63, 76.12, 76.02, 75.51, 69.87, 69.75, 60.92, 60.62, 56.56, 53.39, 47.22, 43.87, 43.09, 41.93, 41.27, 41.22, 40.66, 38.37, 36.13, 29.21, 21.95, 19.96, 19.21, 15.35. **ESI-HRMS** (positive) m/z: [M+Na]$^+$ calcd. for C$_{32}$H$_{50}$O$_{13}$Na 665.31436; found 665.31488.

A4.4 Synthesis and characterization of compounds 34-35

A4.4.1 Synthesis and characterization of compound 34
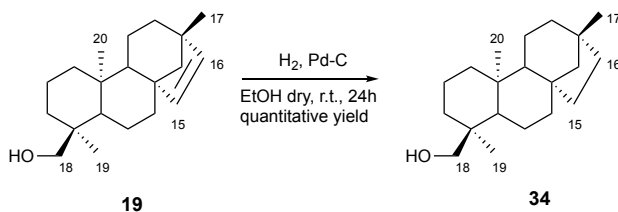
Scheme A4.1 Synthesis of compound **34** from **19**.

A solution of **19** (3.28 mmol, 95 mg) and Pd/C (6.55 mg, 10%) in EtOH dry (16.4 ml) was stirred under a hydrogen atmosphere (10 bar) at room temperature for 24 h. The reaction mixture was filtered, and the solvent was

evaporated under reduced pressure affording compound **34** (3,27 mmol, 95 mg, quantitative yield). (Murillo, J.A. *et al*., 2019).

Compound 34. White powder (quantitative yield); m.p.108 ºC ± 0.5 ºC; $[\alpha]_D$ -4.4°(CHCl$_3$). **^{1}H NMR** (CDCl$_3$, 400 MHz): δ (ppm) = 3.39 (d, 1H, J = 10.8 Hz, H-18a); 3.10 (d, 1H,J = 10.8 Hz, H-18b); 2.03 (m, 1H, H-3eq.); 0.95 (s, 3H, CH$_3$-17); 0.93 (s, 3H, CH$_3$-19); 0.75 (s, 3H, CH$_3$-20); **^{13}C NMR** (CDCl$_3$, 100 MHz): δ (ppm)= 72.52, 57.86, 57.03, 49.74, 45.13, 41.08, 40.21, 39.52, 39.48, 37.84, 37.71, 35.46, 33.97, 29.92, 27.39, 20.70, 20.15, 17.99, 17.97, 15.81.

A4.4.1 Synthesis and characterization of compound 35
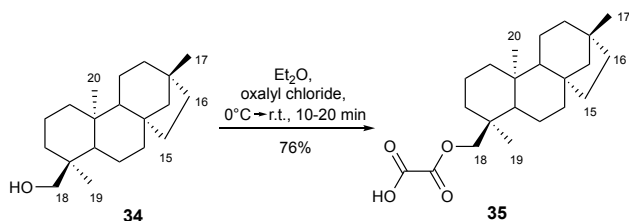
Scheme A4.2 Synthesis of compound **35** from **34**.

To a solution of **24** (0.257 mmol, 75 mg, 1 equiv.) in Et$_2$O (0.192 mmol/ml, 1.34 ml) oxalyl chloride (0.55 mmol, 0.275 ml, 4 equiv.) was added dropwise at 0 °C and the reaction mixture was stirred at reflux for 30 minutes. Then the reaction mixture was cooled down and quenched by slow addition of distilled water. The aqueous layer was extracted with Et$_2$O and the organic layer was washed with

water for two times and with brine, dried over anhydrous Na_2SO_4 and evaporated to dryness under reduced pressure. The residue was purified by flash column chromatography on silica gel and eluted with $CHCl_3$: CH_3OH: HCOOH (98: 2: 1%) affording compound **35** (0.196 mmol; 71 mg, 76%). (Zhang, X. *et al*., 2016).

Compound 35. Pale yellow oil (yield 76%); $[\alpha]_D$ -3.9° ($CHCl_3$). **^{1}H NMR** ($CDCl_3$, 400 MHz): δ (ppm) = 4.10 (d, 1H, J = 10.8 Hz, H-18a); 3.90 (d, 1H, J = 10.8 Hz, H-18b); 2.03 (m, 1H, H-3eq.); 0.96 (s, 3H, CH_3-17); 0.93 (s, 3H, CH_3-19); 0.89 (s, 3H, CH_3-20). **^{13}C NMR** ($CDCl_3$, 100 MHz): δ (ppm) = 158.64, 157.78, 57.74, 56.95, 50.69, 45.05, 40.88, 40.11, 39.51, 39.19, 37.82, 37.78, 37.02, 35.90, 33.91, 29.92, 27.34, 20.64, 20.53, 17.69, 17.66, 15.76. **ESI-HRMS** (negative) m/z: ESI-HRMS (negative): [M -H]$^-$ calcd. for $C_{22}H_{33}O_4$ 361.23843; found 361.23816.

CHAPTER A5

Bibliography

Allen, H. K. *et al.* Call of the wild: Antibiotic resistance genes in natural environments. *Nat. Rev. Microbiol.* 8, 251–259 (2010).

Aminov, R. I. A brief history of the antibiotic era: Lessons learned and challenges for the future. *Front. Microbiol.* 1, 1–7 (2010).

Apostolakos, I. & Piccirillo, A. A review on the current situation and challenges of colistin resistance in poultry production. *Avian Pathol.* 47, 546–558 (2018).

Avent, A. G., Hanson, J. R. & De Oliveira, B. H. Hydrolysis of the diterpenoid glycoside, stevioside. *Phytochemistry* 29, 2712–2715 (1990).

Baron, S., Hadjadj, L., Rolain, J. M. & Olaitan, A. O. Molecular mechanisms of polymyxin resistance: knowns and unknowns. *Int. J. Antimicrob. Agents* 48, 583–591 (2016).

Bassetti, M., Peghin, M., Vena, A. & Giacobbe, D. R. Treatment of Infections Due to MDR Gram-Negative Bacteria. *Front. Med.* 6, 1–10 (2019).

Batista, R., Humberto, J. L., Chiari, E. & de Oliveira, A. B. Synthesis and trypanocidal activity of ent-kaurane glycosides. *Bioorganic Med. Chem.* 15, 381–391 (2007).

Blair, J. M. A., Webber, M. A., Baylay, A. J., Ogbolu, D. O. & Piddock, L. J. V. Molecular mechanisms of antibiotic resistance. *Nat. Rev. Microbiol.* 13, 42–51 (2015).

Brown, D. G., Lister, T. & May-Dracka, T. L. New natural products as new leads for antibacterial drug

discovery. *Bioorganic Med. Chem. Lett.* 24, 413–418 (2014).

Brown, D. G. Drug discovery strategies to outer membrane targets in Gram-negative pathogens. *Bioorganic Med. Chem.* 24, 6320–6331 (2016).

Brown, L., Wolf, J. M., Prados-Rosales, R. & Casadevall, A. Through the wall: Extracellular vesicles in Gram-positive bacteria, mycobacteria and fungi. *Nat. Rev. Microbiol.* 13, 620–630 (2015).

Cabeen, M. T. & Jacobs-Wagner, C. Bacterial cell shape. *Nat. Rev. Microbiol.* 3, 601–610 (2005).

Casciaro, B.; Calcaterra, A.; Cappiello, F.; Mori, M.; Loffredo, M.R.; Ghirga, F.; Mangoni, M.L.; Botta, B.; Quaglio, D., Nigritanine as a New Potential Antimicrobial Alkaloid for the Treatment of *Staphylococcus aureus*-Induced Infections, *Toxins.*, 11, 511 (2019)

Ceunen, S. & Geuns, J. M. C. Steviol Glycosides: Chemical Diversity, Metabolism, and Function. (2013).

Chaturvedula, V. S. P., Klucik, J., Upreti, M. & Prakash, I. Synthesis of ent-kaurane diterpene monoglycosides. *Molecules* 16, 8402–8409 (2011).

Clinical and Laboratory Standards Institute (CLSI): Performance standards for antimicrobial susceptibility testing; Twenty-sixth informational supplement. *CLSI document M100-S26*. Wayne, PA: Clinical and Laboratory Standards Institute (2016).

Cragg, G. M. & Newman, D. J. Natural products: A continuing source of novel drug leads. *Biochim. Biophys. Acta - Gen. Subj.* 1830, 3670–3695 (2013).

Das, R., & Mukhopadhyay, B. Chemical O-Glycosylations: An Overview. *ChemistryOpen*, 5(5), 401-433 (2016).

Delle Monache, F. Contributo allo studio delle balche il vino rituale dei Maya, *Simposio internazionale sulla medicina indigena e popolare dell'America latina* (1977).

Delle Monache, F.; Botta, B.; Nicoletti, M.; De Barros Coêlho, J. S.; De Andrade Lyra, F.D. Three New Xanthones and Macluraxanthone from *Rheedia benfharniana* PI. Triana (Guttiferae), *Journal of the Chemical Society, Perkin Transaction*. 484-488 (1981).

Delle Monache, G.; Gonzalez Gonzalez, .J.; Delle Monache, F.; Marini Bettolo, G.B. Prenylated benzophenones from *Vismia Decipiens*, *Phytochemistry*. 19, 2025-2028 (1980).

Delle Monache, F; Marquina Mc Quhae, M.; Ferrari, F.; Marini-Bettolo, G.B. Ferruginin A and B and ferruanthrone, new triprenylated anthranoids form *Vismia*

baccifera var. ferruginea, *Tetrahedron*, *35*, 2143-2149 (1979).

Erazo, S.; Zaldívar, M.; Delporte C.; Backhouse, N.; Tapia, P.; Belmonte, E.; Delle Monache, F.; Negrete, R. Antibacterial diterpenoids from *Fabiana densa* var. *ramulosa*, *Planta Medica*. 68, 361-363 (2002).

Fernandes, P. & Martens, E. Antibiotics in late clinical development. *Biochem. Pharmacol.* 133, 152–163 (2017).

Fernandes, P. Antibacterial discovery and development - The failure of success? *Nat. Biotechnol.* 24, 1497–1503 (2006).

Fleming, A., Nobel Lecture, December 11, 1945 (1945).

Frieri, M., Krishan K. & Boutin, A. Antibiotic resistance. *Journal of infection and public health*. 10.4, 369-378 (2017).

Garaev, E. E.; Mahiou-Leddet, V.; Mabrouki, F.; Herbette, G.; Garaev, E. A.; Ollivier, E. Chemical constituents from roots of Cephalaria media, *Chemistry of Natural Compounds*. *50*, 4, 756-758 (2014).

Geuns, Jan MC. "Stevioside." *Phytochemistry*. 64.5, 913-921 (2003)

Giacobbe, D. R., Mikulska, M. & Viscoli, C. Recent advances in the pharmacological management of infections due to multidrug-resistant Gram-negative bacteria. *Expert Rev. Clin. Pharmacol.* 11, 1219–1236 (2018).

Giamarellou, H. Epidemiology of infections caused by polymyxin-resistant pathogens. *Int. J. Antimicrob. Agents* 48, 614–621 (2016).

Gould, K. Antibiotics: From prehistory to the present day. *J. Antimicrob. Chemother.* 71, 572–575 (2016).

Guglielmi, P.; Carradori, S.; Poli, G.; Secci, D.; Cirilli, R.; Rotondi, G.; Chimenti, P.; Petzer A.; Petzer, J.P. Design, Synthesis, Docking Studies and Monoamine Oxidase Inhibition of a Small Library of 1-acetyl- and 1-thiocarbamoyl-3,5-diphenyl-4,5-dihydro- (1*H*)-pyrazoles, *Molecules* . 24, 484 (2019).

Hall, D. G., Sukhdev, M. and Fan, W. "Solution- and solid-phase strategies for the design, synthesis, and screening of libraries based on natural product templates: a comprehensive survey." *Journal of combinatorial Chemistry*. 3.2, 125-150 (2001).

Hanson, J. R. & De Oliveira, B. H. Stevioside and related sweet diterpenoid glycosides. *Nat. Prod. Rep.* 10, 301–309 (1993).

Hanson, J. R. Skeletal rearrangements of rings C and D of the kaurene and beyerene tetracyclic diterpenoids. *J. Chem. Res.* 42, 75–180 (2018).

Hanson, J. R. The biosynthesis of the diterpenes. *Fortschritte der Chemie Org. Naturstoffe* 29, 395–416 (1971).

Harborne, J.B. The flavonoids: advances in research since 1986, *Chapman and Hall 1st edition*. 676 (1993) ISBN 0412480700.

Harvey, A. L., Edrada-Ebel, R. & Quinn, R. J. The re-emergence of natural products for drug discovery in the genomics era. *Nat. Rev. Drug Discov.* 14, 111–129 (2015).

Hernando-amado, S., Coque, T. M., Baquero, F. & Martínez, J. L. One Health and Global Health perspectives. 4, (2019).

Hong, Y. J. & Tantillo, D. J. Formation of beyerene, kaurene, trachylobane, and atiserene diterpenes

by rearrangements that avoid secondary carbocations. *J. Am. Chem. Soc.* 132, 5375–5386 (2010).

Hu, Q.; Ying-Ying, C.; Qi-Yang, J.; Afsar, K.; Jimiao, S.; Gui- Dong; C.; Feng, L.; Chao, Z.; Hong-Xiang, L. Polyphenolic compounds from *Malus hupehensis* and their free radical scavenging effects, *Natural Product Research*. 32, 18, 2152-2158 (2017).

Infante, P.; Alfonsi, R.; Ingallina, C.; Quaglio, D.; Ghirga, F.; D'Acquarica, I.; Bernardi, F.; Di Magno, L.; Canettieri, G.; Screpanti, I., et al. Inhibition of Hedgehog-dependent tumors and cancer stem cells by a newly identified naturally occurring chemotype. *Cell death & disease*. 7 (2016).

Infante, P.; Mori, M.; Alfonsi, R.; Ghirga, F.; Aiello, F.; Toscano, S.; Ingallina, C.; Siler, M.; Cucchi, D.; Po, A., et al. Gli1/DNA interaction is a druggable target

for Hedgehog-dependent tumors. *Embo J.* 34, 200-217 (2015).

Jayol, A., Nordmann, P., André, C., Poirel, L. & Dubois, V. Evaluation of three broth microdilution systems to determine colistin susceptibility of Gram-negative bacilli. *J. Antimicrob. Chemother.* 73, 1272–1278 (2018).

Jeannot, K., Bolard, A. & Plésiat, P. Resistance to polymyxins in Gram-negative organisms. *Int. J. Antimicrob. Agents* 49, 526–535 (2017).

Kaye, K. S., Pogue, J. M., Tran, T. B., Nation, R. L., & Li, J. Agents of last resort: polymyxin resistance. *Infectious disease clinics of North America*, *30*(2), 391-414 (2016).

Kinghorn, A. D., Soejarto, D. D., Nanayakkara, N. P. D., Compadre, C. M., Makapugay, H. C., Hovanec-Brown, J. M., ... & Kamath, S. K. (1984). A phytochemical

screening procedure for sweet ent-kaurene glycosides in the genus Stevia. *Journal of natural products*, *47*(3), 439-444. (1984)

Kinghorn, A. Douglas, and Djaja Djendoel Soejarto. "Discovery of terpenoid and phenolic sweeteners from plants." *Pure and Applied Chemistry* 74.7 (2002): 1169-1179

Kline, T., Trent, M. S., Stead, C. M., Lee, M. S., Sousa, M. C., Felise, H. B., H. V. Nguyen, H. V., Miller, S. I. Synthesis of and evaluation of lipid A modification by 4-substituted 4-deoxy arabinose analogs as potential inhibitors of bacterial polymyxin resistance. *Bioorganic & medicinal chemistry letters*. *18*(4), 1507-1510 (2008)

Lairson, L. L., Henrissat, B., Davies, G. J. & Withers, S. G. Glycosyltransferases: Structures, Functions, and Mechanisms. *Annu. Rev. Biochem.* 77, 521–555 (2008).

Landman, D., Georgescu, C., Martin, D. A. & Quale, J. Polymyxins revisited. *Clin. Microbiol. Rev.* 21, 449–465 (2008).

Leitão, S.G.; Da Fonseca, E. N.; Dos Santos, T.C.; França, F.; Delle Monache, F. Caffeoylquinic acid derivatives from two Brazilian Vitex species, *Biochemical Systematics and Ecology*. *36*, 312-315 (2008).

Lemus-Mondaca, R., Vega-Gálvez, A., Zura-Bravo, L. & Kong, A. H. Stevia rebaudiana Bertoni, source of a high-potency natural sweetener: A comprehensive review on the biochemical, nutritional and functional aspects. *Food Chem.* 132, 1121–1132 (2012).

Lewis, K. New approaches to antimicrobial discovery. *Biochemical pharmacology*, *134*, 87-98 (2017).

Li, B. & Webster, T. J. Bacteria antibiotic resistance: New challenges and opportunities for implant-

associated orthopedic infections. *J. Orthop. Res.* 36, 22–32 (2018).

Li, J. & Nation, R. L. Colistin in the 21st century. *Curr. Opin. Infect. Dis.* 22, 535–543 (2009).

Li, J., Nation, R. L., Turnidge, J. D., Milne, R. W., Coulthard, K., Rayner, C. R., & Paterson, D. L. Colistin: the re-emerging antibiotic for multidrug-resistant Gram-negative bacterial infections. *The Lancet infectious diseases*, *6*(9), 589-601 (2006).

Lo Sciuto, A. & Imperi, F. Aminoarabinosylation of lipid a is critical for the development of colistin resistance in pseudomonas aeruginosa. *Antimicrob. Agents Chemother.* 62, 17–20 (2018).

Lohoelter, C., Schollmeyer, D. & Waldvogel, S. R. Derivatives of (-)-isosteviol with expanded ring D and various oxygen functionalities. *European J. Org. Chem.* 2, 6364–6371 (2012).

Lohoelter, C., Weckbecker, M. & Waldvogel, S. R. (-)-Isosteviol As a Versatile Ex-Chiral-Pool Building Block for Organic Chemistry. *European J. Org. Chem.* 201300447, 5539–5554 (2013).

Minlon, H. (1946). A simple modification of the Wolff-Kishner reduction. *Journal of the American Chemical Society*, *68*(12), 2487-2488 (1946).

Li, Z. & Velkov, T. Polymyxins: Mode of Action. *Polymyxin Antibiotics: From Laboratory Bench to Bedside*. Springer, Cham, 37-54 (2019).

Manshuo, L.; Pin, L.; Rongqiang, L.; Yulin, Z.; Yang, B. Synthesis, characterization and biological activity of Rhein-cyclodextrin conjugate, *Journal of Molecular Structure*. 1128, 239-244 (2017).

Mascarello, A.; Mori, M.; Chiaradia-Delatorre, L.D.; Menegatti, A.C.; Delle Monache, F.; Ferrari, F.; Yunes, R.A.; Nunes, R.J.; Terenzi, H.; Botta, B., et al.

Discovery of Mycobacterium tuberculosis protein tyrosine phosphatase B (PtpB) inhibitors from natural products. *PloS one*. 8 (2013).

Messner, P., Schäffer, C., & Kosma, P. Bacterial cell-envelope glycoconjugates. In *Advances in carbohydrate chemistry and biochemistry* (Vol. 69, pp. 209-272). Academic Press (2013).

Moffatt, J. H., Harper, M. & Boyce, J. D. Mechanisms of Polymyxin Resistance. 55–71 (2019).

Moons, N., De Borggraeve, W. & Dehaen, W. Isosteviol as a Starting Material in Organic Synthesis. *Curr. Org. Chem.* 15, 2731–2741 (2011).

Mosettig, E. & Nes, W. R. Stevioside. II. The structure of the aglucon. *J. Org. Chem.* 20, 884–899 (1955).

Mosettig, E., Beglinger, U., Dolder, F., Lichti, H., Quitt, P., & Waters, J. A. The absolute configuration of

steviol and isosteviol. *Journal of the American Chemical Society*, *85*(15), 2305-2309 (1963).

Murillo, J. A., Gil, J. F., Upegui, Y. A., Restrepo, A. M., Robledo, S. M., Quiñones, W., Echeverri, F. San Martin, A, Olivo, H. F., & Escobar, G. Antileishmanial activity and cytotoxicity of ent-beyerene diterpenoids. *Bioorganic & medicinal chemistry*, *27*(1), 153-160 (2019).

Napolitano, J. G., Simmler, C., McAlpine, J. B., Lankin, D. C., Chen, S. N., & Pauli, G. F. Digital NMR profiles as building blocks: assembling 1H fingerprints of steviol glycosides. *Journal of natural products*, *78*(4), 658-665 (2015).

Needham, B. D. & Trent, M. S. Fortifying the barrier: The impact of lipid A remodelling on bacterial pathogenesis. *Nat. Rev. Microbiol.* 11, 467–481 (2013).

Newman, D. J. & Cragg, G. M. Natural Products

as Sources of New Drugs from 1981 to 2014. *J. Nat. Prod.* 79, 629–661 (2016).

Newman, D. J. & Cragg, G. M. Natural products as sources of new drugs over the last 25 years. *J. Nat. Prod.* 70, 461–477 (2007).

Newman, D. J. Natural products as leads to potential drugs: An old process or the new hope for drug discovery? *J. Med. Chem.* 51, 2589–2599 (2008).

O'Neill, J., Davies, S., Rex, J., White, L. J., & Murray, R. Review on antimicrobial resistance, tackling drug-resistant infections globally: final report and recommendations. *London: Wellcome Trust and UK Government* (2016).

Ogawa, T., Nozaki, M. & Matsui, M. Total synthesis of stevioside. *Tetrahedron*. 36, 2641–2648 (1980).

Olaitan, A. O., Morand, S. & Rolain, J. M.

Mechanisms of polymyxin resistance: Acquired and intrinsic resistance in bacteria. *Front. Microbiol.* 5, 1–18 (2014).

Oulmi, D., Maillard, P., Guerquin-Kern, J. L., Huel, C., & Momenteau, M. Glycoconjugated porphyrins. 3. Synthesis of flat amphiphilic mixed meso-(glycosylated aryl) arylporphyrins and mixed meso-(glycosylated aryl) alkylporphyrins bearing some mono-and disaccharide groups. *The Journal of Organic Chemistry*, *60*(6), 1554-1564 (1995).

Parker, J. Bacteria. 254-257 (2001).

Peng, C.; Zhang, W.; Dai, C.; Li, W.; Shen, X.; Yuan, Y.; Yan, L.; Zhang, W.; Yao, M. Study of the aqueous extract of *Aloe vera* and its two active components on the Wnt/β-catenin and Notch signaling pathways in colorectal cancer cells, *Journal of Ethnopharmacology*. 243, 112092 (2019).

Peters, R. J. Two rings in them all: The labdane-related diterpenoids. *Nat. Prod. Rep.* 27, 1521–1530 (2010).

Petrou, V. I. *et al.* Structural biology: Structures of aminoarabinose transferase ArnT suggest a molecular basis for lipid A glycosylation. *Science (80-.).* 351, 608–612 (2016).

Poirel, L., Jayol, A., & Nordmann, P. Polymyxins: antibacterial activity, susceptibility testing, and resistance mechanisms encoded by plasmids or chromosomes. *Clinical microbiology reviews*, *30*(2), 557-596 (2017).

Raetz, C. R. H., Reynolds, C. M., Trent, M. S. & Bishop, R. E. Modification, Lipid A In, Systems. *Annu Rev Biochem.* 76, 295–329 (2007).

Rogers, K & Kadner, R.J. Bacteria. *Encyclopedia Britannica*. (2019).

https://www.britannica.com/science/bacteria.

Roy, A., Roberts, F. G., Wilderman, P. R., Zhou, K., Peters, R. J., & Coates, R. M. 16-aza-ent-beyerane and 16-aza-ent-trachylobane: Potent mechanism-based inhibitors of recombinant ent-kaurene synthase from arabidopsis thaliana. *Journal of the American Chemical Society*, *129*(41), 12453-12460 (2007).

Sabnis, A., Klöckner, A., Becce, M., Evans, L. E., Furniss, R. C. D., Mavridou, D. A., Stevens, M. M., Edwards, A. M. Colistin kills bacteria by targeting lipopolysaccharide in the cytoplasmic membrane. *bioRxiv*, 479618 (2019).

Scarpati, M.L. and Delle Monache, F. Isolamento dal Verbascum sinuatum di due nuovi glucosidi: il verbascoside e l'isoverbascoside*, estratto dagli Annali di Chimica*. 53 (1963).

Shen, B. A new golden age of natural products

drug discovery. *Cell*, *163*(6), 1297-1300 (2015).

Silhavy, T. J., Kahne, D. & Walker, S. The bacterial cell envelope. Cold Spring Harb. Perspect. Biol. 2, 1–17 (2010).

Silver, L. L. Challenges of antibacterial discovery. *Clinical microbiology reviews*, *24*(1), 71-109 (2011).

Storm, D. R., Rosenthal, K. S., & Swanson, P. E. Polymyxin and related peptide antibiotics. *Annual review of biochemistry*, *46*(1), 723-763 (1977).

Tacconelli, E. *et al.* Discovery, research, and development of new antibiotics: the WHO priority list of antibiotic-resistant bacteria and tuberculosis. *Lancet Infect. Dis.* 18, 318–327 (2018).

Tahara, S.; Moriyama, M.; Ingham, J.L.; Mizutani, J. Structure revision of piscidone, a major isoflavonoid in the root bark of *Piscidia erythrina*, *Phytochemistry*. 31, 2,

679-682 (1992).

Thomford, N. E. *et al.* Natural products for drug discovery in the 21st century: Innovations for novel drug discovery. *Int. J. Mol. Sci.* 19, (2018).

Torres, R., Delle Monache F., Bertolo G. B. M., Cossels, B. K. Coumarins and cinnamic acid from *Gymnophyton isatidicarbom*, *Journal of Natural Products 42*, 532-533 (1979).

Tsuji, B. T. *et al.* International Consensus Guidelines for the Optimal Use of the Polymyxins: Endorsed by the American College of Clinical Pharmacy (ACCP), European Society of Clinical Microbiology and Infectious Diseases (ESCMID), Infectious Diseases Society of America (IDS. *Pharmacotherapy* 39, 10–39 (2019).

Tyers, M. & Wright, G. D. Drug combinations: a strategy to extend the life of antibiotics in the 21st century.

Nat. Rev. Microbiol. 17, 141–155 (2019).

Typas, A., Banzhaf, M., Gross, C. A. & Vollmer, W. From the regulation of peptidoglycan synthesis to bacterial growth and morphology. *Nat. Rev. Microbiol.* 10, 123–136 (2012).

Vaara, M. Polymyxin derivatives that sensitize Gram-negative bacteria to other antibiotics. *Molecules*, *24*(2), 249 (2019).

Velkov, T. *et al.* A review on the current situation and challenges of colistin resistance in poultry production. *Int. J. Antimicrob. Agents* 48, 614–621 (2019).

Velkov, T. Pharmacology of polymyxins: new insights into an 'old' class of antibiotics. *Futur. Microbiol.* 8, 1–20 (2013).

Velkov, T., Thompson, P. E., Nation, R. L. & Li, J. Structure-activity relationships of polymyxin antibiotics. *J. Med. Chem.* 53, 1898–1916 (2010).

Vollmer, W., Blanot, D. & De Pedro, M. A. Peptidoglycan structure and architecture. *FEMS Microbiol. Rev.* 32, 149–167 (2008)

Wang, T. T., Liu, Y. & Chen, L. Synthesis and cytotoxic activity of nitric oxide-releasing isosteviol derivatives. *Bioorganic Med. Chem. Lett.* 24, 2202–2205 (2014).

Wang, Z. Comprehensive Organic Name Reactions and Reagents. *Wiley.* 2930-2036 (2010).

Wellsow, J. *et al.* Insect-antifeedant and antibacterial activity of diterpenoids from species of Plectranthus. *Phytochemistry* 67, 1818–1825 (2006).

Wölwer-Rieck, U. The leaves of Stevia rebaudiana (Bertoni), their constituents and the analyses thereof: A review. *J. Agric. Food Chem.* 60, 886–895 (2012).

Wood, H. B., Allerton, R., Diehl, H. W. & Fletcher, H. G. Stevioside. I. The structure of the glucose

moieties. *J. Org. Chem.* 20, 875–883 (1955).

Wright, G. D. Antibiotic Adjuvants: Rescuing Antibiotics from Resistance. *Trends Microbiol.* 24, 862–871 (2016).

Yan, A., Guan, Z. & Raetz, C. R. H. An undecaprenyl phosphate-aminoarabinose flippase required for polymyxin resistance in Escherichia coli. *J. Biol. Chem.* 282, 36077–36089 (2007).

Zhang, X. & MacMillan, D. W. C. Alcohols as Latent Coupling Fragments for Metallaphotoredox Catalysis: Sp 3 -sp 2 Cross-Coupling of Oxalates with Aryl Halides. *J. Am. Chem. Soc.* 138, 13862–13865 (2016).

Part B

A molecular level investigation
of the protein machinary essential
for bacterial cell wall biosynthesis

The present part of the thesis deals with a research activity carried out at the Department of Physiology and Cellular Biophysics at Columbia University in the city of New York, under the supervision of Prof. Filippo Mancia

CHAPTER B1

INTRODUCTION

B1.1 A brief history of cryogenic electron microscopy (cryo-EM)

Structural characterization of proteins has always been a major achievement, not least as a fundamental step toward the rational design of new therapeutic targets. The ability to design drugs with improved specificity and efficacy relies on the knowledge of the specific three-dimensional structure that is characteristic of every single enzyme or protein molecule. Thus, structural biologists have always been constantly improving known techniques (such as X-ray crystallography and nuclear magnetic resonance or NMR) as well as developing new ones in order to push the resolution at which protein molecules can be imaged and, as final goal, structurally characterized. In the last decade we have witnessed the rapid development of single particle cryo-electron microscopy (cryo-EM) to

unveil the structural complexity of challenging protein targets as well as massive protein complexes. This technique, that has been for long complementary to X-ray crystallography and NMR, is now widely expected to be the dominant one, changing the field of structural biology in a profound and unprecedented way, facilitating new major discoveries.

The possibility to use an electron source to directly image biological samples was first discovered in the early 1970s, when cryo-EM was developed (Frank, J., 1975; Dubochet, J. *et al*., 1988; Henderson, R. *et al*., 1975 and 1990). The imaging process was made possible by applying a purified protein sample onto a small carbon grid, removing the excess of aqueous protein solution, and covering the grid with an electron rich stain such as uranyl acetate or formate. The beam, generated by an electron gun and focused by means of a series of electronic lenses,

was directed on the grid inserted in the high-vacuum of the microscope, and the image was recorded as a negative of the actual sample, since the electrons were only able to pass easily through the holes generated in the staining where the single protein molecules were localized. The images thus recorded contained the 2D projections of the biological macromolecules. De Rosier and Klug immediately demonstrated that such structures could be reconstructed by combining 2D projection images of the same object along different directions or orientations (De Rosier, D.J. and Klug, A., 1968). A further development was reached in the 1980s, when the plunge freezing technique made it possible to flash freeze a protein sample applied to a grid covered in a thin holey carbon film in liquid ethane, allowing to image macromolecules directly in the frozen aqueous solution (Adrian, M. *et al*., 1984). After that, the frozen grid was transferred to the electron

microscope and kept at near-liquid nitrogen temperature for imaging. This method is still used routinely without major changes, except that now a machine is used to blot and plunge grids with tunable parameters. Another limitation that had to be overcome was the poor signal to noise ratio (SNR) that was acquired because of the radiation damage by the high-energy electron beam limiting the total electron dose that a biological sample can handle. At first the use of 2D protein crystals was therefore mandatory in order to collect data at high resolution combining the phases calculated from the Fourier transformations of images and the amplitudes obtained from diffractions. Frank, in 1975, proposed an idea to determine protein structures without any crystallization required, by computationally combining images of many individual protein particles of the same type (Frank, J., 1975). A large number of images is needed to both

enhance SNR and to provide different views needed for the 3D reconstruction (Fernandez-Leiro, R. and Scheres, S.H.W., 2016). Furthermore, what electron micrographs record are projections of the specimen convoluted by a contrast transfer function (CTF), a sine function oscillating in a frequency-dependent manner. This CTF is determined by how much off the focus of an image is recorded, the so-called "defocus". To retain the highest resolution, images must be collected as close as possible to focus, but such images, however, have a very limited contrast. Images of a radiation sensitive frozen hydrated biological sample have to be recorded with a large defocus in order to generate sufficient contrast, thus limiting the high-resolution signal. This limits nonetheless the imaging of small macromolecules (smaller than 100 KDa) for which the contrast in the image is so low that a larger

defocus is needed, thus losing irreversibly the higher resolution information needed for 3D reconstruction.

The recent surge in high-resolution EM structures has gone by the name of "resolution revolution" (Cheng, Y., 2015 and 2018). The underlying reason for such enormous achievement is in a combination of transformative technological breakthroughs arising from the development of direct electron detection camera, as well as the implementation of new image processing algorithms. The exploitation of this kind of cameras strongly enhances the final quality of the produced micrographs since those are able to detect charges generated directly from electrons striking the camera sensor, thus localizing the electron with much greater precision than older methods would allow. These sensors also run at high frame rates, enabling cryo-EM images to be recorded as a stack of movie frames, each is recorded

in a short period of time. Being able to record images as movie stacks facilitated many new imaging approaches that are critical for maximizing the achievable resolution. Most importantly, it allows the correction of beam-induced image motion and partially mitigates radiation damage (Scheres, S.H.W., 2014; Brilot, A. F. *et al*., 2012; Li, X. *et al*., 2013).

An impressive amount of innovation has therefore led single particle cryo-EM to become, over the past 40 years, a routine and powerful method to determine atomic structures, shedding a whole new light on the field of structural biology (Figure B1.1).
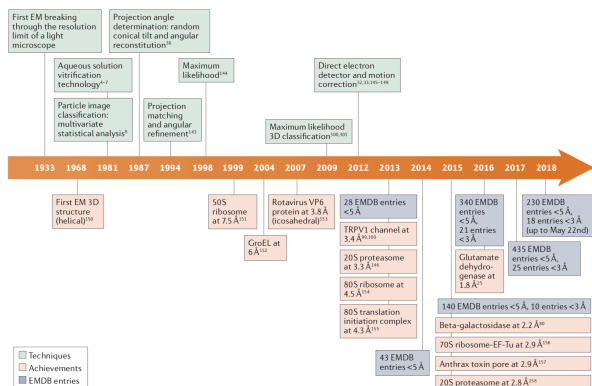
Figure B1.1 Cryo-EM timeline. EMDB: electron microscopy data bank; TRPV1, transient receptor potential cation channel subfamily V member 1 (Renaud, J.P. *et al*., 2018).

B1.2 Cryo-EM protein structure determination: how does it work?

In order to determine the atomic resolution structure of a protein by cryo-EM the first step required is to obtain a pure and monodispersed sample of the protein of interest (Thompson, R.F. *et al.*, 2016) (Figure B1.2).
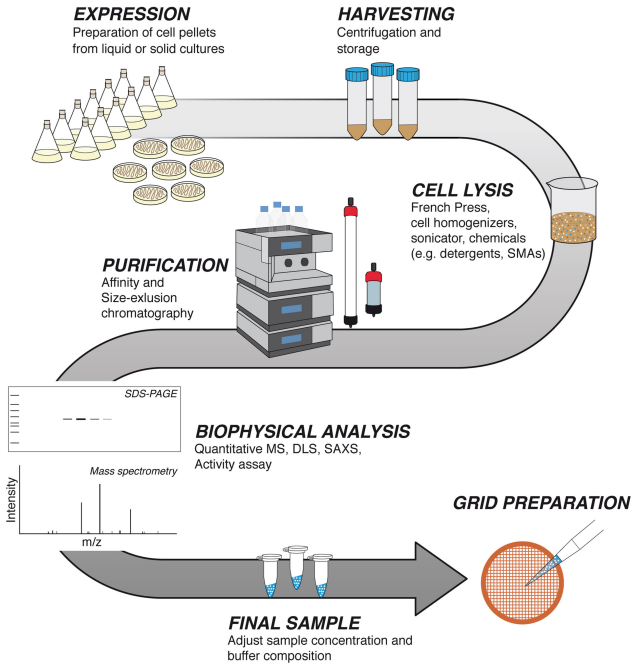
Figure B1.2 Generic protein purification workflow (Sgro, G.G. *et al*., 2018).

Chapter B1

First of all, typically the protein is expressed in a specific cell line in order to maximize the amount of expressed folded and functional protein.

Membrane proteins are classically trickier to purify in comparison to their soluble counterparts. An integral membrane protein has to be extracted from the native lipidic environment of the cell membrane by means of detergents capable of disrupting the lipidic double layer and cover and protect the protein thanks to their amphipatic nature (Seddon, A.M. et al., 2004). The solubilized protein can then be purified by different techniques including affinity chromatography and gel filtration size-exclusion chromatography. To further stabilize the membrane protein, it's then often necessary to reconstitute the protein of interest in a more native environment. Many different systems have been developed to give the best possible stability to

reconstituted membrane proteins and nowadays amphipols, styrene-maleic acid copolymer (SMA), diisobutyl-maleic acid copolymer (DIBMA) and nanodiscs are, among others, the most common ones (Skrzypek, R. *et al*., 2018). The reconstitution into nanodiscs of integral membrane proteins is used to best mimic the native lipidic bilayer. Nanodics consists of two truncated apolipoproteins wrapped around a bilayer of phospholipids (Denisov, I.G. and Sligar, S.G., 2016). The need for a broad application of this methodology to proteins of different size, shape and function led to many different versions of this scaffold system, that can be composed by apolipoproteins of different length such as membrane scaffold protein (MSP) 1D1, 1E3D1 or 2N2, and different phospholipidic compositions, enabling the fine tuning of the nanodiscs composition and size for the specific aim. In order to reconstitute the integral

membrane protein into nanodiscs, the detergent has to be removed from the protein surface and solution. Thus, the protein is incubated overnight in the presence of nanodiscs and hydrophobic polymeric beads to generate the best possible condition for the protein to transition to the pre-formed nanodiscs (Figure B1.3).
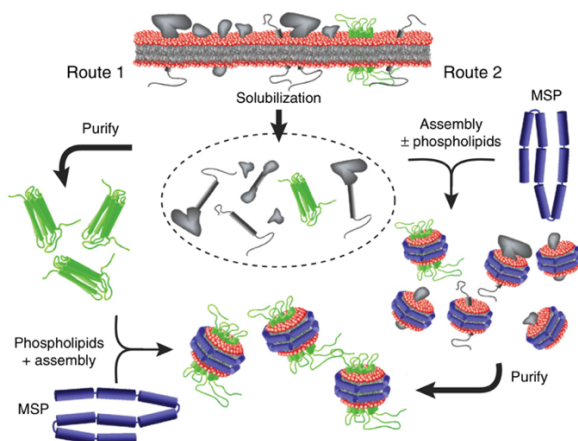
Figure B1.3 Nanodiscs reconstitution of membrane proteins (Denisov, I.G. and Sligar, S.G., 2016).

Once the protein is incorporated into the nanodiscs and its purity assessed by means of size exclusion chromatography and SDS-PAGE, the sample is flash frozen in a liquid ethane solution on cryo-EM grids using a plunge freezing instrument (such as a Vitrobot or a Leica). The grids are then stored in liquid nitrogen until they are imaged on the electron microscope. A grid showing a monodispersed sample with ice thickness of the right size to embed the single protein particles is usually screened on a screening microscope (FEI Tecnai F20, Tecnai T12 BioTWIN) and then collected on a second, more powerful electron microscope (FEI Polara F30, FEI Titan Krios) in order to gather as many micrographs as possible. The data analysis can finally be performed by means of specific software packages (Figure B1.4). Due to the huge number of data involved, researchers are taking advantage from advances in computing technology. The

latest software packages (such as MotionCor2, RELION 3, cryoSPARC 2) exploit graphic processing unit (GPU) acceleration for different parts data processing pipeline, leading to an easy and reproducible reconstruction of the 3D structure of the target protein (Baldwin, P.R. *et al*., 2018).
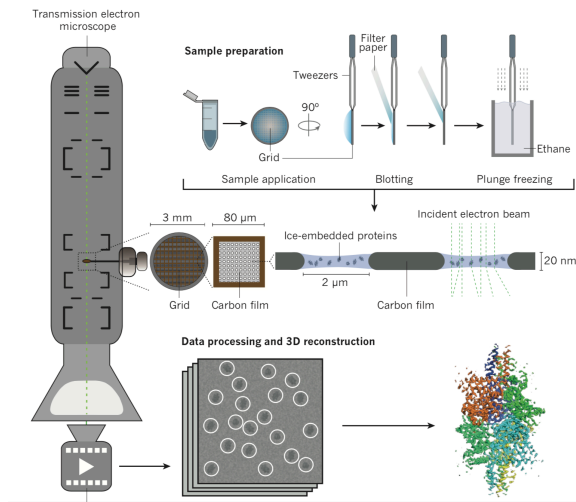
Figure B1.4 Protein structure determination through cryo-EM (Fernandez-Leiro, R. and Scheres, S.H.W., 2016).

A general workflow consists in the initial motion correction step, in which the movie frames are aligned to generate a single micrograph in which the single protein particles are corrected for the beam induced motion. After a contrast transfer function (CTF) estimation, it is possible to select a subset of manually picked particles from which initial 2D class averages are generated. These are consequently used as search models to identify computationally all the particles resembling the protein of interest within the full data sets of micrographs. Once all the protein particles have been picked, they are divided into 2D classes and those are used to reconstitute the initial 3D volume. Further refinement of this volume leads to an improved resolution of the density map, allowing the identification of the helical segments and finally of the side chains of the protein. The model is finally built in the density map, generating a coordinate structure file that

contains the three-dimensional structure of the protein of interest (Figure B1.5).
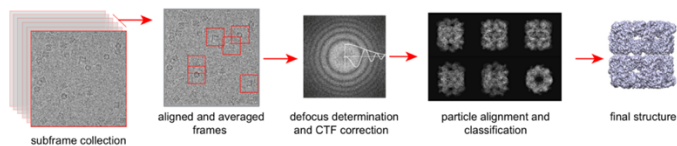
Figure B1.5 Schematic of single-particle protein reconstruction (Carroni, M. and Saibil, H.R., 2016).

B1.3 Aim of work

The development and implementation of antibiotics is one of the most important innovations of the modern era. Although their benefits are undeniable, we are witnessing a pharmaceutical arms race in which bacterial evolution is matching against our ability to discover new antimicrobial compounds.

Chapter B1

Bacteria have many biological resources to fight antibiotics, and we must approach the problem of antibiotic resistance at many levels.

Recommendations and strategies to fight it are several, including the discovery of novel targets to develop new drugs.

The goal of this project is to characterize the structural and functional features of the RodA-PBP2 complex, which is involved in PG biosynthesis. More in general, we believe that a thorough understanding of bacterial biology and such essential processes can pave the way for the pursuit of novel potent antibiotics.

CHAPTER B2

Structural and functional investigation of Roda-PBP2 fusion protein

B2.1 The role of penicillin-binding proteins (PBPs) in peptidoglycan synthesis

All bacteria have a cell wall, which provides them unique structural characteristics and pathogen-host interaction profiles (Messner, P. *et al*., 2013).

Peptidoglycan is a key component of the cell wall in almost all Gram-negative and Gram-positive bacteria. As previously described in the general introduction, PG synthesis involves many enzymes including glycosyltransferase (GTase) to polymerize the glycan chains and transpeptidases (TPase) to crosslink the peptides. The TPase enzymes are the so-called penicillin-binding proteins (PBPs), which were first identified as targets of ß-lactam antibiotic penicillin (Typas, A. *et al*., 2012; Taguchi, A. *et al*., 2019).

The PBPs include several types of enzymes, which vary by species. However, they are mainly categorized according to their molecular weight into low molecular mass (LMM) PBPs and high molecular mass (HMM) PBPs. LMM-PBPs are less defined in their biological roles. They have been implicated in peptidoglycan remodeling during cell division as some members of the sub-type have been identified as having carboxypeptidation and peptide bond hydrolysis activities.

HMM-PBPs are known to be essential and have enzymatic functions related to the transpeptidation and transglycosylation of peptidoglycan. HMM-PBPs can be further classified into class A (aPBPs) and class B (bPBPs). Class A HMM-PBPs have been characterized as dual function enzymes, with both glycosyltransferase and transpeptidase activity. Class B PBPs have been shown to have only transpeptidase activity (Goffin, C. and Ghuysen,

J.M., 1998). Class B PBPs are also essential components of larger protein complexes responsible for either cell shape, growth and elongation (elongasome) and cell division (divisome) (Spratt, B.G., 1975; den Blaauwen, T. *et al.*, 2008; Szwedziak, P. and Lowe, J., 2013). For example, in *H. influenzae* two different protein complexes comprising the cell-elongation-transpeptidase PBP2 and the cell-division-transpeptidase PBP3 were found (Cabeen, M.T. and Jacobs-Wagner, C., 2005).

Beyond its contribution to bacterial biology in general, understanding the protein-protein interactions involving penicillin-binding proteins may be of broader application, since the disruption of protein-protein interfaces may be a promising strategy for future antibiotic development.

B2.1.1 Crystal structure of PBP2 from *Helicobacter pylori*

The rod-shape in Gram-negative bacteria is maintained by a multiprotein "elongase" complex involving, among other proteins, the cell-elongation-transpeptidase PBP2, which belongs to HMM class B PBPs category. It localizes in the lateral bacterial cell wall and at the division site with a temporary role in cell division initiation. PBP2, however, play a major role in the elongation process (Levy, N. *et al*., 2019).

The crystal structure of PBP2 from *H. pylori* (*Hp*PBP2; PDB 5LP4) was solved to 3.0 Å by molecular replacement using the structure of PBP3 from *P. aeruginosa* as a model (Figure B2.1).
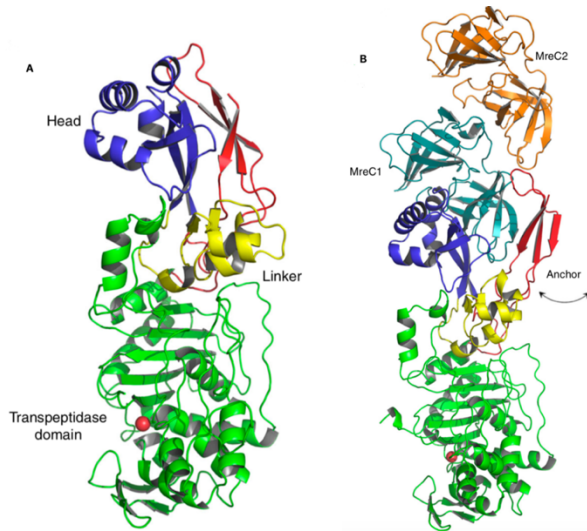
Figure B2.1. Structure of PBP2 from *Heliobacter pylori*. A) The structure of PBP2 from *H. pylori* in its apo state. B) The structure of *H. pylori* PBP2 bound to two MreC molecules, showing a repositioning of the anchor domain to accommodate binding. Figure adapted from Contreras-Martel, C. et al., 2017.

It showed the characteristic fold of class B PBPs containing a nonpenicillin-binding domain and a transpeptidase domain (Contreras-Martel, C. *et al*., 2017). *Hp*PBP2 is made up of a three-part N-terminal domain (the nonpenicillin-binding domain) containing a helical "head," a three beta-strand "anchor", and a mostly helical "linker" region. Following the N-terminal domain is the transpeptidase domain, containing a catalytic site with three conserved sequence motifs.

The structure of the soluble domain of *Hp*PBP2 in complex with the soluble domain of MreC, a bitopic membrane protein that is essential for cell shape, was also solved to 2.7 Å resolution (PDB 5LP5). The overall structure of the complex indicated that MreC binds PBP2 at its N-terminal domain, causing a rearrangement of the N-terminal portion in which the anchor domain swings away from the head domain to accommodate MreC

binding. The interactions between elongasome proteins have a transient nature, so it should be noted that these different interactions with PBP2 are not necessarily mutually exclusive. However, their disruption within the elongasome leads to cell shape perturbations and eventual bacterial cell death, indicating the importance of the tight orchestration of elongasome formation steps (Contreras-Martel, C. *et al*., 2017).

B2.2 The role of <u>s</u>hape, <u>e</u>longation, <u>d</u>ivision and <u>s</u>porulation (SEDS) proteins

Transmembrane enzymes referred to as SEDS proteins are named for their critical roles in bacterial cell wall biology. Bacterial proteins FtsW, RodA and SpoVE are SEDS proteins, that share sequence homology and participate in peptidoglycan synthesis during different growth and maturation processes. RodA participates in elongation before cell division, SpoVE participates in sporulation and FtsW participates in cell division (Ruiz, N., 2015). It is also known they form complexes with type B PBPs.

SpoVE, a sporulation SEDS protein in *B. subtilis*, has been shown to form a direct functional complex with HMM type B PBP, SpoVD. A recombinant fusion of these

two proteins was designed and proved to be functional *in vivo* (Fay, A., *et al*., 2010). It was also shown that the introduction of a loss-of-function point mutation into either individual protein, deleted function of the complex, suggesting cooperative function. Since the characterization of the SpoVE/SpoVD protein-protein functional interactions, other SEDS proteins, FtsW and RodA, have been shown to interact directly with class B PBPs in the divisome and elongasome respectively (Fay, A., *et al*., 2010; Fraipont, C., *et al*., 2011; Cho, H., *et al*., 2016). Though SEDS proteins are understood to be important for peptidoglycan synthesis, having a role in key bacterial processes, and interact with class B PBPs, their precise functional characterization has been somewhat of a debate. FtsW, for example, has been implicated as the Lipid II flippase, and has been demonstrated *in vitro* to promote the movement of Lipid II across a bilayer

(Mohammadi, T., *et al*., 2011; Mohammadi, T., *et al*., 2014). However, a homologous protein RodA, has been recently characterized as a glycosyltransferase, functioning in complex with a class B PBP (PBP2) to complete the first step of peptidoglycan synthesis (Emami, K., *et al*., 2017). Additionally, FtsW has been recently shown to also function as a glycosyltransferase (Taguchi, A.W. *et al*., 2019). There are two hypothesized models in the field (demonstrated in Figure B2.2 fusing RodA as an example): one in which SEDS proteins function as dual purpose enzymes in complex with class B PBPs to flip lipid II across the membrane and then polymerize peptidoglycan, and the other in which the MurJ protein acts as the lipid II flippase and the SEDS-PBP complex function solely to polymerize peptidoglycan.
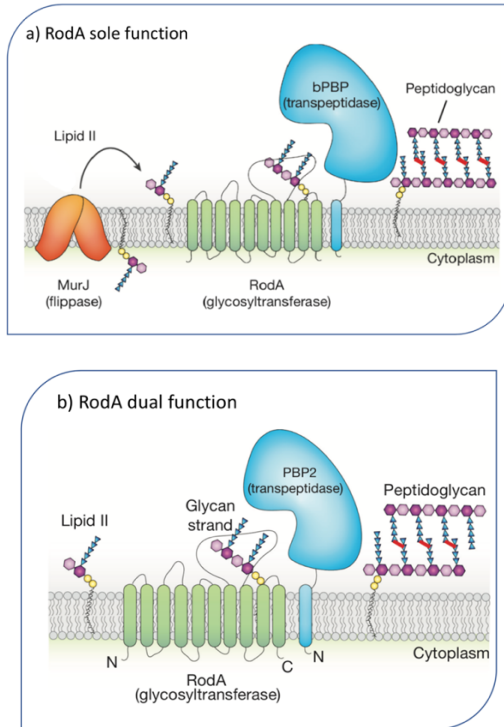
Figure B2.2 Two models of SEDS-PBP function. These models use RodA as an example. They are applicable to SEDS proteins in general. Figure adapted from Sjodt, M. et al., 2018.

B2.2.1 Crystal structure of RodA protein from *Thermus thermophilus*

The precise function of SEDS proteins was for a long time poorly understood, but it recently was revealed that the prototypical SEDS family member RodA is a glycosyltransferase.

In 2018 the crystal structure of RodA from *T. thermophilus* was determined to 2.9 Å resolution using evolutionary coupling-enabled molecular replacement (EC-MR), taking advantage of the fact that protein residues that interact structurally tend to co-evolve to maintain structural and functional integrity (Sjodt, M. *et al*., 2018) (Figure B2.3).

This structure showed ten transmembrane helices connected by loops, with a putative lipid substrate-binding

site between TM2 and TM3, and a central hydrophilic cavity open to the extracellular face of the protein. Within the central cavity, an absolutely conserved salt bridge was identified (E108/K111). The presence of a PBP2 interacting domain located between TM8 and TM9 of RodA was also suggested. Thus, to build a cell wall, a key step is peptide crosslinking catalyzed by the aPBPs and bPBPs. Numerous studies indicated that SEDS proteins and bPBPs are likely to form a complex in cells operating both glycan-strand polymerization and peptide crosslinking.
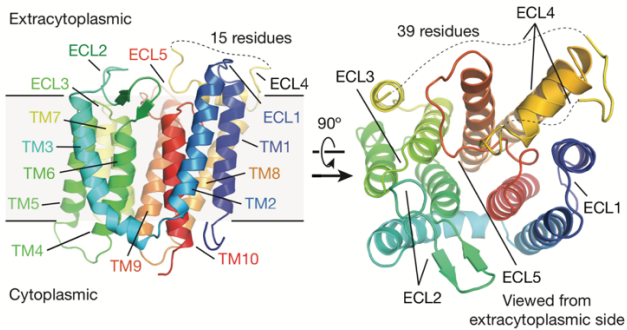
Figure B2.3 Structure of RodA from *Thermus thermophilus*. Architecture of RodA reveals ten transmembrane helices (TM1-10) and 5 extracellular loops (ECL1-5) with a cone shaped central cavity. ECL4 was not resolved (Sjodt, M. *et al.*, 2018).

Up to now, the characterization of this protein-protein interface remains far from being completely understood. Further, there is no experimental evidence that RodA could accomplish the flipping of Lipid II, even though reports suggested that FtsW, a RodA homolog, is a Lipid II flippase (Mohammadi, T., et al., 2011). However, the

216

results reported above give a framework to better understand bacterial cell wall synthesis and SEDS protein function.

B2.3 Cryo-EM investigation of RodA-PBP2 fusion protein structure

Though crystal structures of both RodA (Sjodt, M. *et al*., 2018) and PBP2 (Contreras-Martel, C. *et al.*, 2017; Lovering, A.L., *et al*., 2007; Lovering, A.L., *et al*., 2008) are available, the interaction between the two proteins and their joint enzymatic activity remains poorly characterized. Thus, the structure of RodA protein in complex with PBP2 was investigated by cryo-EM.

Recent advances in the field of cryo-EM, such as the development and implementation of direct detectors

and other computational methods, led to what has been coined the "resolution revolution" (Kuhlbrandt, W., 2014). Achieving high resolution structures by cryo- EM is now possible for macromolecules that were previously too small for this technique (Nitta, R., *et al*., 2018). SEDS proteins by themselves, which are only around 40-50 kDa, would still be too small and featureless to be successfully resolved by cryo-EM, but as fusions with PBPs the complexes are now of a suitable size for cryo-EM given the recent advancements in the field (110-130 kDa).

Thus, based upon the ability of a chimera of the isofunctional RodA-PBP2 genes in *B. subtilis* to complement mutations in the same organism (Sjodt, M. *et al*., 2018), a fusion protein of RodA-PBP2 was made from *E. coli.* More in detail, in collaboration with Jonathan Dworkin's research group in the Department of Microbiology and Immunology at Columbia University,

which already made *in vivo* functional recombinant fusions of SEDS-PBP proteins (SpoVE-SpoVD and FtsW-PBP3) (Fay, A., *et al*., 2010), RodA-PBP2 fusion protein was designed with the PBP linked to the C-terminus of the SEDS protein by a flexible linker bearing the amino acid sequence GSGSGS (Figure B2.4).
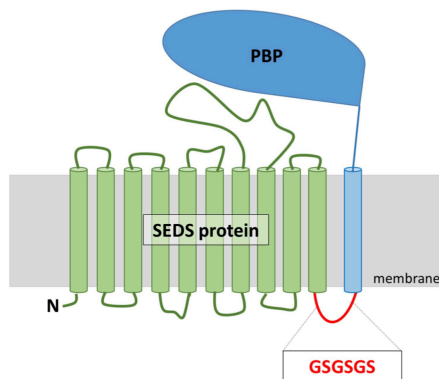
Figure B2.4 Design of SEDS-PBP fusion proteins.

The resulting constructs were tested for expression in small scale and scaled up for purification and structural investigation by cryo-EM.

RodA-PBP2 from E. *coli* was purified in detergent, then reconstituted in an encapsulating lipid-filled nanodiscs carrier protein and run on size exclusion chromatography (Figure B2.5).
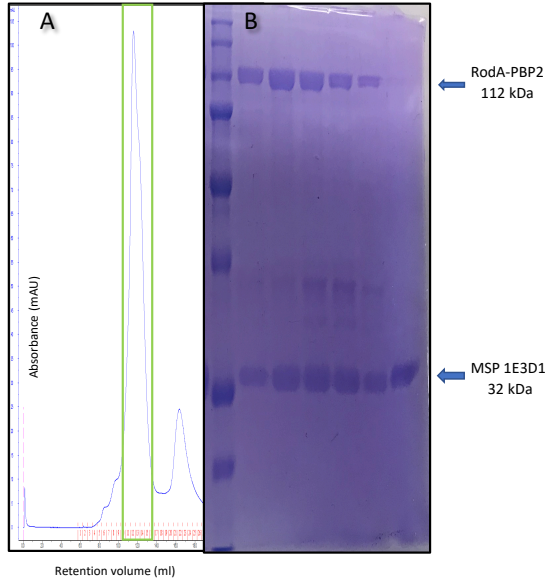
Figure B2.5 A) Size exclusion chromatography profile of RodA-PBP2 after nanodiscs incorporation. Green bar indicates the fraction that was taken for subsequent cryo-EM grid preparation. B) SDS-PAGE analysis of fractions collected from the SEC run shown in A.

The resulting SEC elution profile revealed two main overlapping peaks. The peak further to the right was taken for cryo-EM studies in an attempt to characterize a monomeric protein. Further, SDS-PAGE analysis of the resulting peak suggested successful incorporation into nanodiscs, as the MSP protein is clearly seen on the gel in the same fractions as the RodA-PBP2 fusion protein. The sample concentration and freezing conditions were optimized *via* several rounds of grid preparation followed by screening on a Tecnai F20. A full data collection was performed on the Titan Krios 3 microscope at Simons Electron Microscopy Center (SEMC).

A representative micrograph from this collection is shown in figure and resulting 2D class averages in figure. Comparing these 2D classes to the available structures (Figure B2.6), secondary structural elements of the protein can already be recognized.
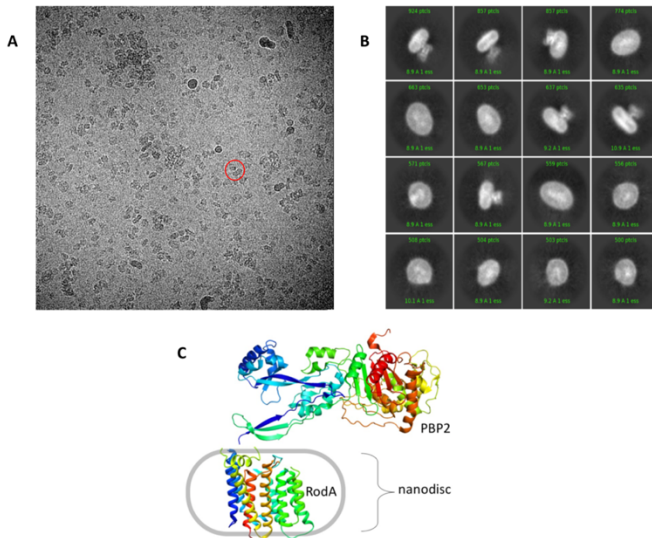
Figure B2.6. A) Representative micrograph from the Titan Krios data collection. B) Resulting 2D classes calculated using cryoSPARC 2. C) Simple composite of available structures of RodA (PDB 6BAR) and PBP2 (PDB 5LP5) of what is expected for the RodA- PBP2 complex.

These data were further processed, and a preliminary 3D map was reconstructed at around 5 Å resolution (Fig. Figure B2.7 **A**). Overlaying this 3D reconstruction with the individual structures of RodA and PBP2 (Figure B2.7 **B**) it can be noticed that the insertion of the single transmembrane spanning helix of PBP2 into the ten membrane spanning helices of RodA causes a conformational dependent domain movement (CDDM) consistent with the rapid lipid II polymerization activity of RodA. Clear changes in the PBP2 structure in both the MreC protein binding domain (MreC-BD) as well as the transpeptidase domain opposite are apparent. The complex also shows that the PBP is orientated parallel to the membrane proving a first idea of the spatial arrangement of these.
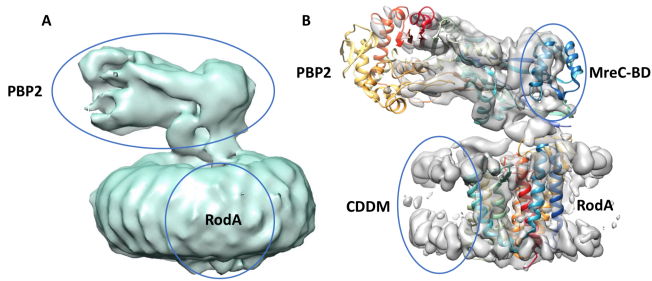
Figure B2.7 A) Preliminary 3D reconstruction of R odA-PBP2 from cryo -EM data using cryoSPARC 2. B) Overlayed 3D reconstruction of RodA-PBP2 with the individual structures of RodA and PBP2.

To date, the main objective is to obtain a high-resolution 3D reconstruction of RodA-PBP2. The distribution of particle views included in this 3D reconstruction showed heavy clustering and suggested a preferred orientation of the particles frozen on the grids. Preferred particle orientation is a classic problem in cryo-EM and methods development to compensate for preferred

orientation have been the focus of many research groups (Drulyte, I. *et al*., 2018; Tan, Y.Z. *et al*., 2017). There are different ways to solve the preferred orientation issue of RodA-PBP2. One way would be to collect data with a tilt as described in Tan, Y.Z. *et al*., 2017, which allows the collection of a larger number of particle views by tilting the grid in the microscope. However, there are some limitations to using this approach. Other ways to solve the issue would be to include additives, such as glycerol, or surfactants in the protein solution before freezing grids that will insulate the particles in the thin aqueous layer from the forces present at the air-water interface that could be influencing the particle orientation. There are also many other approaches that could be taken at the sample preparation level, such as adjusting the pH of the buffering solution or using different blotting paper on the plunge freezer (Drulyte, I., *et al*., 2018).

B2.4 Functional studies of RodA-PBP2 fusion protein

In collaboration with David Roper at the University of Warwick, whose expertise lies in the biochemical investigation of peptidoglycan biosynthesis and antibiotic resistance (Galley, N.F. et al., 2014; Punekar, A.S. *et al*., 2018; Clarke, T.B. *et al*., 2009), the *E. coli* RodA-PBP2 fusion protein reconstituted into nanodiscs was confirmed to be functional *in vitro* as it can complete both the glycosyltransferase reaction as well as the transpeptidase one. The assays performed by David Roper's group are well established, albeit difficult to perform, gel-based techniques (Galley, N.F. et al., 2014; Schägger, H. and von Jagow, G., 1987; Lesse, A.J. *et al*., 1990; Barrett, D. *et al*., 2007; Helassa, N. et al., 2012), in which fluorescently labelled Lipid II variants are

incubated with the purified enzyme and ß-lactam antibiotics to confirm the specificity of the reaction. The discrete glycan products of increasing size can be separated on a 9% acrylamide gel to see the processive glycosyltransferase and transpeptidase activity of the enzyme.

In particular, these assays demonstrated the rapid lipid II polymerization ability of the purified RodA-PBP2 fusion protein in which PG crosslinking is specifically inhibited by PBP2 specific ß-lactams and produces high molecular weight crosslinked PG.

On the contrary, putative flippase activity of SEDS protein RodA still remains unknown. With the purpose to investigate it, four mutants of RodA-PBP2 fusion protein were designed and produced *via* site-directed mutagenesis of specific amino acid residues in RodA

glycosyltransferase and/or PBP2 transpeptidase active sites:

- *E. coli* RodA-PBP2 mutants D262A and D262N, where the mutation is located in the RodA transglycosylase active site abolishing transglycosylase activity;

- *E. coli* RodA-PBP2 mutant D447N with mutation in the PBP2 transpeptidase active site having no effect on the glycosylase activity of RodA;

- *E. coli* RodA-PBP2 the double mutant D262A and D447N with mutations in the RodA and PBP2 domains respectively also abolishing transglycosylase activity.

Thus, it seems likely that blocking glycosyltransferase activity or transpeptidase activity or both for one of these enzymes could potentially block the

flippase activity and trap this complex with lipid II bound. The resulting four constructs were tested for expression in small scale and scaled up for purification. They were purified in detergent and reconstituted successfully in nanodiscs (Figure B2.8). Those mutants are currently under investigation to assay RodA putative flippase activity.
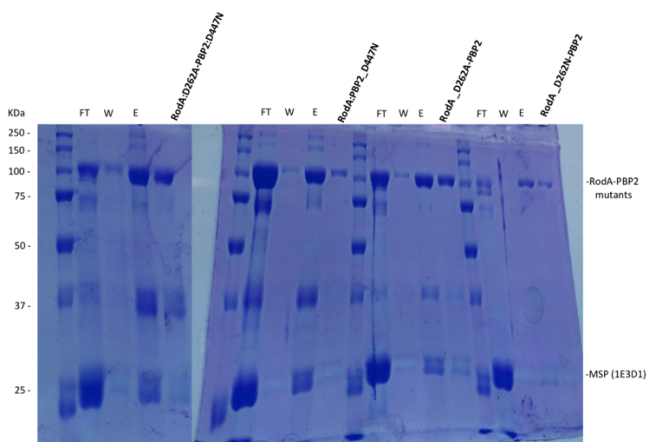
Figure B2.8 SDS-PAGE gels of RodA-PBP2 mutants reconstituted into nanodiscs

B2.5 Conclusions

Recent evidence suggests that the core of the PG biosynthetic complex consists of the class B PBPs such as PBP2 and PBP3, that work together with SEDs proteins, FtsW and RodA, respectively. These enzymatic complexes are involved in peptidoglycan production during cell division (FtsW-PBP3) and cell elongation (RodA-PBP2) and are also the key targets for most clinically used β-lactam compounds. The challenge is thus to understand the molecular interplay between all the protein partners of the PG biosynthetic complex and how this regulates overall cell wall biosynthesis.

Here, the structural and functional properties of RodA-PBP2 complex were investigated.

A preliminary 3D cryo-EM reconstruction of *E. coli* RodA-PBP2 fusion protein reconstituted into lipid

nanodiscs was reported. Further, *E. coli* RodA-PBP2 fusion protein was demonstrated to be functional *in vitro* thanks to the biochemical assays carried out by David Roper at the University of Warwick.

The future objective, which comprises ongoing work, is solving the issue of preferred orientation observed in the RodA-PBP2 cryo-EM data to yield a high-resolution 3D structure of this complex. This latter will inform biochemical functional investigation of the purified enzyme as well as genetic investigation of the complex *in vivo*.

Ultimately, the hope is that a better understanding of how the individual components of the RodA-PBP2 complex achieve their joint function in the biosynthesis of PG will provide clues as to how to disrupt this conserved bacterial feature, in the pursuit of novel potent antibiotics against a classic target.

CHAPTER B3

General Methods

B3.1 Expression and purification of RodA-PBP2 fusion protein (wild-type and mutants)

To express the target protein, BL21 PLysS E. coli strain was transformed with 1 μL RodA-PBP2 in pNYCOMPS-N23 expression vector. 200 μL of this transformation was used to inoculate a starter culture (2xYT containing 100 μg/ml Ampicillin and 35 μg/ml Chloramphenicol), which was grown overnight at 37°C. The next day, 2xYT containing 100 μg/ml Ampicillin and 35 μg/ml Chloramphenicol was inoculated with 10 ml of starter culture. The cultures were grown at 37°C to an OD600 between 0.8 and 1.0. Then they were cooled to room temperature, induced by adding a final concentration of 200 μM IPTG and incubated overnight at 22°C. The

next day the cultures were harvested by spinning at 4000 rpm for 30 minutes at 4°C. The cell pellets were then used immediately for preparing membranes or stored at -80°C for future use.

The volume of culture grown varied with experiment, 20 ml for small-scale expression tests (SDS-PAGE analysis), 250 ml for mid-scale purification (HPLC detergent screening) and minimum of 800 ml for large-scale purification aimed at structural characterization experiments.

To prepare membranes, cell pellets were resuspended in Lysis buffer (20 mM HEPES, pH 7, 200 mM NaCl, 4µL/100mL RNase, 10µg/mL solid DNase, 1mM PMSF, 1mM Complete protease inhibitor cocktail (Roche) and 1mM TCEP) and lysed by sonication with a tip sonicator (small and mid-scale) or by pressure using an Avestin Emulsiflex C3 for 3 passages (large scale). Lysed

cells were centrifuged 34,000 rpm and 4°C for 30 minutes. Supernatants were discarded and the pelleted membrane fraction was resuspended in a high salt buffer (20 mM HEPES, pH 7, 500 mM NaCl, 1 mM PMSF, 1mM Complete protease inhibitor cocktail (Roche) and 1mM TCEP) using a glass homogenizer. The washed membranes were centrifuged at 34,000 rpm and 4°C for 30 minutes. Supernatants were discarded and the membrane fraction was resuspended in Lysis Buffer (20 mM HEPES, pH 7, 500 mM NaCl, 20% glycerol, 4μL/100mL RNase, 10μg/mL solid DNase, 1mM PMSF, 1mM Complete protease inhibitor cocktail (Roche) and 1mM TCEP) at the same volume as in the first step of the membrane preparation protocol using a glass homogenizer, resulting in a membrane resuspension of lysis buffer. The membranes were then used immediately

for subsequent protein purification or stored at -80°C for future use.

The RodA-PBP2 complex is not very stable and cannot be left overnight for binding to nickel resin or for dialysis. To avoid protein precipitation, the purification protocol was performed in one day without any overnight incubation steps.

For protein purification, DDM was added to prepared membranes to a final concentration of 1% (w/v) to solubilize and extract the target proteins from the membrane. Solubilization was carried out for 2 hours at 4°C with gentle agitation or rotation. Samples were then centrifuged at 34,000 rpm at 4°C for 30 minutes to separate the insoluble fraction. The supernatant was added to Ni-NTA resin (Qiagen), which had been washed with water and pre-equilibrated with buffer containing 20mM HEPES, pH 7, 500 mM NaCl, 40mM imidazole reducing

non- specific binding to the nickel resin, and 0.1% DDM. Samples were incubated for 2 hours at 4°C with gentle agitation or rotation to facilitate protein binding to the resin. Samples were incubated on ice to settle the resin, then the supernatant was removed and discarded. The remaining resin was washed with 10 column volumes (C.V.) of wash buffer (20 mM HEPES, pH 7, 500 mM NaCl, 60 mM Imidazole, 20% glycerol, 0.1% DDM and 10 mM ATP Magnesium salt) and eluted with 3-4 C.V. of elution buffer (20 mM HEPES, pH 7, 500 mM NaCl, 300 mM Imidazole, 20% glycerol, 1% DDM). Eluted protein was exchanged to buffer without imidazole (20 mM HEPES, pH 7, 500 mM NaCl, 20% glycerol, 0.1 % DDM) using a G-25 or PD-10 desalting column (GE Healthcare). Protein was concentrated to 13 μM with a concentrator (Amicon® ultra centrifugal filters) with a molecular weight cut-off of 100 kDa. The protein concentration was

measured with a NanoDrop spectrophotometer (Thermo Fisher Scientific) using the calculated extinction coefficient of the target protein. The resulting protein was then reconstituted into lipid nanodiscs.

The same procedure was followed for expression and purification of RodA-PBP2 fusion protein mutants.

B3.2 Reconstitution of RodA-PBP2 fusion protein into lipid nanodiscs

To prepare membrane scaffold proteins (MSPs) 1E3D1, *E. coli* One Shot BL21 Star competent cells (ThermoFisher Scientific) were transformed with pMSP1E3D1 (Addgene) and plated on a LB Agar plate containing 35 μg/ml Kanamycin and grown overnight at 37°C. A single colony from the resulting plate was used to inoculate 50 mL of LB containing 35 μg/ml Kanamycin. The culture was grown overnight at 37°C. 25 mL of the starter culture is added to 800 mL of 2xYT containing 35 μg/ml Kanamycin and grown at 37°C until the OD600 is between 1 and 1.2, when the incubator temperature was reduced to 28°C and 0.4 mM IPTG is added. Cells were grown for an additional 4 hours at this temperature. Cells were harvested at 4000 rpm at 4°C, supernatant removed,

and the resulting cell pellets were used immediately for protein purification or stored at -80°C for subsequent use.

Cell pellets were resuspended in 15 mL pre-chilled lysis buffer (per 800 mL of bacterial culture) containing 20 mM HEPES, pH 7.5, 200 mM sodium chloride, 20 mM magnesium sulfate, RNase, DNase, PMSF, Complete protease inhibitor cocktail (Roche) and 1mM TCEP. Cells were lysed on ice by sonication at an amplitude of 35 W/cm^2 for 20 minutes, alternating 30 seconds on and 30 seconds off. The lysed cells were then centrifuged at 34,000 rpm for 30 minutes at 4°C.

The supernatant was passed through a column of pre-equilibrated Ni-NTA resin (2 mL of nickel resin per 800 mL bacterial culture). The resin was washed with 3 C.V. of Cholate Buffer (20 mM HEPES, pH 7.5, 0.3M sodium chloride and 50mM sodium cholate) and then washed with 10 C.V. of Wash Buffer (20 mM HEPES, pH

7.5, 200 mM sodium chloride, 20 mM Imidazole) and then eluted with 4 C.V. of Elution Buffer (20 mM HEPES, pH 7.5, 200 mM sodium chloride, 300 mM Imidazole). The eluted protein was dialyzed against 1 L of Dialysis Buffer (20mM Hepes pH 7.5, 150mM sodium chloride) in the presence of TEV protease (1 mg TEV protease per 800 mL bacterial culture). Dialysis was carried out overnight at 4°C. Resulting protein was concentrated to about 10 mg/ml and stored in aliquots for future use.

To prepare lipids for nanodiscs reconstitution, 1-palmitoyl-2-oleoyl-sn-glycero-3-phospho-(1'-rac-glycerol) (POPG) (Avanti Polar Lipids) in powder form was weighed into a glass vial. Buffer containing 20 mM HEPES, pH 7 and 150 mM NaCl was added to make a 20 mM lipid solution. The amount of required lipids was calculated from the average molecular weight provided by Avanti Polar Lipids. The lipid mixture was then sonicated

on a low setting with a tip sonicator until the lipid solution was nearly clear and opalescent. This was used immediately or stored in aliquots at -20°C for future use.

RodA-PBP2 was reconstituted into nanodiscs using the previously described MSP and lipids. Pure desalted protein was added to POPG and "medium" MSP 1E3D1 at a molar ratio of 1:300:5 (protein:lipid:MSP). The reaction mixture was incubated for 2 hours at 4°C with gentile agitation and protected from light. After incubation, 100 mg of Bio- Beads (BioRad) per 1 mL of nanodiscs mixture was added to remove the detergent and initiate nanodiscs formation. The mixture with Bio-Beads was incubated overnight at 4°C with gentile agitation. The next day, the mixture was removed from Bio-Beads by careful pipetting. To remove excess lipids and empty nanodiscs the protein incorporated into nanodiscs was then added to fresh Ni-NTA resin, which had been washed with

water and pre-equilibrated with buffer containing 20 mM HEPES and pH 7, 500 mM NaCl, 40 mM imidazole. Binding was carried out for 2 hours at 4°C with gentle agitation or rotation. After binding, the nickel resin was washed with 10 column volumes (C.V.) of wash buffer (20 mM HEPES, pH 7, 500 mM NaCl, 60 mM Imidazole) and eluted with 3-4 C.V. of elution buffer (20 mM HEPES, pH 7, 500 mM NaCl, 300 mM Imidazole) both without detergent. The resulting protein in nanodiscs was subjected to size exclusion chromatography (SEC) in a detergent-free buffer (containing 20 mM HEPES, pH 7 and 200 mM NaCl) to assess protein quality, and collect fractions of pure, stable protein in nanodiscs.

The same procedure was followed for lipid nanodiscs reconstitution of RodA-PBP2 fusion protein mutants.

B3.3 RodA-PBP2 Cryo-EM grids preparation, data collection and processing

For cryo-EM, grids were prepared using a Vitribot (FEI) plunge freezer. 3 µl of purified protein reconstituted into POPG lipid nanodiscs at concentrations ranging from 0.15 to 0.8 mg/ml were applied to C-Flat grids (CF-1.2/1.3-3Cu-50; Electron Microscopy Sciences) or gold grids (Ultra AU Foil R 0.6/1 300 Mesh; QuantaFoil), incubated for 30 seconds, blotted with filter paper for times ranging from 4 to 8 seconds and flash frozen in liquid ethane and stored in liquid nitrogen. Prepared grids were imaged with one of the following microscopes: Tecnai F20 (FEI) housed at SEMC, Tecnai T12 (FEI) housed at SEMC, Tecnai F20 (FEI) housed at Columbia University, Tecnai Polara F30 (FEI) housed at Columbia, Titan Krios (FEI) housed at SEMC. Data were collected

and visualized with either Leginon or EPU. Frame alignment and dose weighting were performed with MotionCor2 and CTF estimation was performed using Gctf. 2D particle alignment, 3D reconstruction and refinement were carried out using RELION 3 and cryoSPARC 2.

CHAPTER B4

Bibliography

Adrian, M., Dubochet, J., Lepault, J., & McDowall, A. W. Cryo-electron microscopy of viruses. *Nature*, *308*(5954), 32 (1984).

Baldwin, P. R., Tan, Y. Z., Eng, E. T., Rice, W. J., Noble, A. J., Negro, C. J., Cianfrocco, M. A., Potter, S. C., Carragher, B. Big data in cryoEM: automated collection, processing and accessibility of EM data. *Current opinion in microbiology*, *43*, 1-8 (2018).

Barrett, D., Wang, T. S. A., Yuan, Y., Zhang, Y., Kahne, D., & Walker, S. Analysis of glycan polymers

produced by peptidoglycan glycosyltransferases. *Journal of Biological Chemistry*. 282(44), 31964-31971 (2007).

Brilot, A. F., Chen, J. Z., Cheng, A., Pan, J., Harrison, S. C., Potter, C. S., Carragher, B., Henderson, R., Grigorieff, N. Beam-induced motion of vitrified specimen on holey carbon film. *Journal of structural biology*, *177*(3), 630-637 (2012).

Cabeen, M. T. & Jacobs-Wagner, C. Bacterial cell shape. *Nat. Rev. Microbiol.* 3, 601–610 (2005).

Carroni, M. & Saibil, H. R. Cryo electron microscopy to determine the structure of macromolecular complexes. *Methods* 95, 78–85 (2016).

Cheng, Y. Membrane protein structural biology in the era of single particle cryo-EM. *Curr. Opin. Struct. Biol.* 52, 58–63 (2018).

Cheng, Y. Single-particle Cryo-EM at crystallographic resolution. *Cell* 161, 450–457 (2015).

Cho, H., Wivagg, C. N., Kapoor, M., Barry, Z., Rohs, P. D., Suh, H., Marto, J. A., Garner, E. C., Bernhardt, T. G. (2016). Bacterial cell wall biogenesis is mediated by SEDS and PBP polymerase families functioning semi-autonomously. *Nature microbiology*. 1(10), 16172.

Clarke, T. B., Kawai, F., Park, S. Y., Tame, J. R., Dowson, C. G., Roper, D. I. Mutational analysis of the substrate specificity of Escherichia coli penicillin binding protein 4. *Biochemistry*, *48*(12), 2675-2683 (2009).

Contreras-Martel, C. *et al.* Molecular architecture of the PBP2-MreC core bacterial cell wall synthesis complex. *Nat. Commun.* 8, 1–10 (2017).

De Rosier, D. J., & Klug, A. Reconstruction of three-dimensional structures from electron micrographs. *Nature*. 217 (5124), 130 (1968).

den Blaauwen, T., De Pedro, M. A., Nguyen-Disteche, M., & Ayala, J. A. Morphogenesis of rod-shaped sacculi. *FEMS microbiology reviews*, *32*(2), 321-344 (2008).

Denisov, I. G., & Sligar, S. G. Nanodiscs for structural and functional studies of membrane proteins. *Nature structural & molecular biology*. 23(6), 481 (2016).

Drulyte, I., Johnson, R. M., Hesketh, E. L., Hurdiss, D. L., Scarff, C. A., Porav, S. A., Ranson, N. A., Muench, S. P., Thompson, R. F. Approaches to altering particle distributions in cryo-electron microscopy sample preparation. *Acta Crystallographica Section D: Structural Biology*, *74*(6) (2018).

Dubochet, J., Adrian, M., Chang, J. J., Homo, J. C., Lepault, J., McDowall, A. W., & Schultz, P. Cryo-electron

microscopy of vitrified specimens. *Quarterly reviews of biophysics*. 21(2), 129-228 (1988).

Emami, K., Guyet, A., Kawai, Y., Devi, J., Wu, L. J., Allenby, N., Daniel, R.A., Errington, J. RodA as the missing glycosyltransferase in Bacillus subtilis and antibiotic discovery for the peptidoglycan polymerase pathway. *Nature microbiology*, *2*(3), 16253 (2017).

Fay, A., Meyer, P., & Dworkin, J. Interactions between late-acting proteins required for peptidoglycan synthesis during sporulation. *Journal of molecular biology*, *399*(4), 547-561 (2010).

Fernandez-Leiro, R. & Scheres, S. H. W. Unravelling biological macromolecules with cryo-electron microscopy. *Nature* 537, 339–346 (2016).

Fraipont, C., Alexeeva, S., Wolf, B., van der Ploeg, R., Schloesser, M., den Blaauwen, T., & Nguyen-Disteche, M. The integral membrane FtsW protein and

peptidoglycan synthase PBP3 form a subcomplex in Escherichia coli. *Microbiology*, *157*, 251-259 (2011).

Frank, J. Averaging of low exposure electron micrographs of non-periodic objects. *Ultramicroscopy*. 1(2), 159-162 (1975).

Galley, N. F., O'Reilly, A. M., & Roper, D. I. Prospects for novel inhibitors of peptidoglycan transglycosylases. *Bioorganic chemistry*, *55*, 16-26 (2014).

Goffin, C., & Ghuysen, J. M. Multimodular penicillin-binding proteins: an enigmatic family of orthologs and paralogs. *Microbiol. Mol. Biol. Rev.*62(4), 1079-1093 (1998).

Helassa, N., Vollmer, W., Breukink, E., Vernet, T., Zapun, A. The membrane anchor of penicillin-binding protein PBP2a from Streptococcus pneumoniae influences

peptidoglycan chain length. *The FEBS journal*, *279*(11), 2071-2081 (2012).

Henderson, R., & Unwin, P. N. T. Three-dimensional model of purple membrane obtained by electron microscopy. *Nature*. 257(5521), 28 (1975).

Henderson, R., Baldwin, J. M., Ceska, T. A., Zemlin, F., Beckmann, E. A., & Downing, K. H. (1990). Model for the structure of bacteriorhodopsin based on high-resolution electron cryo-microscopy. *Journal of molecular biology*. 213(4), 899-929 (1990).

Kühlbrandt, W. The resolution revolution. *Science*, *343*(6178), 1443-1444 (2014).

Lesse, A. J., Campagnari, A. A., Bittner, W. E., Apicella, M. A. Increased resolution of lipopolysaccharides and lipooligosaccharides utilizing tricine-sodium dodecyl sulfate-polyacrylamide gel

electrophoresis. *Journal of immunological methods*, *126*(1), 109-117 (1990).

Levy, N., Bruneau, J. M., Le Rouzic, E., Bonnard, D., Le Strat, F., Caravano, A. Chevreuil, F., Barbion, J., Chasset, S., Ledoussal, B., Moreau, F., Ruff, M. Structural basis for E. coli Penicillin Binding Protein (PBP) 2 inhibition, a platform for drug design. *Journal of medicinal chemistry*. 62(9), 4742-4754 (2019).

Li, X., Mooney, P., Zheng, S., Booth, C. R., Braunfeld, M. B., Gubbens, S., Agard, A. D., Cheng, Y. Electron counting and beam-induced motion correction enable near-atomic-resolution single-particle cryo-EM. *Nature methods*. 10(6), 584 (2013).

Lovering, A. L., De Castro, L. H., Lim, D., & Strynadka, N. C. Structural insight into the transglycosylation step of bacterial cell-wall biosynthesis. *Science*, *315*(5817), 1402-1405 (2007).

Lovering, A. L., De Castro, L., & Strynadka, N. C. Identification of dynamic structural motifs involved in peptidoglycan glycosyltransfer. *Journal of molecular biology*, *383*(1), 167-177 (2008).

Lovering, A. L., Gretes, M., & Strynadka, N. C. Structural details of the glycosyltransferase step of peptidoglycan assembly. *Current opinion in structural biology*, *18*(5), 534-543 (2008).

Messner, P., Schäffer, C., & Kosma, P. Bacterial cell-envelope glycoconjugates. In *Advances in carbohydrate chemistry and biochemistry* (Vol. 69, pp. 209-272). Academic Press (2013).

Mohammadi, T. *et al.* Identification of FtsW as a transporter of lipid-linked cell wall precursors across the membrane. *EMBO J.* 30, 1425–1432 (2011).

Mohammadi, T., Sijbrandi, R., Lutters, M., Verheul, J., Martin, N. I., den Blaauwen, T., de Kruijff, B.,

Breukink, E. Specificity of the transport of lipid II by FtsW in Escherichia coli. *Journal of biological chemistry.* 289(21), 14707-14718 (2014).

Nitta, R., Imasaki, T., Nitta, E. Recent progress in structural biology: lessons from our research history. *Microscopy*, *67*(4), 187-195 (2018).

Punekar, A. S., Samsudin, F., Lloyd, A. J., Dowson, C. G., Scott, D. J., Khalid, S., & Roper, D. I. The role of the jaw subdomain of peptidoglycan glycosyltransferases for lipid II polymerization. *The Cell Surface*, *2*, 54-66 (2018).

Renaud, J. P., Chari, A., Ciferri, C., Liu, W. T., Remigy, H. W., Stark, H., & Wiesmann, C. Cryo-EM in drug discovery: achievements, limitations and prospects. *Nature Reviews Drug Discovery*, *17*(7), 471-492 (2018).

Ruiz, N. Lipid flippases for bacterial peptidoglycan biosynthesis. *Lipid insights*, *8*, LPI-S31783 (2015).

Schägger, H., & Von Jagow, G. Tricine-sodium dodecyl sulfate-polyacrylamide gel electrophoresis for the separation of proteins in the range from 1 to 100 kDa. *Analytical biochemistry*, *166*(2), 368-379 (1987).

Scheres, S. H. Beam-induced motion correction for sub-megadalton cryo-EM particles. *Elife*, *3*, e03665 (2014).

Seddon, A. M., Curnow, P., & Booth, P. J. Membrane proteins, lipids and detergents: not just a soap opera. *Biochimica et Biophysica Acta (BBA)-Biomembranes*. 1666(1-2), 105-117 (2004).

Sgro, G. G. & Costa, T. R. D. Cryo-EM Grid Preparation of Membrane Protein Samples for Single Particle Analysis. *Front. Mol. Biosci.* 5, 1–8 (2018).

Sjodt, M., Brock, K., Dobihal, G., Rohs, P. D., Green, A. G., Hopf, T. A., Meeske, A. J., Veerasak, S., Kahne, D., Walker, S., Marks, D. S., Bernhardt, T. G., Rudner, D. Z., Marks, D. S. Structure of the peptidoglycan polymerase RodA resolved by evolutionary coupling analysis. *Nature*. 556(7699), 118 (2018).

Skrzypek, R., Iqbal, S., & Callaghan, R. Methods of reconstitution to investigate membrane protein function. *Methods*. 147, 126-141 (2018).

Spratt, B. G. Distinct penicillin binding proteins involved in the division, elongation, and shape of Escherichia coli K12. *Proceedings of the National Academy of Sciences*. 72(8), 2999-3003 (1975).

Szwedziak, P., & Löwe, J. Do the divisome and elongasome share a common evolutionary past?. *Current opinion in microbiology*, *16*(6), 745-751 (2013).

Taguchi, A., Welsh, M. A., Marmont, L. S., Lee, W., Sjodt, M., Kruse, A. C., Kahne, D., Bernhardt, T. G., Walker, S. FtsW is a peptidoglycan polymerase that is functional only in complex with its cognate penicillin-binding protein. *Nature microbiology*. 4(4), 587 (2019).

Tan, Y. Z., Baldwin, P. R., Davis, J. H., Williamson, J. R., Potter, C. S., Carragher, B., & Lyumkis, D. Addressing preferred specimen orientation in single-particle cryo-EM through tilting. *Nature methods*, *14*(8), 793 (2017).

Thompson, R. F., Walker, M., Siebert, C. A., Muench, S. P., & Ranson, N. A. An introduction to sample preparation and imaging by cryo-electron microscopy for structural biology. *Methods*. 100, 3-15 (2016).

Typas, A., Banzhaf, M., Gross, C. A. & Vollmer, W. From the regulation of peptidoglycan synthesis to

bacterial growth and morphology. *Nat. Rev. Microbiol.* 10, 123–136 (2012)

Acknowledgments

Beside Botta's family, I'd like to thank the American one: Prof. Dr. Filippo Mancia and his group. In particular I'd like to mention Dr. Rie Nygaard.

Finally, I wish to thank my "real" family, my grandparents, my mother and who has always been there supporting me.

I couldn't have done it without you. Thank you.